

Review

# Recent Advancement of Ullmann Condensation Coupling Reaction in the Formation of Aryl-Oxygen (C-O) Bonding by Copper-Mediated Catalyst

Choong Jian Fui <sup>1</sup>, Mohd Sani Sarjadi <sup>1</sup> , Shaheen M. Sarkar <sup>2</sup> and Md Lutfor Rahman <sup>1,\*</sup>

<sup>1</sup> Faculty of Science and Natural Resources, University Malaysia Sabah, Sabah 88400, Malaysia; jianfui@hotmail.com (C.J.F.); msani@ums.edu.my (M.S.S.)

<sup>2</sup> Bernal Institute, Department of Chemical Sciences, University of Limerick, V94 T9PX Limerick, Ireland; Shaheen.Sarkar@ul.ie

\* Correspondence: lotfor@ums.edu.my; Tel.: +60-16-939-9011

Received: 18 August 2020; Accepted: 9 September 2020; Published: 24 September 2020



**Abstract:** Transition metal-catalyzed chemical transformation of organic electrophiles and organometallic reagents belong to the most important cross coupling reaction in organic synthesis. The biaryl ether division is not only popular in natural products and synthetic pharmaceuticals but also widely found in many pesticides, polymers, and ligands. Copper catalyst has received great attention owing to the low toxicity and low cost. However, traditional Ullmann-type couplings suffer from limited substrate scopes and harsh reaction conditions. The introduction of homogeneous copper catalyst with presence of bidentate ligands over the past two decades has totally changed this situation as these ligands enable the reaction promoted in mild condition. The reaction scope has also been greatly expanded, rendering this copper-based cross-coupling attractive for both academia and industry. In this review, we will highlight the latest progress in the development of useful homogeneous copper catalyst with presence of ligand and heterogeneous copper catalyst in Ullmann type C-O cross-coupling reaction. Additionally, the application of Ullmann type C-O cross coupling reaction will be discussed.

**Keywords:** Ullmann cross-coupling; copper catalyst; C-O bond; heterogeneous catalyst; homogeneous catalyst; biaryl ether

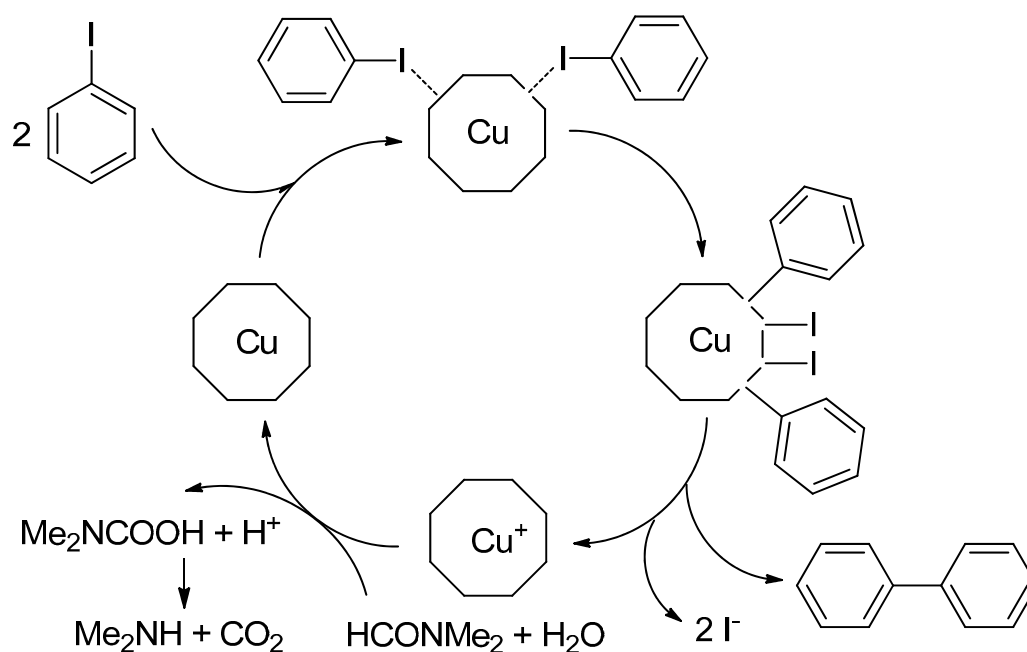
## 1. Introduction

The transition metal-catalyzed chemical transformation of organic electrophiles, and organometallic reagents have turned up as an exceedingly robust synthetic tool. The evolution of transition metal catalysts have attained a stage of civilization that authorizes for an extensive scope of chemical bonds formation partners to be combined efficiently [1]. In the last century, C-C bond transformation (catenation) has permitted chemists to assemble intricate molecular frameworks of diversified interests encompassing complete synthesis of natural products, pharmaceuticals, and industrial process improvement, as well as biochemistry, materials, and nanotech [2,3]. The evolution of chemicals through the transition-metal catalyzed reaction is an exciting era for the chemistry of palladium [4], ruthenium [5], platinum [6], etc., and has been significantly adopted by the industry. For example, ruthenium-catalyzed N-H insertion reaction for the formation of benzofused six/five-membered azaheterocycles [7] which have a wide range of significant biological activity, such as anti-bacterial, -fungal, -tubercular, helminthic, -plasmodial, -cancer, -inflammatory, cardiotoxic, -hypertensive, -thrombotic, histaminic, -ulcer, analgesic, neuroleptic, etc. [8]. In contrast, the low cost and high abundance of copper metal seemed to be the left in the cold as a trend of a breakthrough in this area. However, the copper-mediated C-C, C-O, C-N, and C-S bond formation is a part of one oldest reactions, emphasizing the Ullmann cross-coupling reaction [9,10].

In the early 20th century, Ullmann and Goldberg have reported the first and primary cleavage of an aromatic carbon-halide bond in the presence of a stoichiometric amount of copper as catalyst (Table 1) [11,12]. In this reaction, two moles of aryl halides are coupled in the presence of a stoichiometric amount of copper salt to afford the homocoupling product at 210–260 °C (Scheme 1) [12,13]. Even though these homocoupling reactions received considerable attention from the synthetic industry, it contributed several applications in that century. Still, this reaction suffered from harsh conditions, which included high temperature, strong base, a large amount of copper catalyst, limited substrate scope, etc. [14]. Later, Ullmann and Goldberg also reported a copper-catalyzed C-N [15] and C-O heteroatomic bonds formation reaction [16]. In 1929, Hurtley found that 3-bromobenzoic acid might be utilized for the formation of C-C bond through the homocoupling reaction [17,18] in the presence of copper-bronze and copper acetate in diketones and malonates. Unfortunately, this reaction generally needs harsh conditions, like the Ullmann and Goldberg reaction, and inadequate functional groups tolerance have restricted the applications of Ullmann and Ullmann-type reactions through their study.

**Table 1.** History of Ullmann-type reaction by Ullmann, Goldberg, and Hurtley.

Bond Type	Author	Year	Catalyst Source	Temperature	Ref.
C-C	Ullmann	1901	Copper powder (stoichiometric)	200 °C	[12]
C-N	Ullmann	1903	Copper (stoichiometric)	Reflux	[19]
C-O	Ullmann	1905	Copper	200 °C	[20]
C-N	Goldberg	1906	Copper	Reflux	[21]
C-C	Hurtley	1929	Copper nanoparticle	Reflux	[22]



**Scheme 1.** Typical copper-mediated Ullmann condensation reaction and presumptive mechanism.

To modernize this prominent and classical Ullmann reaction, it is essential to establish a novel composition and morphology of catalyst, suitable solvents, and reducing agents. Back in 1970, many researchers applied various metal-based catalysts involved in Ullmann's reaction, and most included palladium, nickel, and gold [23]. However, palladium and nickel were found to be the best catalysts for Ullmann reaction due to high reactivity and regioselectivity. Unfortunately, metal catalysts have several drawbacks, such as high cost, highly toxic, and generally required poisonous organic phosphines as a stabilizing ligands [24]. Gold is the most stable metal and exhibits marvelous features, such as assemblage of different types involving materials science, the development of its own particles,

size-related electronic, magnetic, and optical properties, and utilization as a catalysis in biology [25]. Besides these precious metals, silver [26], nickel [27,28], and rhodium [29] were also studied and applied to the Ullmann coupling reaction. The cooperative stimulus of the polymetallic unlocked different view to the field of catalysis when a unique constituent is adequately investigated. Bimetallic catalysts revealed outstanding performance than the monometallic catalysts for their catalytic performance, stability, and selectivity [30].

The research on Ullmann reaction is a persistent process and has adapted interested reaction today. Under this framework and history, it is so valuable for us to investigate the reactivity and mechanism of Ullmann's reactions. These can assist us in scheme the new vital catalysts for the breakthrough of the related field. In the meantime, countless work has been put in to explore the Ullmann reaction process at the molecular level.

This review focuses summary of the evolution of catalysts in Ullmann reaction for aryl C-O-C (diaryl ether) bond formation, the choice of reductants, and provides an ordinary outline of the reaction mechanism. The corresponding outcomes were managed in brief here to permit this review to stand alone.

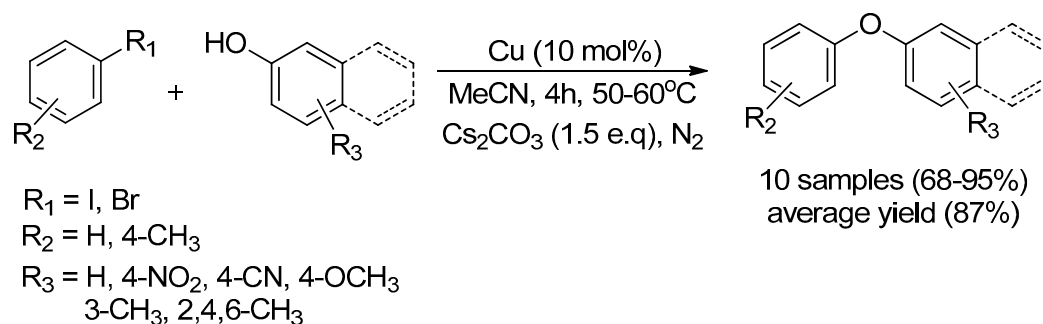
## 2. Aryl C-O Bond Formation Catalyzed by Copper Metal

### 2.1. Heterogeneous Catalyst

A heterogeneous catalyst is referred to as a catalytic reaction where the catalyst has the phase difference with the reactants. In short, it is an insoluble catalyst in a solution. A heterogeneous catalyst generally continues creating the active site with the reactant under suitable reaction conditions. These sites change the rates of chemical reactions of the reactants localized on them without changing the thermodynamic equilibrium between the materials [31].

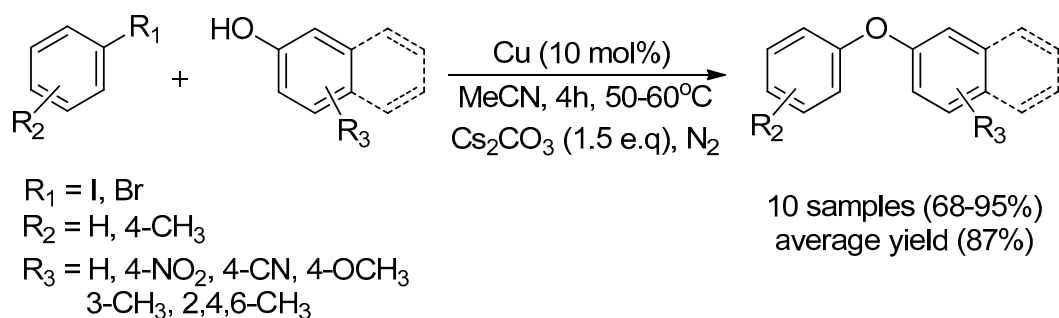
#### 2.1.1. The Mono-Element of Cu Nanoparticle

In 2007, Kidwai research group reported using mono element copper nanoparticles as a catalyst for the O-arylation through the Ullmann coupling reaction. The biaryl ether was rapidly formed using 10 mol% of the catalyst in the presence of 1.5 equivalent (equiv.) of  $\text{Cs}_2\text{CO}_3$  under mild reaction conditions (50–60 °C) in acetonitrile (Scheme 2). The cross-coupling reactions were highly selective in a wide variety substituted phenols and aryl halides. A very successful finding in this study was the low reactive aryl bromides efficiently promoted the Ullmann coupling reaction. The steric hindered 2,6-disubstituent, and bicyclic phenols also resulted with the biaryl ether in an acceptable to high yield. The copper nanoparticle size was  $18 \pm 2$  nm, and it was determined by TEM, as well as quasi-elastic light scattering data (QELS). It should be expressed that the size of the nanoparticle profoundly affect the catalytic cross-coupling reactions [32]. Unfortunately, these copper nanoparticles did not performed well in the reusability experiment. The catalytic activity started to decrease after the second run of the coupling reaction (iodobenzene and phenol) with increasing of the reaction time: 87% (6 h), 81% (9 h), 72% (11 h), and 63% (12 h), respectively [33].



Scheme 2. The formation of biaryl ether using Cu-nanoparticles.

Shortly afterward, Schouten and Wheatly described Ullmann coupling (C-O) reaction using copper nanoparticles (CuNPs) (~9.6 nm) under microwave irradiation conditions without the presence of a base to afford the corresponding biaryl ether with high yield [34,35]. Continuing, Yuto Isomura, and his co-workers used colloidal CuNPs (~2 nm) as an efficient catalyst in the formation biaryl ethers. Their finding showed that the reaction was conducted according to the inferiority of catalyst loading and ligand-free environment at 110 °C in dimethylformamide (DMF) for a day (Scheme 3). The copper nanoparticle was synthesized by a surfactant-free in DMF reduction method. These colloidal CuNPs were investigated by HRTEM, along with the dynamic light scattering (DLS) spectrum. The characterization of colloidal CuNPs demonstrated that copper species is predominantly low oxidation state and high probability protected by a layer of an oxide. This unwarranted copper nanoparticle facilitated the coupling of an aryl halide with phenol in the presence of 0.01 mM loading of nanoparticles. The aryl-iodide and bromide were efficiently forwarded to the O-arylation Ullmann coupling reaction with a variety of substituted phenols. However, iodothiophene was not forwarded to the coupling reaction under this reaction conditions, and no product was extracted after the reaction. Additionally, the colloidal CuNPs was dramatically deactivated after three consecutive runs when iodobenzene and 3,5-dimethylphenol were used: 51% and 18% [36].

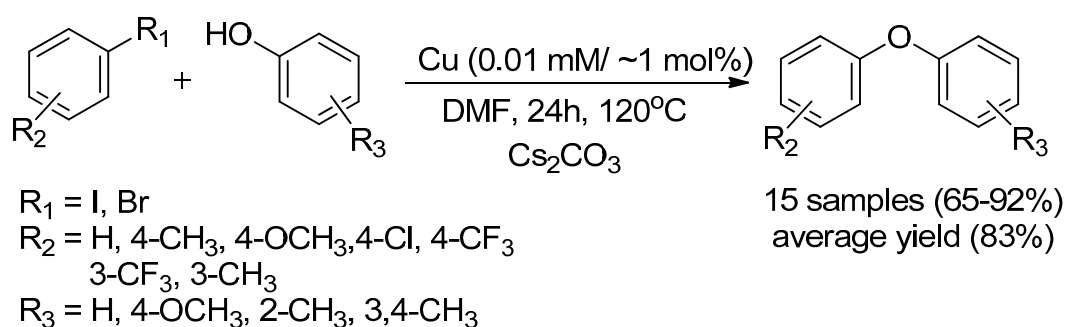


**Scheme 3.** Colloidal CuNPs catalyzed synthesis of diphenyl ethers.

In 2014, researcher Mahmoud Nasrollahzadeh's team described a green synthesis method for the formation of copper nanoparticles via phytoextraction and rhizofiltration of the *Euphorbia esula* L. leaves (Figure 1). The synthesized Cu-NPs used in Ullmann O-arylation to evaluate its catalytic ability without adding of any surfactant. The Cu-NPs (20–110 nm) was characterized by using XRD, TEM, and UV-Vis. All electrons rich and electrons poor aryl halides efficiently reacted with phenols and provided the corresponding aryl ether in the presence of  $\text{Cs}_2\text{CO}_3$  in DMF at 120 °C (Scheme 4). The formation of biaryl ether formation was quite impressive and provided 65–92% yield [37].

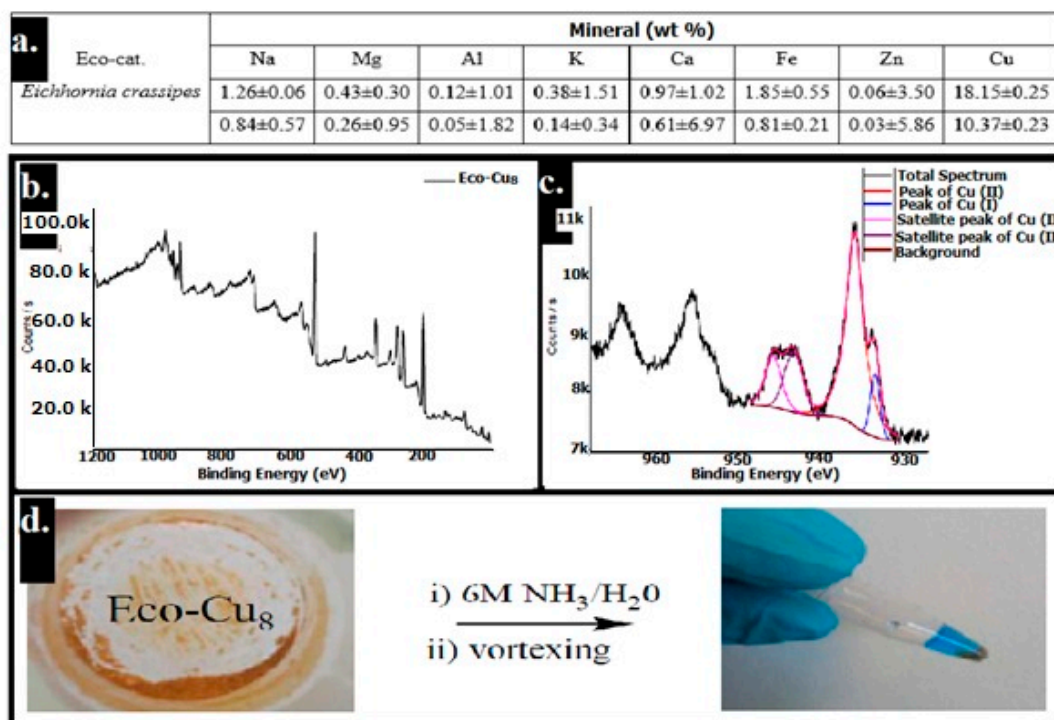


**Figure 1.** Image of *Euphorbia esula* L.

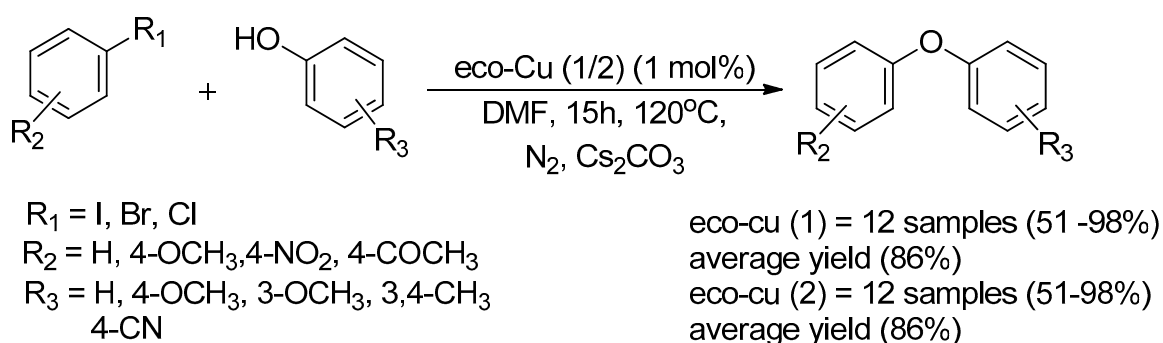


**Scheme 4.** O-arylation of phenol with substituted aryl halides using Cu-NPs.

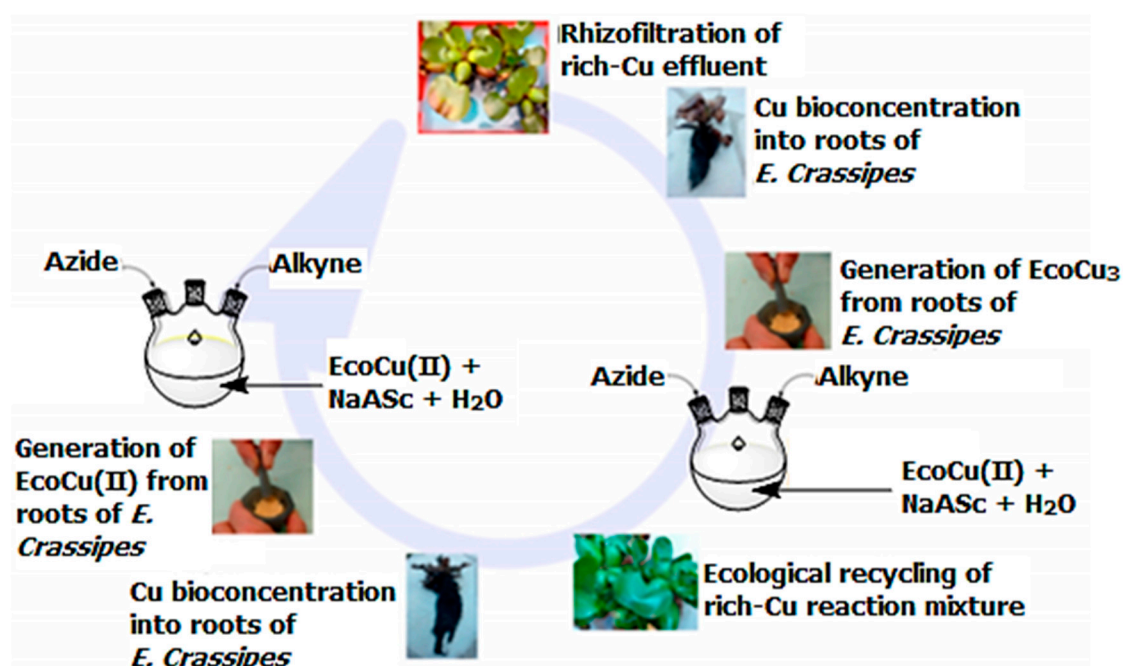
Two years later, Claude Grison's team followed the same method in the synthesis of eco-Cu-NPs via the *Eichhornia crassipes* plant. The synthesis of this bio-eco catalyst is based on the extraction of metals via phytoremediation and innovative chemical valorization [38,39]. The Cu-NPs was adsorbed on the surface of *Eichhornia crassipes* root via phytoextraction with rhizofiltration methods and utilized as a heterogeneous catalyst in the O-arylation Ullmann coupling reaction. The eco-Cu-NPs was characterized by inductively coupled plasma mass spectrometry (ICP-MS), transmission electron microscope (TEM), X-ray diffraction (XRD), and model reactions to clarify the chemical constitution and catalytic performance of the eco-Cu NPs. Based on the study, the *Eichhornia crassipes* extract about 10.3–18.1 wt% of  $\text{Cu}^{2+}$  with 4–8 nm average particles size (Figure 2). The synthesized bio-Cu-NPs were used for the synthesis of biaryl ether where 50  $\mu\text{mol}$  (1 mol%) of catalyst was loaded. The reaction was carried out under inert condition for 15 h to give a promising yield of the biaryl ether (Scheme 5). The quite exciting result is that bio-cat can be compatible for a wide range of functionalities aryl halides and phenol, including nitriles, ketones, ethers, alkyl, and nitro groups with regeneration of the eco-Cu NPs (Figure 3) [40].



**Figure 2.** (a) Chemical composition on the eco-Cu-NPs *Eichhornia crassipes*; (b,c) the XPS analysis of eco-Cu-NPs; (d) The analytical characterization eco-Cu-NPs. Reproduced by permission of Royal Society of Chemistry. [40]



**Scheme 5.** O-arylation of phenol with substituted aryl halides. (1) NPs by Claude Grison and eco-Cu; (2) NPs by Tomasz K. Olszewski in standard condition.

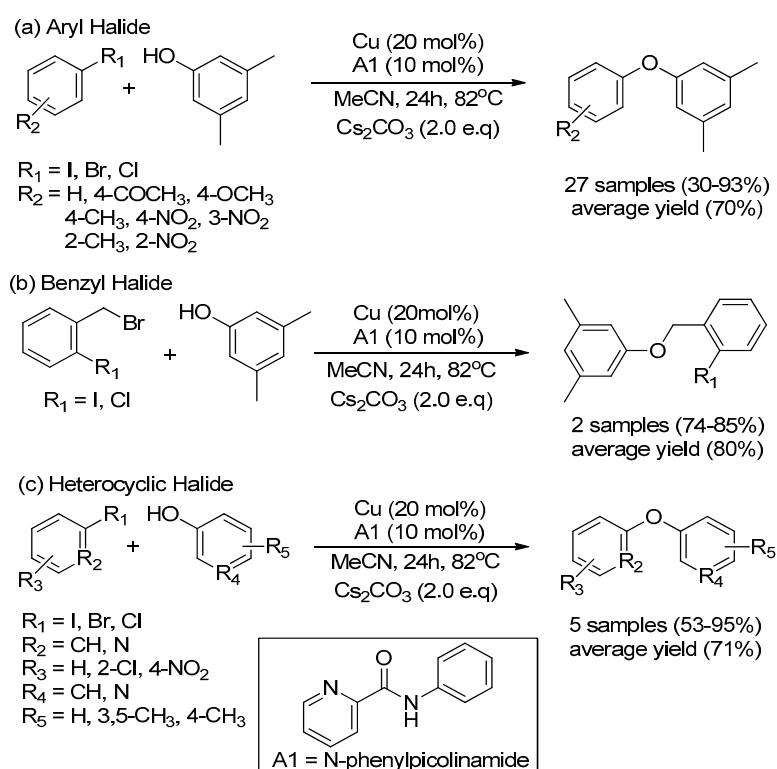


**Figure 3.** The eco-Cu-NPs was recycled based on the rhizofiltration.

In 2019, researcher Tomasz K. Olszewski et al. also applied the same method in the synthesizing of bio-Cu-NPs via rhizofiltration and biosorption of copper contaminant effluent using *Eichhornia crassipes* root. The Cu-NPs were well characterized using ICP-MS, XRD, XPS, and Brunauer-Emmett-Teller (BET) analyses. Tomasz K. Olszewski found that *Eichhornia crassipes* root can adsorb around 10.37 wt% of  $\text{Cu}^{2+}$ -NPs. The synthesized Cu-NPs provided high yield of the biaryl product (51–98%) using 1 mol% of Cu-NPs within 15 h (Scheme 5). The rhizofiltration and adsorption technique was applied to refill the copper nanoparticles that were lost on the *Eichhornia crassipes* root (Figure 3) so that the bio-Cu-NPs can efficiency promote the reaction [41].

### 2.1.2. Cu-Nanoparticles in the Presence of Ligands (A)

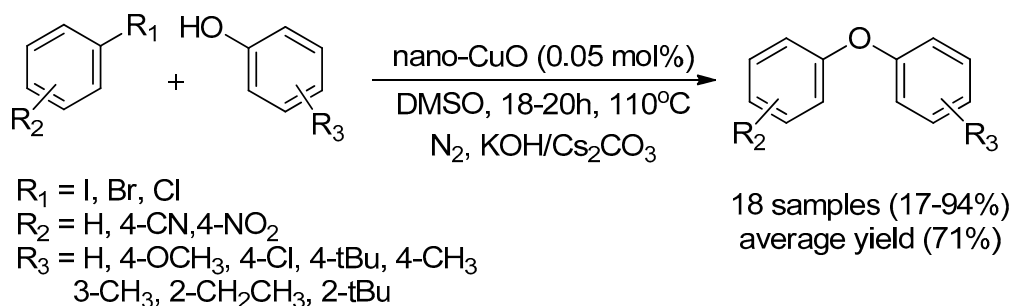
In 2017, researcher Damkaci's team described commercially nano-sized Cu-catalyzed C-O bond formation of phenols with a variety of aryl halides efficiently in the presence of N-phenylpicolinamide (A1) as a ligand (Scheme 6). The hetero(aromatic)aryl halides and phenols provided 30–93% yield of the corresponding O-arylation products selectively [42].



**Scheme 6.** (a) C-O bond formation in the presence of nano-sized copper with ligand (A1); (b) selectivity of benzyl halides vs. aryl halides; (c) heterocyclic biaryl ether.

### 2.1.3. Copper Oxide Nanoparticle

In 2008, Zhang Jin Tang first discovered the nanocrystalline copper oxide nanoparticle, and it was applied to the O-arylation of Ullmann reaction. The CuO-NPs was synthesized from an aqueous solution of copper (II) nitrate trihydrate in pH 10 at room temperature. The CuO-NPs was collected and calcinated at 350 °C for 24 h. The synthesized CuO-NPs (28.5 nm) was employed to the Ullmann etherification reaction of a variety of substituted phenols and aryl halides in the presence of base (KOH/Cs<sub>2</sub>CO<sub>3</sub>) in dimethyl sulfoxide (DMSO) at ~100 °C under an inert atmosphere (Scheme 7). The result suggested that the phenols substituted with electron-donating groups provided a better yield compare to the electron-withdrawing substituted group. The reactivity of the aryl halide was followed by Ph-I > Ph-Br > Ph-Cl. The substituted aryl chloride played significantly role in the coupling reaction. For example, neutral chlorobenzene provided only 17% of diphenyl ether, whereas 4-nitrochlorobenzene afforded the respective product with 87% yield. In the study, the aryl-iodine and aryl-bromide showed little substituent effect that attached to the benzene ring [43].



**Scheme 7.** Ullmann etherification using CuO NPs.

One year later, Jee Yong Kim's research group has synthesized copper oxide nanoparticle in cubic shape. The color of the CuO nano cubic was yellow, with an average size of  $45.1 \pm 3.1$  nm (Figure 4). A number of functionalized biphenyl ethers were smoothly produced from the respective nucleophiles and substituted aryl halides (I, Br, Cl) at  $150^\circ\text{C}$  in the presence of 0.1 mol% of CuO nano cubic (Scheme 8). The overall reaction combination provides the competitive advantages of low catalyst loading, wide-ranging substrate applicability, good recoverability of the catalyst, and excellent yield of biaryl ether in short reaction time [44].

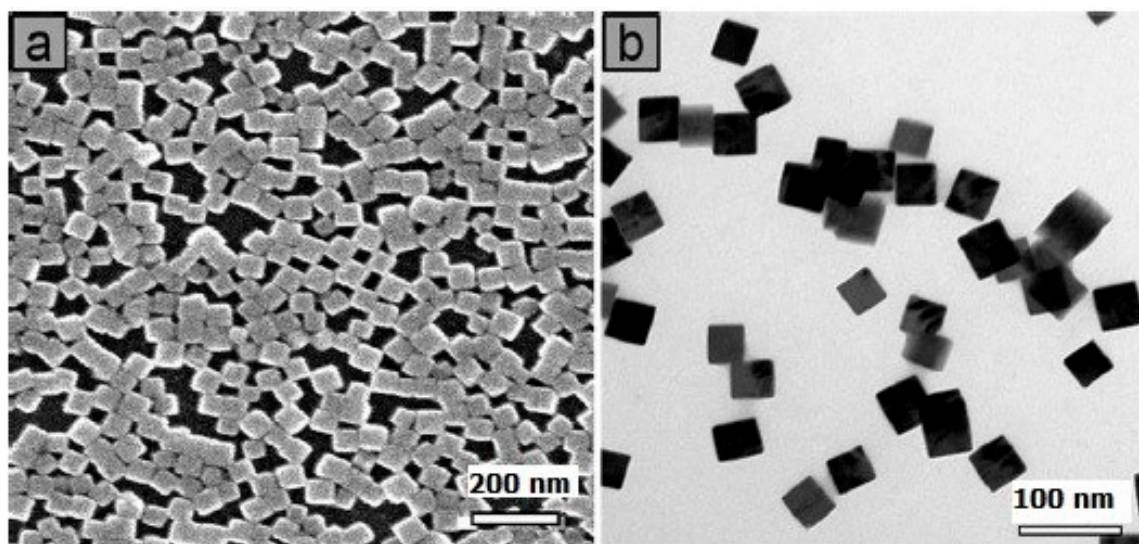
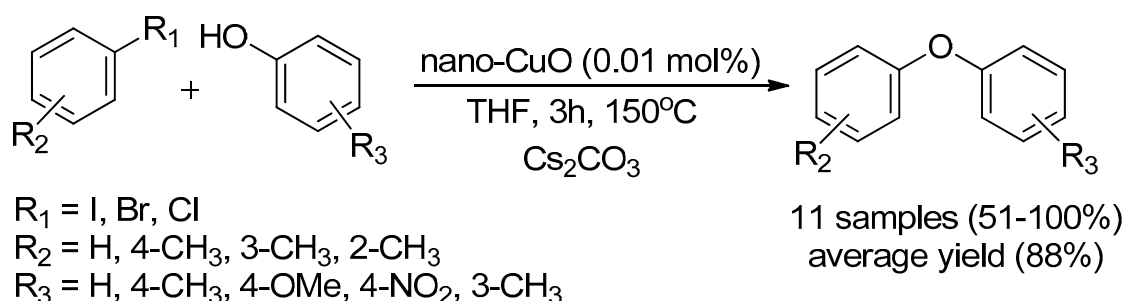


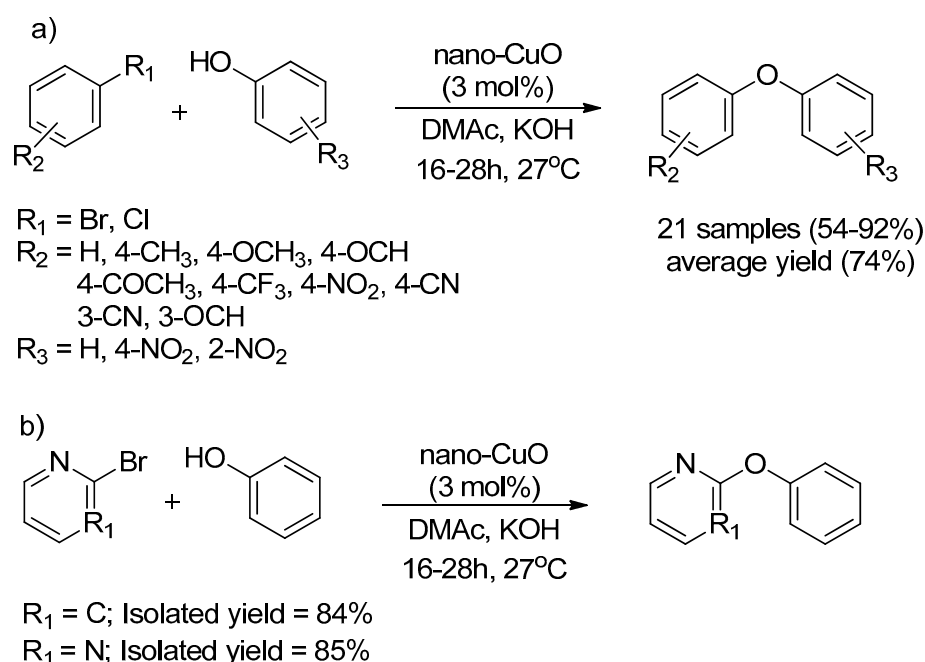
Figure 4. (a) SEM image of cubic formed CuO; (b) TEM image of CuO nano cubic.



Scheme 8. Formation of diphenyl ethers in the presence of CuO nano cube.

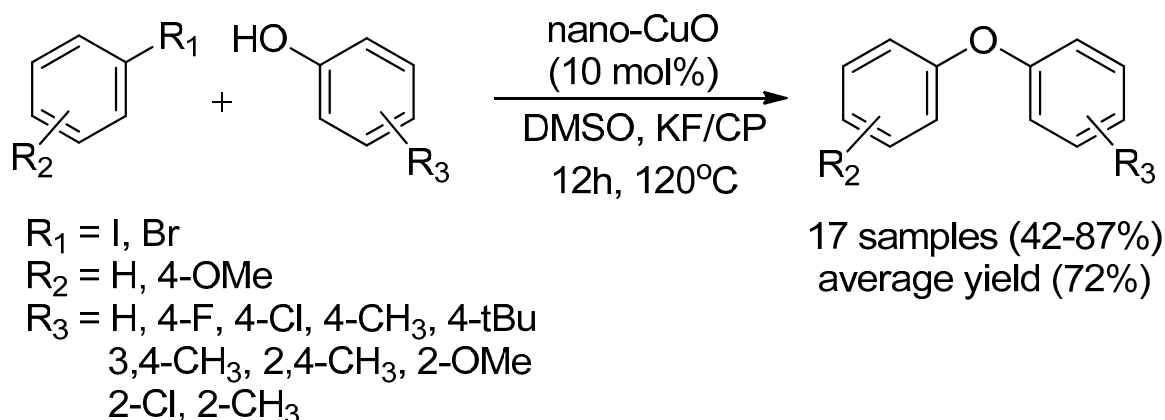
A few years later, S. Ganesh Babu and R. Karvembu designed a gentler method for the formation of biphenyl ether derivatives through Ullmann etherification reaction. A variety of substituted biaryl ethers were produced from respective nucleophiles and substituted aryl bromide/chloride at room temperature in the presence of 3 mol% CuO-NPs and 2 mol equivalent of KOH in *N,N*-dimethyl acetamide (DMAc) under inert condition (Scheme 9). Additionally, CuO-NPs catalyzed C-O bond formation reaction of phenol with (hetero)phenyl bromide smoothly to afford the respective heteroaryl ethers in excellent yield [45].



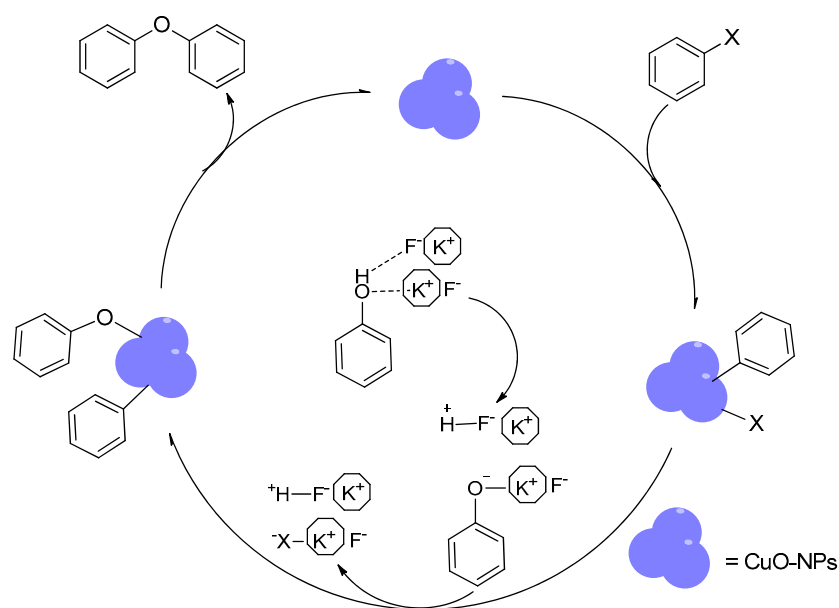


**Scheme 9.** (a) Formation of biaryl ethers in the presence of CuO-NPs; (b) heterocyclic biaryl ether.

In 2014, Mohammad A. Khalilzadeh research team described Ullmann coupling (C-O) reaction using CuO-NPs as a catalyst in the presence of base potassium fluoride (KF)/clinoptilolite [46]. Clinoptilolite (CP) is a natural zeolite mineral, with an open aluminosilicate framework and inner surface area with broad applications in the catalytic reaction [47]. Clinoptilolite has a high cation switching capacity, especially for  $\text{K}^+$  [48]. Thus, the utilization of this feature by impregnation of KF on CP causes a freer  $\text{F}^-$  anion that has ability to work as an active base for the etherification reaction. The cross-coupling result showed 10 mol% of CuO-NPs efficiently provided good to high yield of biaryl ethers (Scheme 10). Base on the study, a probable mechanism for CuO-NPs catalyzed reductive O-arylation coupling reaction shown in Scheme 11. The reaction was started by (i) adsorption of aryl halide on the surface of CuO-NPs through an oxidative addition. (ii) A proton was abstracted by a negatively charged fluoride moiety from phenol to generate a phenoxide anion stabilized at the potassium surface. (iii) Then, the reaction underwent anion substitution and followed by a reductive elimination process on the surface of the CuO-NPs to produce biphenyl ether [46].



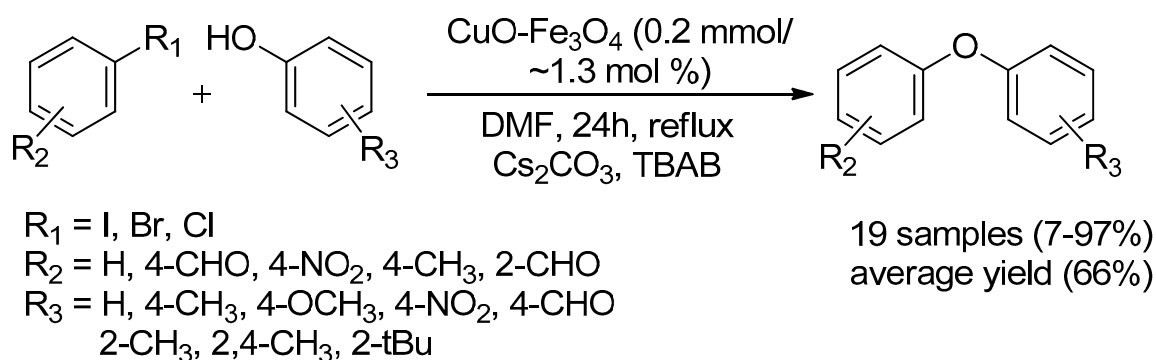
**Scheme 10.** The formation of biaryl ether using CuO-NPs and KF/CP as the base.



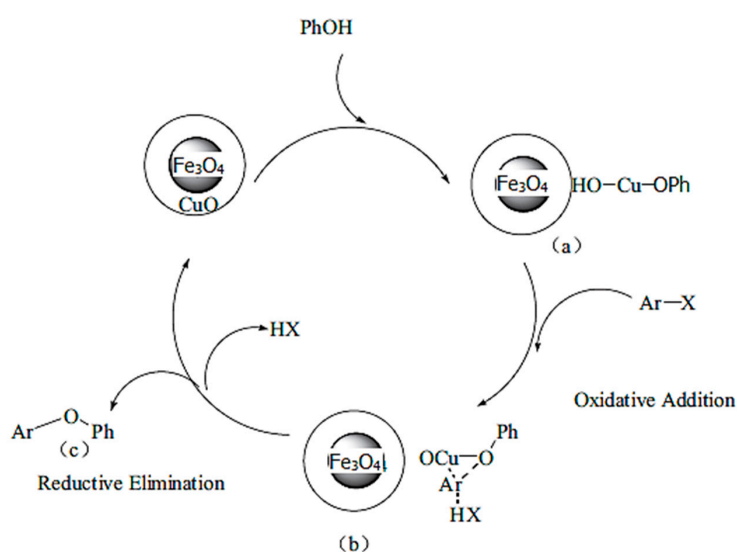
**Scheme 11.** The mechanism of KF/clinoptilolite (CP) as the base with CuO-NPs.

#### 2.1.4. Maghemite-Copper Nanoparticles (CuFe<sub>2</sub>O<sub>4</sub> Nanoparticles)

In 2014, Zhang Yi Peng's research group reported impregnation of copper into magnetic substrate as a heterogeneous catalyst for Ullmann etherification reaction. The CuFe<sub>2</sub>O<sub>4</sub> nanoparticles synthesized by Fe<sub>3</sub>O<sub>4</sub> encapsulated CuO. This magnetic CuFe<sub>2</sub>O<sub>4</sub> catalyst smoothly affords respective biphenyl ethers without using any ligand, and it can be quickly recovered by using of an additional magnet and could be reused up to three times without loss of activity (Scheme 12). The quite exciting results explored by Zhang using CuO-Fe<sub>3</sub>O<sub>4</sub> as the catalyst are: (1) electron-rich substituted phenol lead to produce higher yield of biphenyl ethers, even the substituent in ortho- or meta-location which proficient of providing a steric bias. (2) The electron-rich phenol performs differently from electron-deficient one; the phenol is bearing strong withdrawing group is challenging to undergo an O-arylation reaction. For example, *p*-nitrophenol and *p*-hydroxybenzaldehyde dramatically decreased the yield of the product. (3) The electron-withdrawing substituted aryl halides give an excellent yield. (4) The reactivity of aryl iodide showed better reactivity compare to aryl chlorides I > Br > Cl. A reasonable mechanism for the CuO-Fe<sub>3</sub>O<sub>4</sub>-catalyzed O-arylation is shown in Scheme 13 [49].

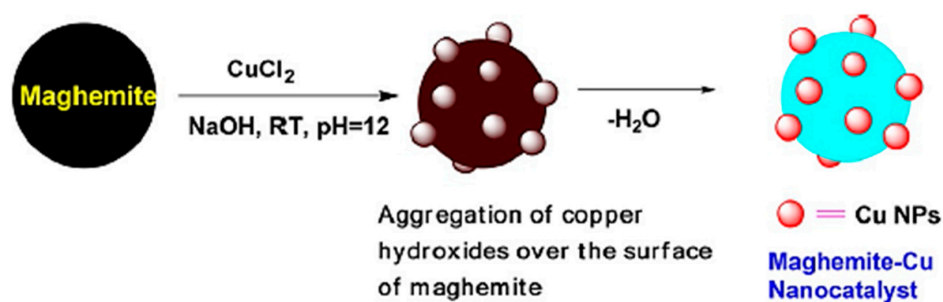


**Scheme 12.** The C-O bond formation in the presence of maghemite-Copper nanoparticles.

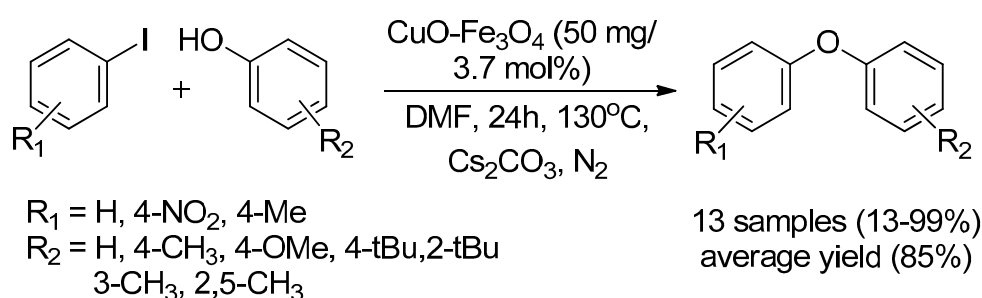


**Scheme 13.** The mechanism of CuO-Fe<sub>3</sub>O<sub>4</sub>-catalyzed C-O bond formation reaction; (a) oxidative addition, (b) intermediate (c) reductive elimination.

Similarly, Sharma et al. also employed a magnetically copper nanoparticles from cost-effective precursors, and it was utilized for C-O, C-N, and C-S bonds formation reactions. The CuFe<sub>2</sub>O<sub>4</sub> nanoparticles were synthesized and characterized by a dull wet impregnation technique and dehydration technique (Figure 5) [50] and XRD, atomic adsorption spectroscopy (AAS), TEM, field emission gun scanning electron microscope energy dispersive X-ray (FEG-SEM-EDS), XPS, Mossbauer spectroscopy, and high-angle annular dark-field imaging scanning transmission electron microscopy (HAADF-STEM), respectively. The size of the magnetic-copper nanoparticles was 28.7 nm and containing 4.7 mol% of copper in the Fe<sub>2</sub>O<sub>4</sub>. The catalytic activity of CuFe<sub>2</sub>O<sub>4</sub> was then investigated using various type of substituted phenols and aryl iodide in present Cs<sub>2</sub>CO<sub>3</sub> in DMF at 130 °C (Scheme 14). The result showed that phenol with substituents at *ortho* and *meta* position gave a lower yield of the corresponded ether [51].

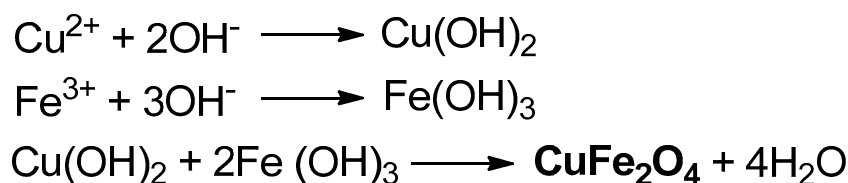


**Figure 5.** Synthesis of maghemite-Cu nanocatalyst. Reproduced by permission of Wiley [51].



**Scheme 14.** Maghemite-Copper oxide nanoparticles catalyzed synthesis of biphenyl ethers.

A few years later, an improvement method was described by Nasim Kazemi groups using  $\text{CuFe}_2\text{O}_4$  under ligand-free conditions. In his study, the maghemite-copper nanoparticles are in the form of spherical-spinal phase with the average diameter  $37.47 \pm 4.92$  nm. The spinel maghemite-copper nanoparticles were prepared by the formation of hydroxyl co-precipitation of  $\text{Cu}(\text{OH})_2$  and  $\text{Fe}(\text{OH})_3$  in aqueous ethanol. Then, the  $\text{Cu}(\text{OH})_2$  and  $\text{Fe}(\text{OH})_3$  react together to give spinel  $\text{CuFe}_2\text{O}_4$  (Scheme 15). The spinel phase of  $\text{CuFe}_2\text{O}_4$  exhibited superparamagnetic behavior;  $56.3 \text{ emu g}^{-1}$ , and it can be easily removed by using a magnetic bar after the reaction (Figure 6). The nanocat- $\text{CuFe}_2\text{O}_4$  utilized in the etherification reaction with various type of substituted phenols and aryl halides under ligand-free conditions at  $70^\circ\text{C}$ . The proposed mechanism is presented in Scheme 16 [52].



Scheme 15. Chemical reaction of Spinel maghemite-copper nanoparticles.

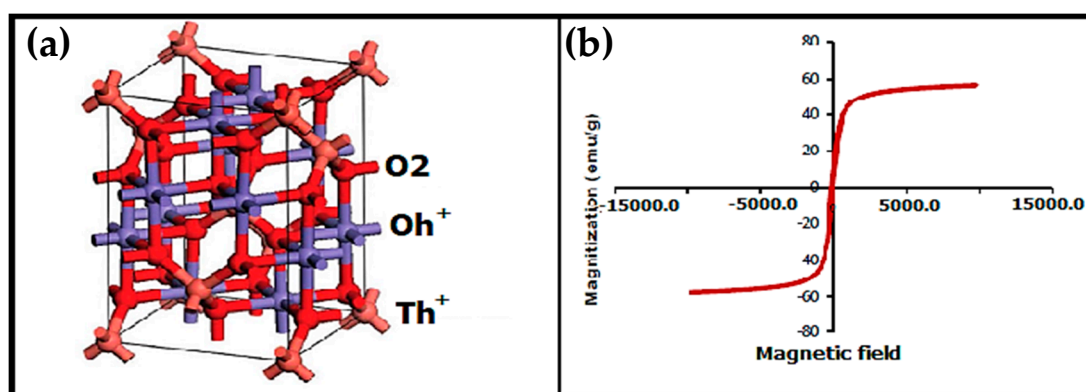
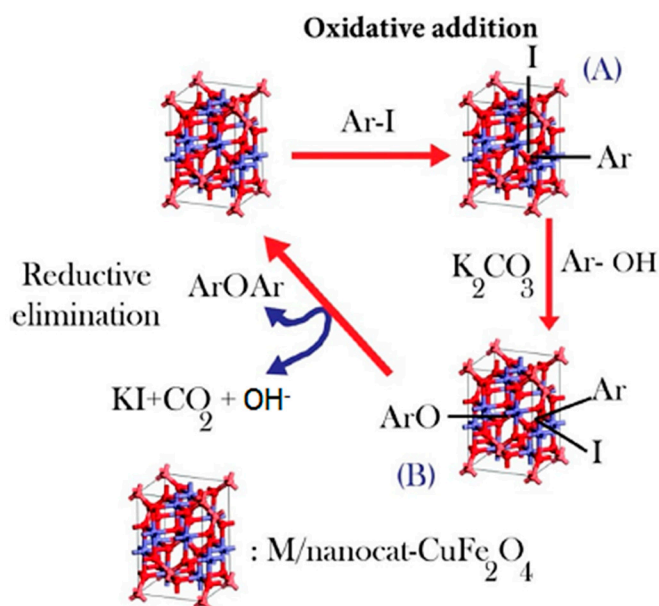


Figure 6. (a) Crystal structure of  $\text{CuFe}_2\text{O}_4$ ; (b) magnetization curve of  $\text{M/nanocat-CuFe}_2\text{O}_4$ .



Scheme 16. The proposed mechanism of biaryl ether formation using maghemite-copper nanoparticles.

### 2.1.5. Supported-Copper Nanoparticles Catalyst

#### Maghemite-Copper Nanoparticles ( $\text{CuFe}_3\text{O}_4$ Nanoparticles)

As more attention on reusable of waste and waste control of by-product after the reaction, many researchers are more likely using the waste as a source in synthesis of catalyst. The agglomeration of nanoparticles is a drawback in the catalytic reaction which causes the decrease of catalytic activity. The ideal support is one of the methods that can reduce the agglomeration of nanoparticles during the reaction [53]. In 2015, Mahmoud Nasrollahzadeh's team first discovered that extracted fruit juice from Barberry *vulgaris* fruit is an excellent reducing and stabilizing agent in the synthesis of  $\text{Cu/RGO-Fe}_3\text{O}_4$  nanocomposite. The preparation of nanocomposite of  $\text{Cu/RGO-Fe}_3\text{O}_4$  are involved in 4 steps: (1) Formulation of GO from natural graphite powder by a modified Hummers method [54]. (2) The reduced graphene oxide (RGO) (Figure 7) nanosheets were prepared by the reduction of a colloidal suspension of graphene oxide-based on glucose [55]. (3) The coprecipitation route was used to synthesize the  $\text{RGO-Fe}_3\text{O}_4$  magnetic nanocomposite [55]. (4) The barberry fruit juice was used in the synthesis of copper nanoparticles onto the  $\text{RGO-Fe}_3\text{O}_4$  surface by treating of  $\text{RGO-Fe}_3\text{O}_4$  magnetic nanocomposite with  $\text{CuCl}_2$  in water at  $60^\circ\text{C}$  for 7 h (Scheme 17) [56]. The synthesized  $\text{Cu/RGO-Fe}_3\text{O}_4$  nanoparticles were 35 nm, and the magnetic saturation was  $22.4\text{ emug}^{-1}$ . The catalytic activity of  $\text{Cu/RGO-Fe}_3\text{O}_4$  provides good to excellent yield, even in electron-donation and electron-withdrawing substituted of aryl halides (Scheme 18) [56].

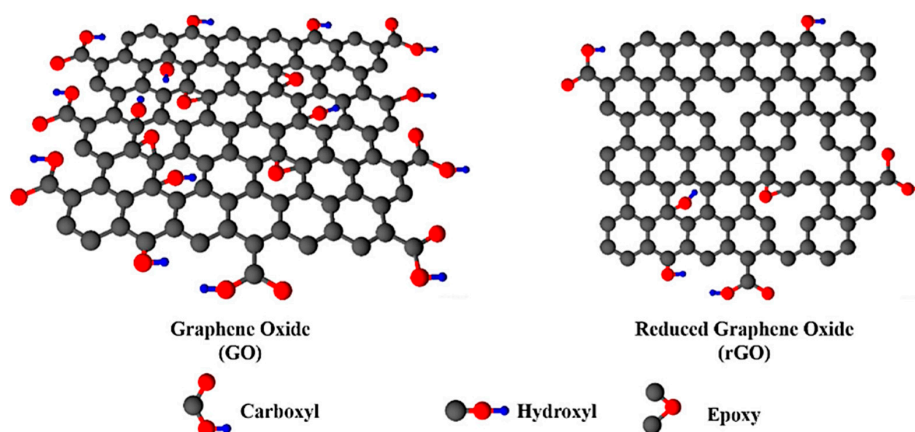
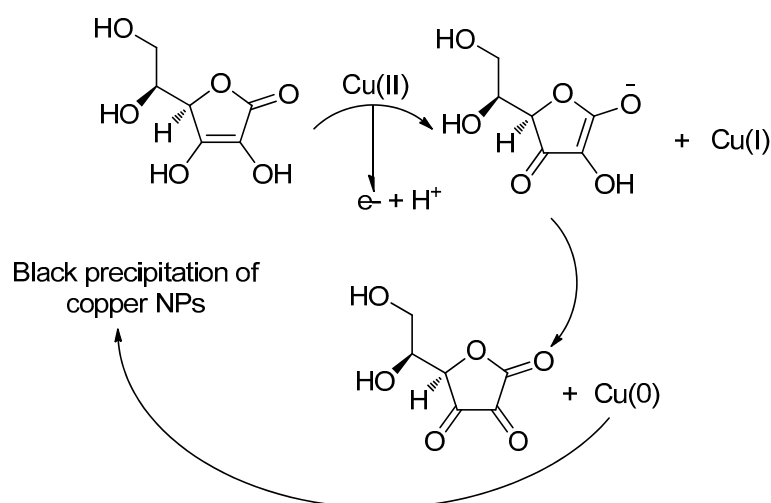
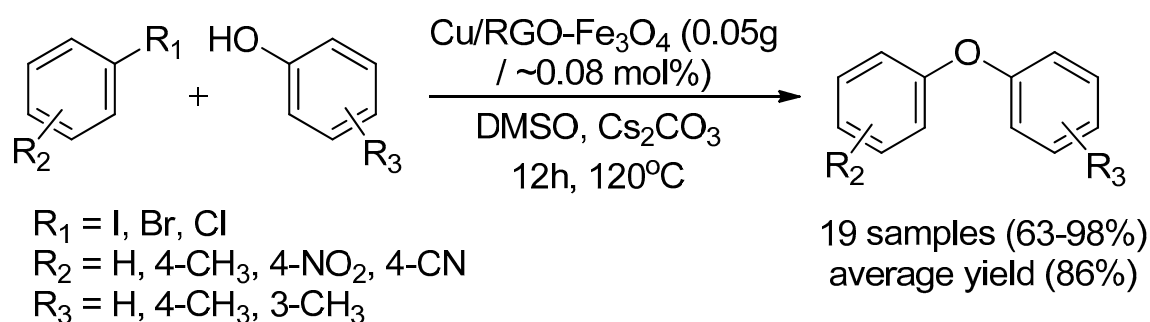


Figure 7. The image of graphene oxide and reduced graphene oxide (RGO).

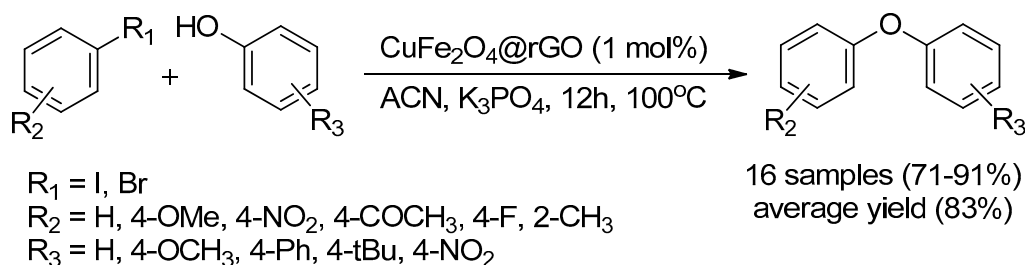


Scheme 17. *Barberis vulgaris* fruits extracted as an eco-synthesis of copper NPs.

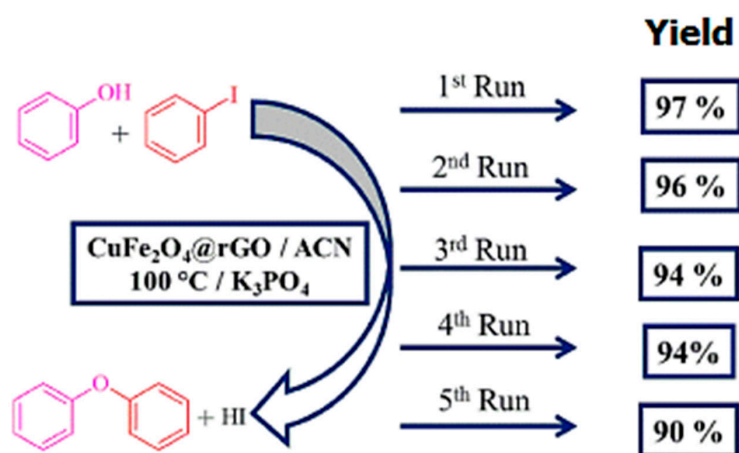


**Scheme 18.** Maghemite-Reduce RGO Copper nanoparticles catalyzed synthesis of biphenyl ethers.

Similarly, Akhil V. Nakhate and Ganapati D. Yadav also reported the catalytic performance of Cu NPs/RGO/Fe<sub>3</sub>O<sub>4</sub> nanocomposite in the O-arylation Ullmann cross-coupling reaction. The difference in their study is the synthesized method of Cu NPs/RGO/Fe<sub>3</sub>O<sub>4</sub>. In Akhil's study, synthesis of supported RGO copper ferrite is done through solvothermal process, using ethane-1,2-diol as a solvent and sodium acetate as a reducing agent. Akhil also focused on the optimization process and comparison in using of copper ferrite-supported RGO with homogeneous copper catalyst and other types of heterogeneous catalysts. In this study, he observed that combination of CuNPs/RGO/Fe<sub>3</sub>O<sub>4</sub> was the best catalyst. The optimization showed that the best agitation rate 600 rpm and only  $1 \times 10^{-3} \text{ g/cm}^3$  of CuFe<sub>2</sub>O<sub>4</sub>@RGO catalyst is needed to obtain the highest yield of the products (Scheme 19). The kinetic study of the C-O bond formation was the second-order rate of reaction where the activation energy was observed to be 14.36 kcal/mol, and the catalyst could be reused up to five times without losing its catalytic activity (Figure 8) [57].

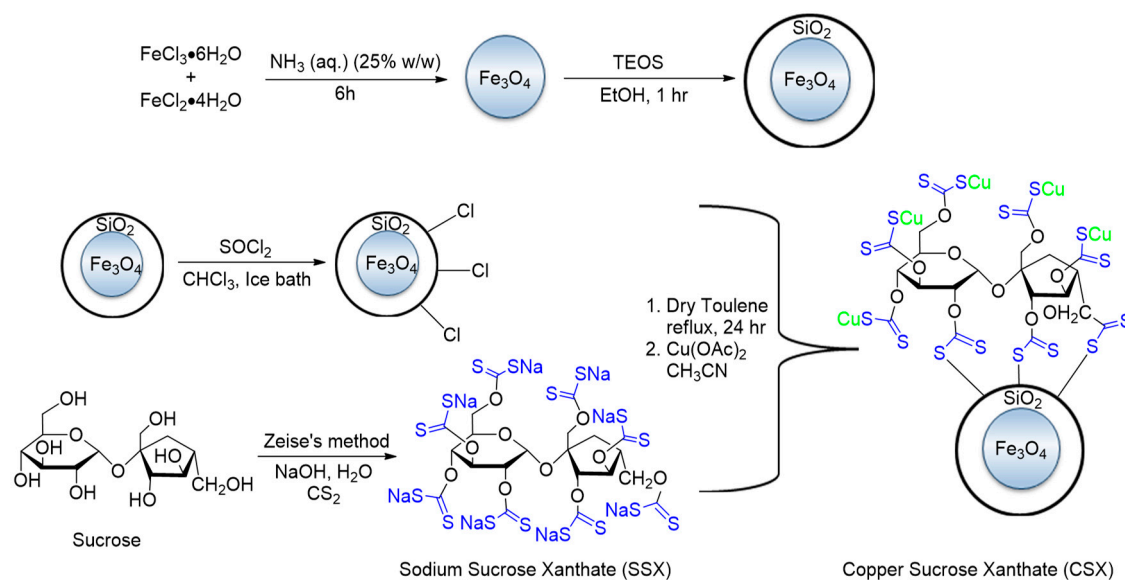


**Scheme 19.** Maghemite-Reduce GO Copper nanoparticles catalyzed synthesis of biphenyl ethers.



**Figure 8.** The reusability of the synthesized catalyst and the yield of ether product.

In a continuous study on the preparation of new recoverable magnetic nanoparticles, Iman Radfar et al. proposed a new magnetic nanoparticle functionalized sugar onto the silicon dioxide solid (Scheme 20). In that study,  $\text{Fe}_3\text{O}_4@\text{SiO}_2$ -copper(I) sucrose xanthate provided an excellent catalytic activity in the formation of ether bond, and it can be recycled up to five times without loss of its catalytic activity [58].



**Scheme 20.** Synthetic route of  $\text{Fe}_3\text{O}_4@\text{SiO}_2$ -copper sucrose xanthate.

In 2019, a few research groups also involved in utilization of ideal solid support in the synthesis of magnetically copper catalyst for O-arylation Ullmann cross-coupling reaction. These research groups are included Sepideh Bagheri (Tables 2 and 3, Entry 1) [59], Muhammad Aqeel Ashraf (Tables 2 and 3, Entry 2) [60], Dariush Khalili (Tables 2 and 3, Entry 3) [61], Mohammad Mehdi Khodaei (Tables 2 and 3, Entry 4) [62], Seyed Ali Mousavi Mashhadi (Tables 2 and 3, Entry 5) [63], and Razieh Zahedi (Tables 2 and 3, Entry 6) [64]. Different solid supports for the synthesis of magnetic copper nanocomposites and O-arylation reactions are depicted in Tables 2 and 3, respectively.

**Table 2.** The complete synthesis route of corresponding recoverable magnetic nanoparticles catalyst.

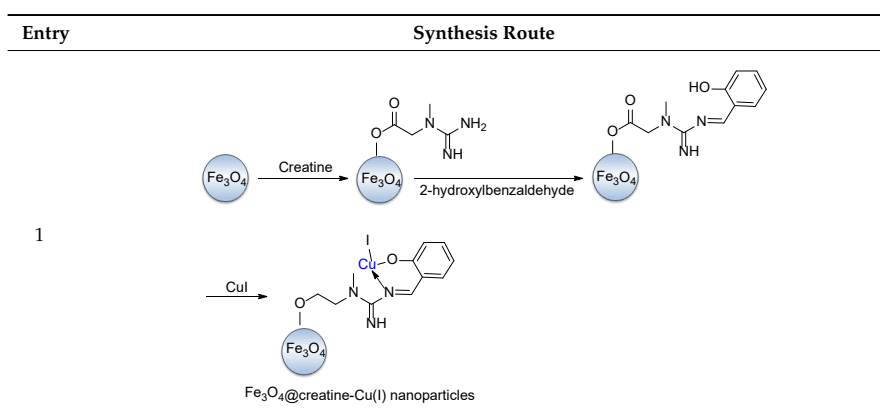


Table 2. Cont.

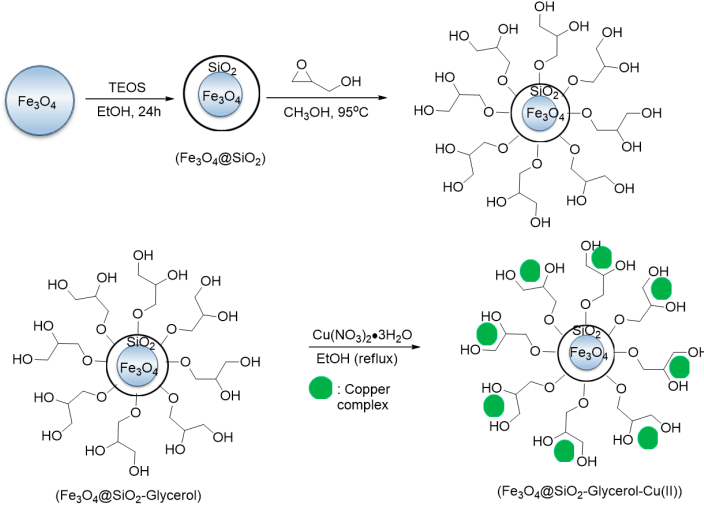
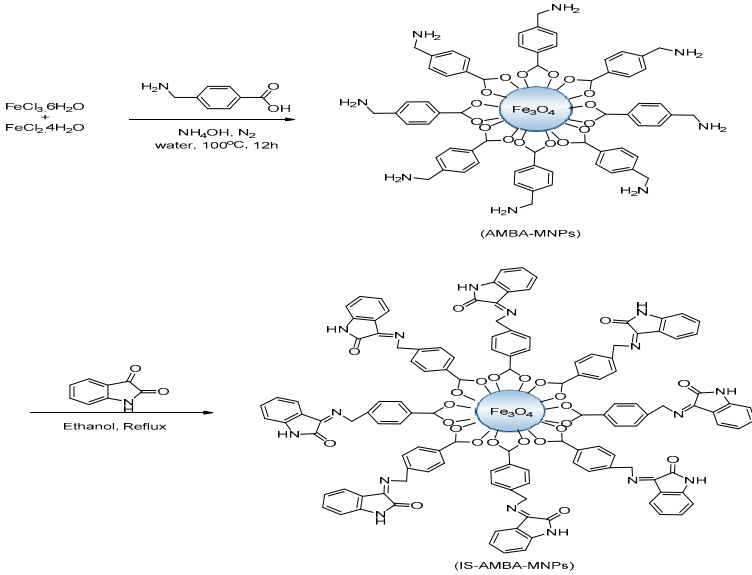
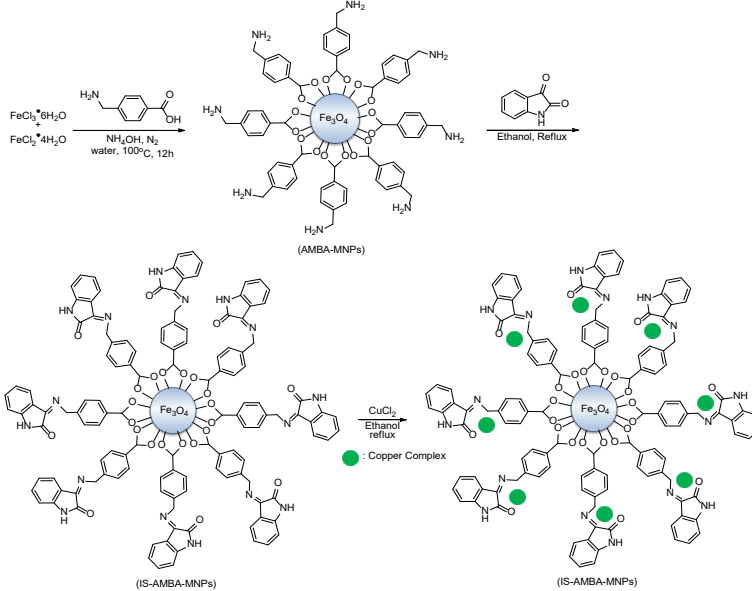
Entry	Synthesis Route
2	 <p>The synthesis route for <math>(\text{Fe}_3\text{O}_4@ \text{SiO}_2\text{-Glycerol-Cu(II)})</math> involves three steps:     <ol style="list-style-type: none"> <li><math>\text{Fe}_3\text{O}_4</math> reacts with TEOS in EtOH for 24h to form <math>(\text{Fe}_3\text{O}_4@ \text{SiO}_2)</math>.</li> <li><math>(\text{Fe}_3\text{O}_4@ \text{SiO}_2)</math> reacts with glycerol in <math>\text{CH}_3\text{OH}</math> at <math>95^\circ\text{C}</math> to form <math>(\text{Fe}_3\text{O}_4@ \text{SiO}_2\text{-Glycerol})</math>.</li> <li><math>(\text{Fe}_3\text{O}_4@ \text{SiO}_2\text{-Glycerol})</math> reacts with <math>\text{Cu}(\text{NO}_3)_2 \cdot 3\text{H}_2\text{O}</math> in EtOH at reflux to form <math>(\text{Fe}_3\text{O}_4@ \text{SiO}_2\text{-Glycerol-Cu(II)})</math>.</li> </ol>     A legend indicates that a green dot represents a Copper complex.   </p>
3	 <p>The synthesis route for <math>(\text{IS-AMBA-MNPs})</math> involves two steps:     <ol style="list-style-type: none"> <li><math>\text{FeCl}_3 \cdot 6\text{H}_2\text{O}</math> and <math>\text{FeCl}_2 \cdot 4\text{H}_2\text{O}</math> react with 4-aminobenzoic acid in the presence of <math>\text{NH}_2\text{OH}</math> and <math>\text{N}_2</math> in water at <math>100^\circ\text{C}</math> for 12h to form <math>(\text{AMBA-MNPs})</math>.</li> <li><math>(\text{AMBA-MNPs})</math> reacts with isatin in Ethanol at Reflux to form <math>(\text{IS-AMBA-MNPs})</math>.</li> </ol> </p>
4	 <p>The synthesis route for <math>(\text{IS-AMBA-MNPs})</math> with a copper complex involves three steps:     <ol style="list-style-type: none"> <li><math>\text{FeCl}_3 \cdot 6\text{H}_2\text{O}</math> and <math>\text{FeCl}_2 \cdot 4\text{H}_2\text{O}</math> react with 4-aminobenzoic acid in the presence of <math>\text{NH}_2\text{OH}</math> and <math>\text{N}_2</math> in water at <math>100^\circ\text{C}</math> for 12h to form <math>(\text{AMBA-MNPs})</math>.</li> <li><math>(\text{AMBA-MNPs})</math> reacts with isatin in Ethanol at Reflux to form <math>(\text{IS-AMBA-MNPs})</math>.</li> <li><math>(\text{IS-AMBA-MNPs})</math> reacts with <math>\text{CuCl}_2</math> in Ethanol at reflux to form <math>(\text{IS-AMBA-MNPs})</math> with a copper complex.</li> </ol>     A legend indicates that a green dot represents a Copper Complex.   </p>



Table 2. Cont.

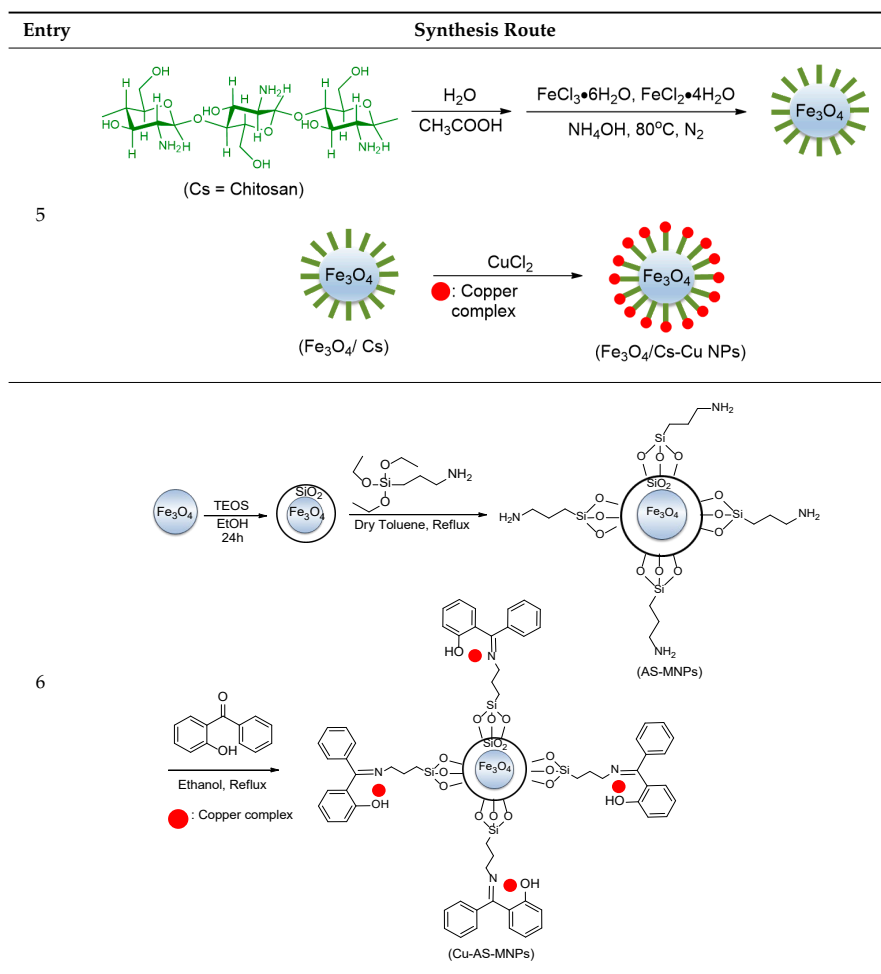


Table 3. The various type of Maghemite-supported Copper nanoparticles catalyzed synthesis of biphenyl ethers.

Entry	Type of Supported Catalyst	Substrates		Condition	Yield (%)	Reusability	Ref.
		Ar-X	Nucleophile				
1	Creatine	Aryl-Br	Phenol	Glycerin, 24 h, 80 °C, K <sub>2</sub> CO <sub>3</sub>	35–80	Up to 5 times	[59]
2	Glycerol	Aryl-I, Br, Cl	Phenol	H <sub>2</sub> O, 5 min–18 h, reflux, KOH	I-84–97 Br-62–91 Cl-38–86	Up to 5 times	[60]
3	Mesoporous graphitic carbon nitrile (mpg-C <sub>3</sub> N <sub>4</sub> )	Aryl- I, Br, Cl	Phenol	DMF, 5 h, 110 °C, K <sub>2</sub> CO <sub>3</sub>	I-75–90 Br-77–82 Cl-33–40	Up to 5 times	[61]
4	Isatin@4-(aminomethyl) benzoic acid- functionalized (IS-AMBA)	Aryl-I, Br	Phenol	DMF, 4 h, 110 °C, K <sub>2</sub> CO <sub>3</sub>	I-21–98 Br-30–63	Up to 5 times	[62]
5	Chitosan	Aryl-I	Phenol	DMSO, 15 h, 120 °C, K <sub>2</sub> CO <sub>3</sub>	55–95	Up to 5 times	[63]
6	Covalent anchoring of the ligand (AS)	Aryl-Br	Phenol	DMF, 24 h, reflux, Cs <sub>2</sub> CO <sub>3</sub>	45–98	Up to 4 times	[64]

### Carbon-Based Materials Supported

Carbon-based materials owe several specialities in the applied physical chemistry due to its comparative broadness in aqueous media, cost-effectiveness, and being chemically inert in most

of the electrolyte solutions [65,66]. There are various type of accessible microstructures of carbon materials, such as graphite, carbon fiber, nanotube, amorphous powders, and diamond [67]. With the persist breakthrough of nanotech in materials science, carbon nanomaterials, especially carbon nanotubes (CNT) and carbon nanofiber (CNF), have gained considerable focus in electroanalysis [68], electronic [69,70], optics [70], polymer composite [71], catalyst [72–74], and other related fields. In 2014, researcher Zhai Zhao Yang's team described the using graphene as solid support in synthesis the catalyst and applied in O-arylation Ullmann cross-coupling reaction. This carbon-supported catalyst can prevent the oxidation of nanosize copper oxide and increase the catalytic performance in coupling reaction [75,76]. The copper oxide supported graphene catalyst was synthesized through two-step liquid-phase procedure, using ethane-1,2-diol as the reducing agent (Figure 9). These methods can provide copper oxide nanoparticles with an average size of 8 nm dispersed homogeneously on the surface of the graphene sheet and show outstanding performance in the organic transformation. The  $\text{Cu}_2\text{O}$ /graphene catalyst shows a very high turnover frequency (TOF) of  $1282 \text{ h}^{-1}$  for the etherification of phenol and aryl iodide in the optimized condition (Scheme 21) [76].

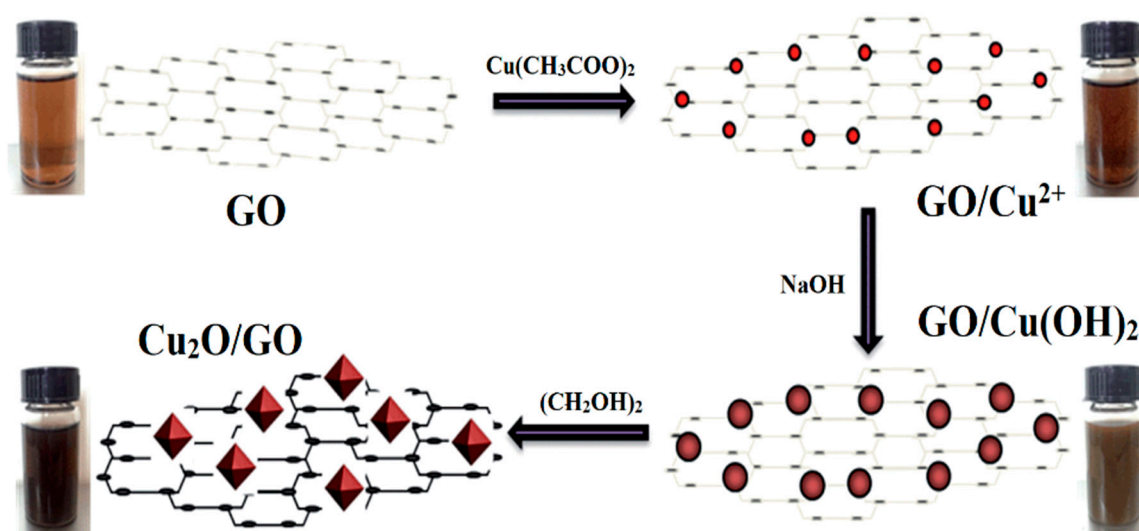
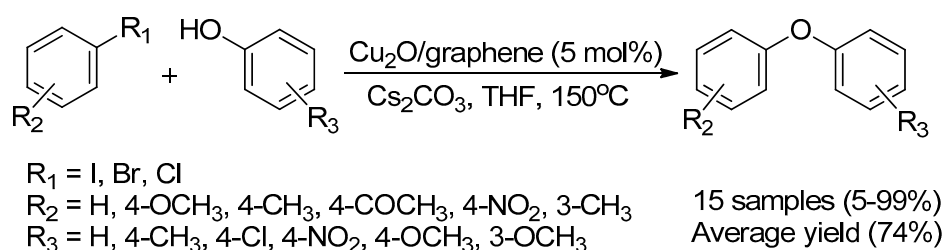


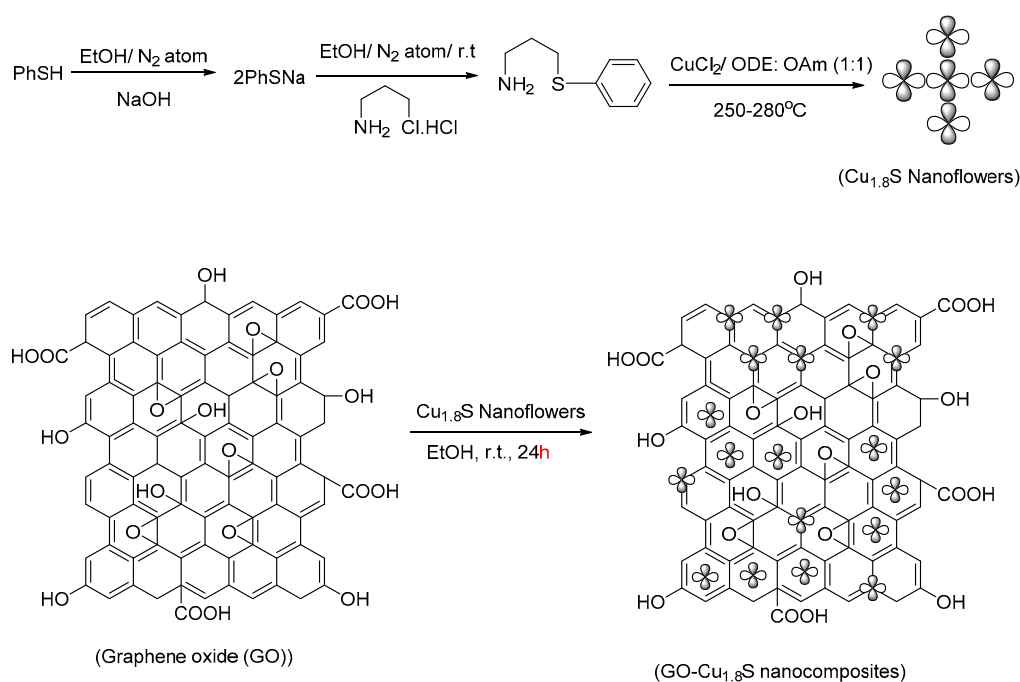
Figure 9. Preparation method of  $\text{Cu}_2\text{O}$ /graphene.



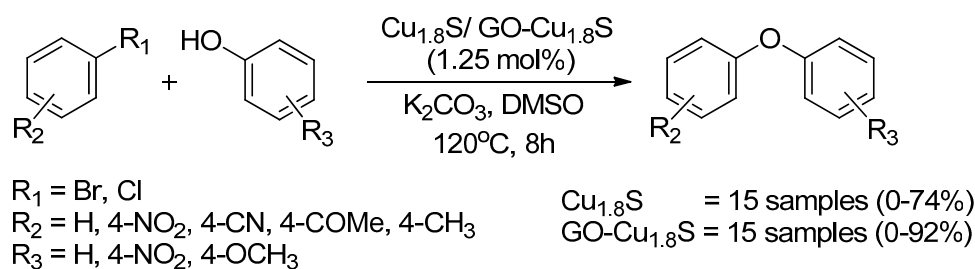
Scheme 21. Graphene Oxide (GO)-supported Copper nanoparticles catalyzed synthesis of biphenyl ethers.

In 2018, Ved Vati Singh and Ajai Kumar Singh first discovered the nanoparticles of phase,  $\text{Cu}_{1.8}\text{S}$  in a blossom-shape by the reaction of 3-(phenylthiol)propylamine in octadecene as the source of sulfur with copper chloride at  $250\text{--}280^\circ\text{C}$ . The nanoflowers of  $\text{Cu}_{1.8}\text{S}$  were anchored onto the graphene oxide (GO) at room temperature to give nanocomposite ( $\text{GO-Cu}_{1.8}\text{S}$ ) (Scheme 22) [77]. The synthesis method of nanoflowers  $\text{Cu}_{1.8}\text{S}$  and  $\text{GO-Cu}_{1.8}\text{S}$  composites are different than earlier report [78,79], which required expensive trioctylphosphine (TOP) that is highly toxic and has pyrophoric nature. Besides, the choosing of GO other than RGO is due to that fact that graphene oxide has a number of functional groups that are important to bind  $\text{Cu}_{1.8}\text{S}$  nanoparticles strongly onto the solid surface. These characteristics minimize

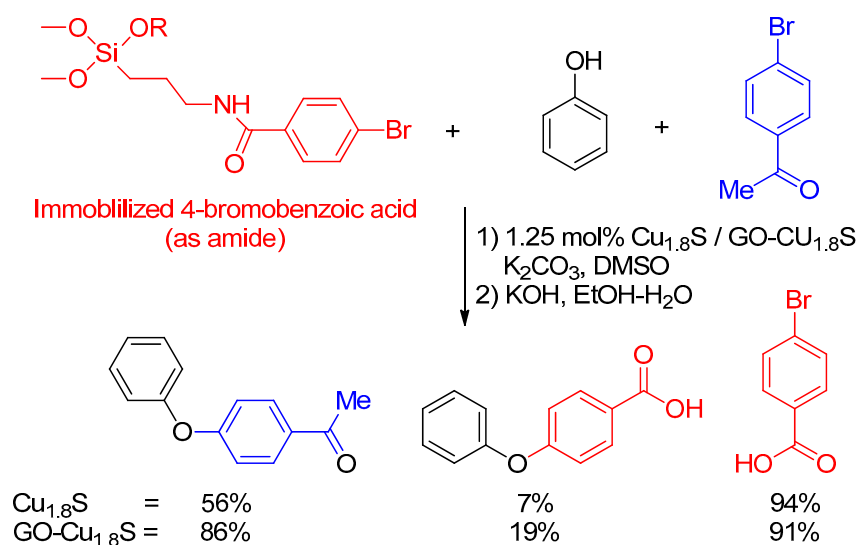
the metal leaching problem during the reaction. The average size of nanoflowers of  $\text{Cu}_{1.8}\text{S}$  was  $\sim 14\text{--}21\text{ nm}$  (high surface area). The  $\text{Cu}_{1.8}\text{S}$  nanoflower and  $\text{GO-Cu}_{1.8}\text{S}$  nanocomposite were explored as a catalyst for Ullmann etherification reaction for several substituted aryl halides with phenols. Based on the studies, the  $\text{GO-Cu}_{1.8}\text{S}$  nanocomposite significantly enhanced the catalytic performance ( $>30\%$ ) than the  $\text{Cu}_{1.8}\text{S}$  nanoflowers. The ether bond formation efficiency follows the order  $\text{ArBr} > \text{ArCl}$  (Scheme 23). Both anchored and unanchored nanoflowers copper particles were found recyclable three times without decreasing its catalytic performance. The heterogeneous nature and chemo selectivity of synthesized catalyst was determined by using a three-phase test (Scheme 24). For a total heterogeneous process, the immobilized  $\text{ArX}$  is not expected to undergo conversion to the coupled product. 4-bromobenzoic acid was anchored on silica (Scheme 24). In the presence of 4-bromoacetophenone, it reacted with phenol under optimum reaction conditions. The yield of the 4-phenoxyphenylacetophenone was 56% and 86% for  $\text{Cu}_{1.8}\text{S}$  nanoflowers and  $\text{GO-Cu}_{1.8}\text{S}$  nanocomposites, respectively. The coupling of immobilized aryl benzoic acid afforded 4-phenoxybenzoic acid in 7% and 19% yield for  $\text{Cu}_{1.8}\text{S}$  and  $\text{GO-Cu}_{1.8}\text{S}$  nanoflowers, respectively. If there was any leaching of Cu from the catalyst, immobilized aryl benzoic acid would have given better yield. This explanation was proved by several reports [80,81], which show good yield of coupled product from heterogeneous halide due to the leaching of metal. The substrate 4-bromoacetophenone present in the solution was converted to 4-phenoxyacetophenone in good yield. Thus, both nanoflowers and composite behave predominantly as a heterogeneous catalyst [77].



**Scheme 22.** Synthesis scheme of  $\text{Cu}_{1.8}\text{S}$  nanoflowers and  $\text{GO-Cu}_{1.8}\text{S}$  nanocomposite.

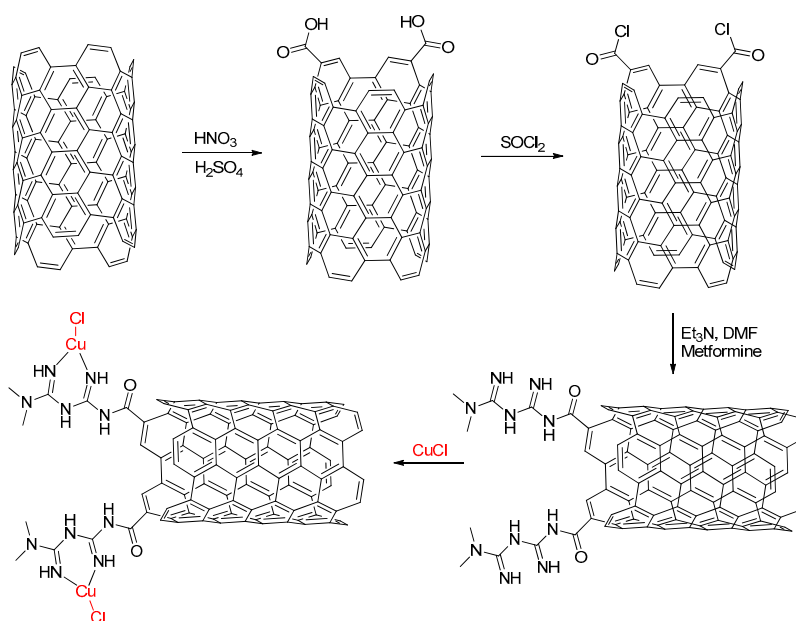


**Scheme 23.**  $\text{GO-Cu}_{1.8}\text{S}$  nanoparticles catalyzed synthesis of biphenyl ethers.

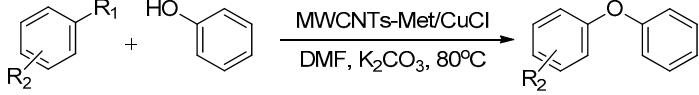


**Scheme 24.** Three-phase tests for nanoflowers of  $\text{Cu}_{1.8}\text{S}$  and  $\text{GO-Cu}_{1.8}\text{S}$  nanocomposite.

Carbon nanotubes (CNTs) regularly hold the promise of molecular ‘properties-by-design’ toward countless daily life applications from electronics to energy to biomedicine [82]. CNTs can be in single-wall (SW) and multiwall-CNTs (MWCNTs). Both nanotubes are useful owing to substantial mechanical, electrical properties, and thermal conductivity. Besides, the turnable surface area, as well as perfect mechanical and chemical stability, makes them a potentially and ideal useful selection for the various field [83]. The reactivity of nanotubes was associated with its diameter and morphology, disclosing the SW-CNTs as the most reactive representative [84]. In 2018, Marym Akhavan et al. described a synthesized MWCNTs-Met/ $\text{CuCl}$  nanocatalyst for Ullmann coupling reaction. The synthesis of MWCNTs-Met/ $\text{CuCl}$  nanocatalyst is through grafting of metformin covalent on the surface of carbon nanotubes and anchored copper nanoparticles onto the MWCNTs-Met (Scheme 25). The MWCNTs-Met/ $\text{CuCl}$  nanocatalyst exhibit higher conversion yield, high stability, and high reusability compared to other reported catalyst (Table 4) [85].

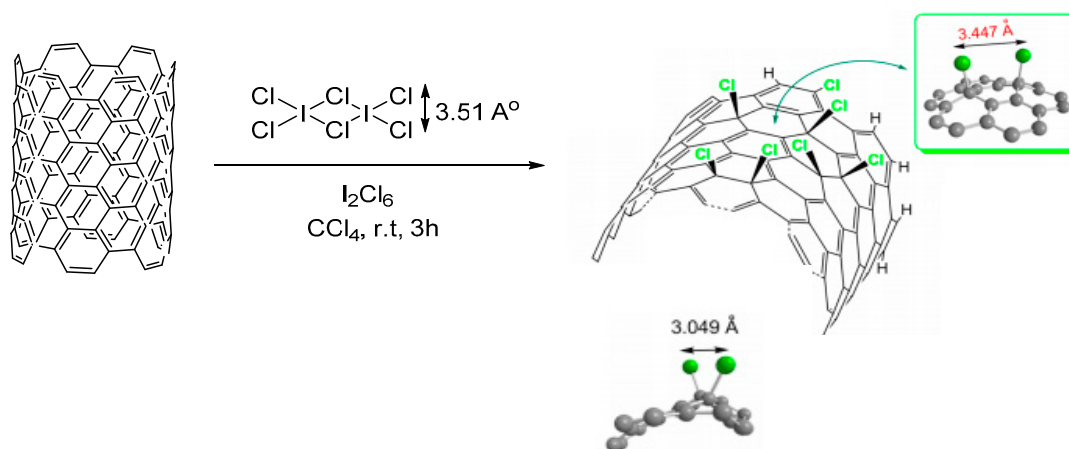


**Scheme 25.** The route of synthesis of multiwall-carbon nanotubes (MWCNTs)-Met/ $\text{CuCl}$  nanocomposite.

**Table 4.** The MWCNTs-Met/CuCl catalyzed synthesis of biphenyl ethers.


Type of Supported Catalyst	Substrates		Yield (%)	Reusability
	Ar-R <sub>1</sub> , R <sub>2</sub>	Nucleophile		
MWCNTs-Met/CuCl	R <sub>1</sub> = I, Br, Cl R <sub>2</sub> = H, 4-CN, 4-CH <sub>3</sub> , 4-OCH <sub>3</sub> , 2-OCH <sub>3</sub>	Phenol	55–96	Up to 8 times

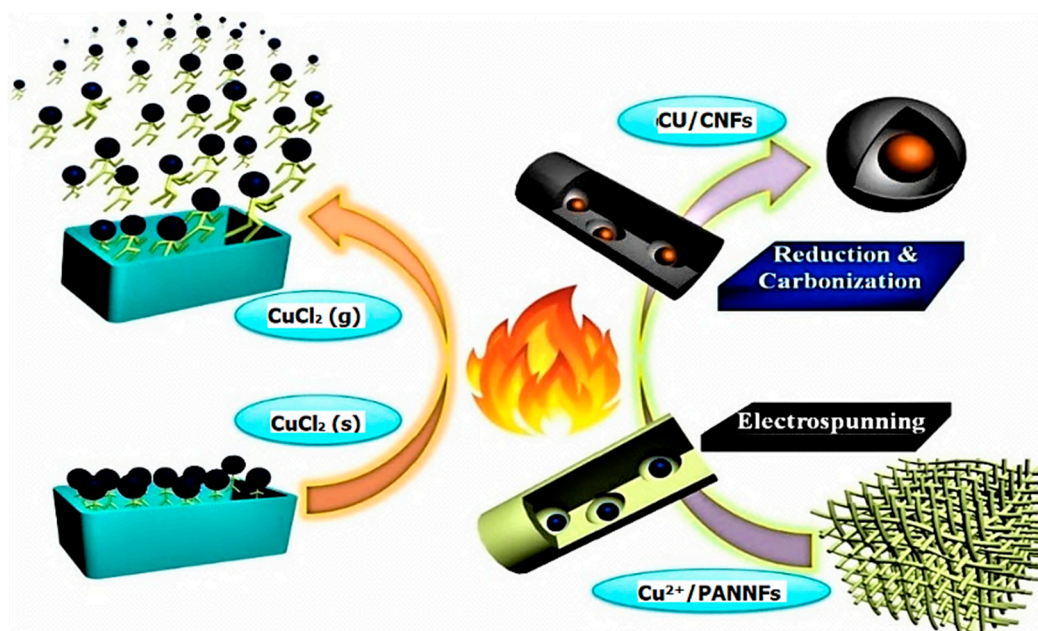
In 2019, Kolanowska reported the synthesis method of MWCNTs with iodine monochloride. Kolanowska's team modified the current method (ultrasonication step) to magnetically stirred method to maintain the integrity of the MWCNTs carpet. They applied 'wet chemistry' method during chlorination of carbon nanotubes. This method can hypothetically enable preferential bis-1,4-addition over bis-1,2-addition from ICl<sub>3</sub> existing in solution as a dimer (I<sub>2</sub>Cl<sub>6</sub>) (Scheme 26). The characteristic of in-house synthesis nanotube and purchasing nanotube is shown in Table 5. The synthesized MWCNTs-Cl with copper was applied in Ullmann O-arylation to determine its catalytic activity. Nevertheless, the chlorinated-CNTs needed new extensive studies due to the fact that CNT-Cl was inactive to promote the reaction when aryl-Cl as the substrate. Therefore, the aryl substrate must be replaced by aryl-Br/aryl-I with presence of the electron-withdrawing group (e.g., carboxylic, nitro groups) [86].

**Scheme 26.** General scheme of the favorite sites of chlorination of carbon nanotubes (CNTs) by their treatment with ICl<sub>3</sub>.**Table 5.** Characteristics of different type of CNTs.

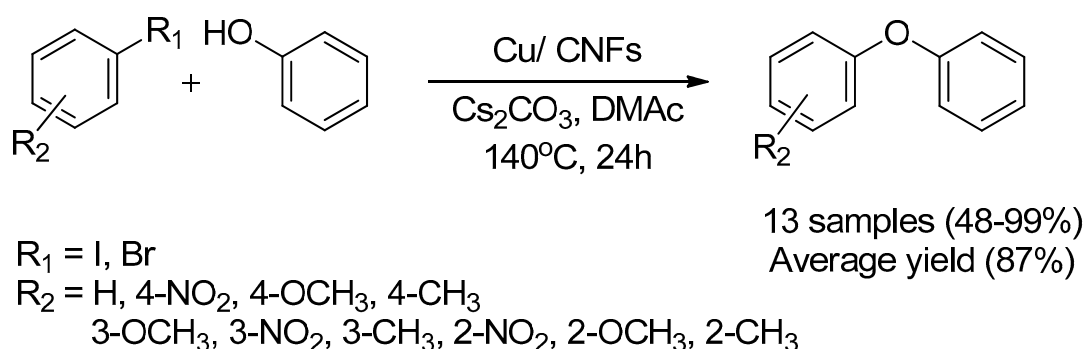
Characteristics	Nanocyl™ NC7000	In-House MWCNTs	TUBALL™ SWCNTs
Average outer diameter, nm	9.5	60–70	1.6
Average length, μm	1.5	200	>5
Aspect ratio	150	3000	3000
Carbon purity, wt. %	90	98	85
Fe-base catalyst residue, wt. %	<1	5.4	<1.5

In 2018, Mu Hong Chun et al. utilized carbon nanofiber to synthesis of Cu/CNFs catalysis. The composite catalyst (Cu/CNFs) was prepared using a homogeneous polymeric solution through electrospinning and high-temperature in-situ carbonization process (Scheme 27). Hong Chun chosen carbon nanofiber due to its one-dimensional structure comparing with carbon nanotube, carbon films,

and carbon sphere [87]. With this characteristics, nanofiber has perfect reducibility, high specific strength, specific modulus, low density, light and excellent thermal stability, making it easy to be reused [88,89]. In this study, the Cu(0) was impregnated through in-situ carbothermic reduction during the carbonization process for the first time. The Cu/CNFs showed extraordinary performance in the Ullmann etherification and can be reused up to five times without loss of activity (Scheme 28) [87].



Scheme 27. Schematic diagram for the synthesis of Cu/carbon nanofibers (CNFs) composite catalysts.

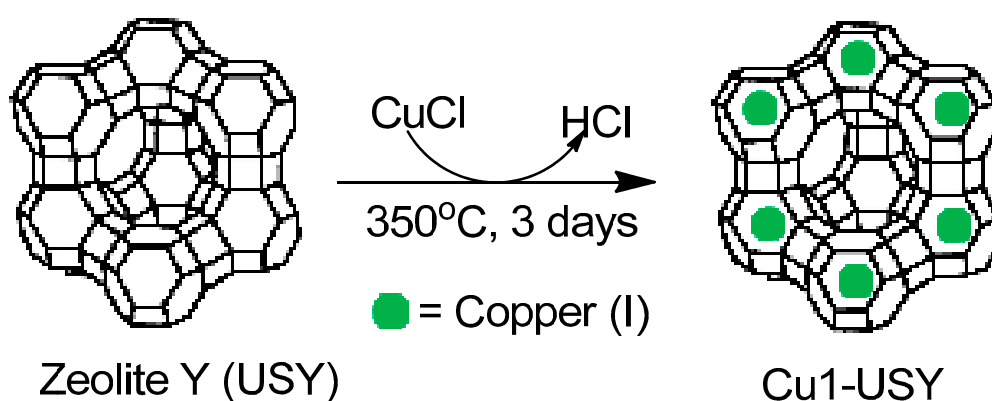


Scheme 28. Cu/CNFs nanocomposite catalyzed synthesis of biphenyl ethers.

### Zeolite Supported

Zeolite is classified as an open-structure aluminosilicate material consisting of neatly scattered micropores in a molecular arrangement. The structure of zeolites could be present into rings of various sizes, which comprise the pore opening windows of zeolites [90]. The negative charges of zeolite frameworks are usually compensated by extra-framework mono or divalent cations. These specific characters allow zeolite exchanged by other cations [91]. In addition, the spatial confinement of zeolite pores joined with catalytically active sites in their structure endows zeolites with extraordinary shape-selective catalysis toward the formation of certain products. Eventually, zeolites can serve as host matrices to encapsulate and stabilize metal clusters or nanoparticles, forming multipurpose composite materials with superior properties. Zeolites have been widely utilized as high-performance catalysts, detergents, adsorbents, and ion-exchangers in various chemical processes due to their specific

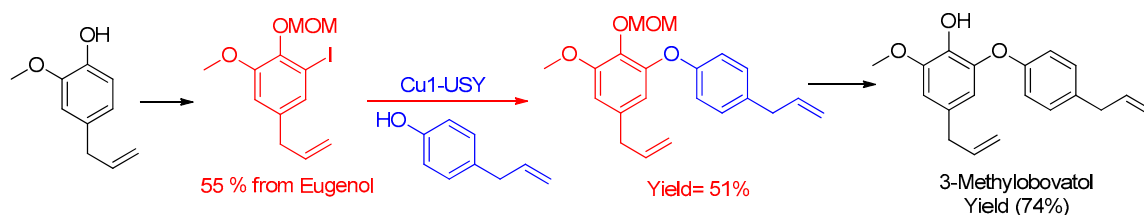
characteristics, as well as their high hydrothermal stability and low production costs [92]. In 2015, researcher Valentin Magnee's team described the utilization of zeolite as a catalyst in the Ullmann coupling reaction. They used a number of zeolite (ultrastable Y (USY), mordenite (MOR), beta ( $\beta$ ), and zeolite socony mobil-5 (ZSM-5)) as a solid support in the synthesis of a heterogeneous copper catalyst. Among these four zeolites, USY is the best heterogeneous catalyst in term of doping of copper species (Scheme 29). The USY-supported copper catalyst showed excellent catalytic activity under a ligand-free condition in toluene at 120 °C (Table 6) [93]. In 2018, Tony Garnier also used USY type zeolite for versatile, efficient, and recyclable Copper(I) catalyst for Ullmann etherification reactions (Table 6). In this study, the electron-poor 4-cyano- and 4-nitrophenol show relatively low yield of product in the Ullmann reaction, even when conducting the experiment in higher temperature, which resulted in only 0–5% yield of product [93]. They utilized this catalyst for the total synthesis of 3-methylobovatoI (Scheme 30) [94]. 3-methylobovatoI is a naturally occurring biphenyl ether that has biphenolic anti-inflammatory, anxiolytic, and nootropic properties [95].



**Scheme 29.** Schematic diagram for the synthesis of Cu<sup>I</sup>-USY composite catalysts via solid/solid exchange procedure.

**Table 6.** Cu<sup>I</sup>-USY composite catalyzed synthesis of biphenyl ethers.

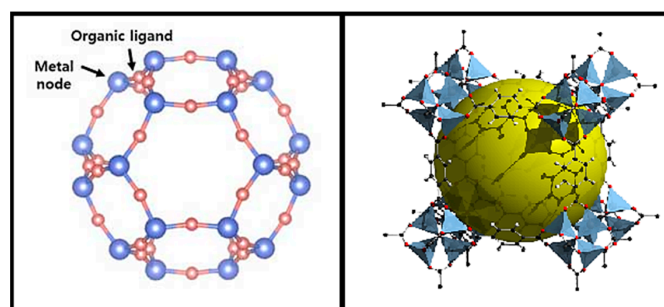
Type of Supported Catalyst	Substrates		Yield (%)	Reusability	Ref.
	Ar-R <sub>1</sub> , R <sub>2</sub>	Nucleophile			
Cu <sup>I</sup> -USY composite catalysts	R <sub>1</sub> = I, Br R <sub>2</sub> = H, 4-OEt, 4-NEt, 4-CN, 4-NO <sub>2</sub> , 2-CH <sub>3</sub> , 2,6-CH <sub>3</sub>	R <sub>3</sub> = H, 3,5-CH <sub>3</sub> , 4-CN, 4-NO <sub>2</sub> , 4-CH <sub>3</sub>	0–85%	Up to 5 times	[93]
	R <sub>1</sub> = I, Br R <sub>2</sub> = H, 4-OEt, 4-NEt, 4-CN, 4-NO <sub>2</sub> , 2-CH <sub>3</sub> , 2,6-CH <sub>3</sub> , etc.	R <sub>3</sub> = H, 3,5-CH <sub>3</sub> , 4-CN, 4-NO <sub>2</sub> , 4-CH <sub>3</sub> , etc.	4–85%		[94]



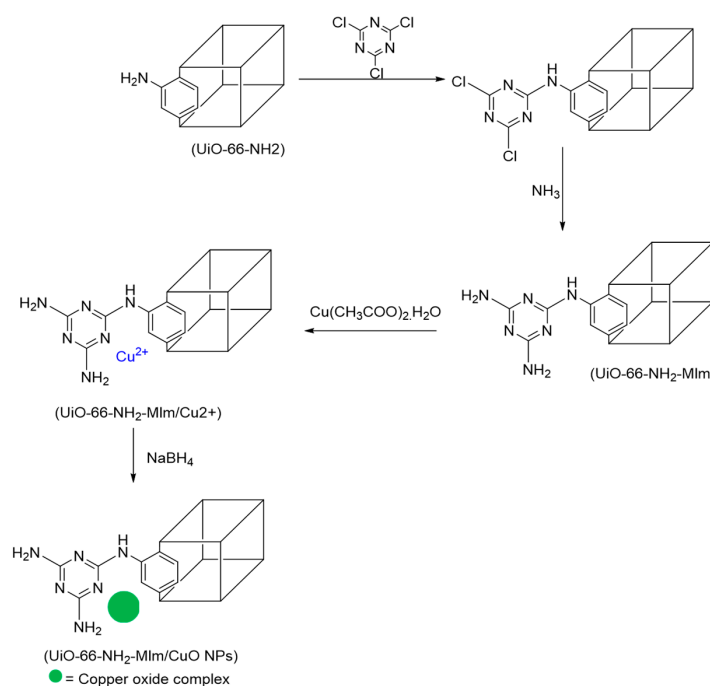
**Scheme 30.** Total synthesis of 3-methylobovatoI via the zeolite-based organic synthesis (ZeoBOS) strategy in the presence of copper (I)-USY.

## Metal-Organic Framework (MOF) Supported

Metal-organic frameworks (MOFs) are hybridized crystalline porous materials of organic and inorganic components that consist of an ordinary order of positively charged metal ions surrounded by organic 'linker' molecules (Figure 10) [96]. The metal ions from nodes that bind the arms of the organic linkers together to form a repeating one-, two-, or three-dimensional extended coordination networks, cage-like structure [97,98]. The chemical mutability, turnable pore structures are large, readily accessible internal surface areas of metal-organic frameworks facilitate possible applications in heterogeneous catalysis [98,99]. The MOF-supported catalytic function depends on the active metal sites, the organic ligands covalently linked to the MOFs during the synthesis process, or a dopant introduced via a post-synthetic modification [98]. In 2017, Samira Sadeghi et.al. introduced UiO-66-NH<sub>2</sub> MOFs as the initial modification with melamine via a post-synthesis approach. The copper oxide was doped on the surface of MOF by available amine group and  $\pi$ -electron interaction of melamine and ligand; UiO-66-NH<sub>2</sub>-Mlm/CuO NPs composite (Scheme 31). The UiO-66-NH<sub>2</sub>-Mlm/CuO NPs was well characterized by SEM and it was utilized as a heterogeneous catalyst in the Ullmann etherification reaction. The UiO-66-NH<sub>2</sub>-Mlm/CuO NPs efficiently (5 mol%) promoted C-O bond formation reaction (Scheme 32), and only 1.2 wt% of copper was leached out after several runs of the experiment [100].

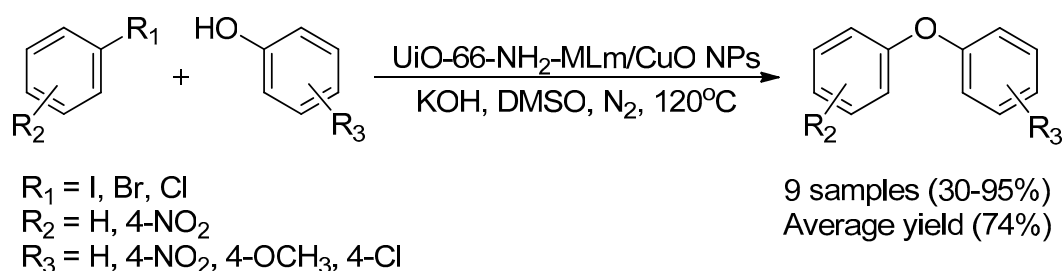


**Figure 10.** Schematic diagram of a metal-organic framework (MOF). The MOF, consisting of metal ions and organic ligands, is a highly porous material with an ultra-high surface area.



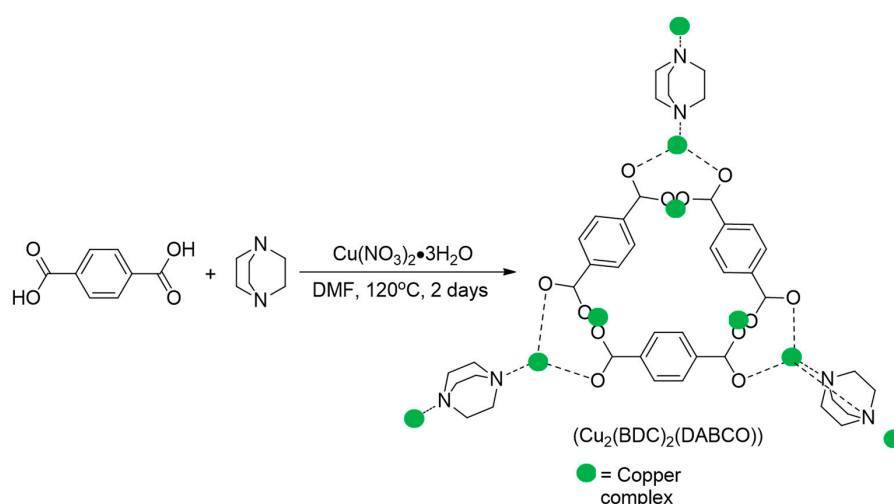
**Scheme 31.** Scheme reaction for the synthesis UiO-66-NH<sub>2</sub>-Mlm/CuO NPs.



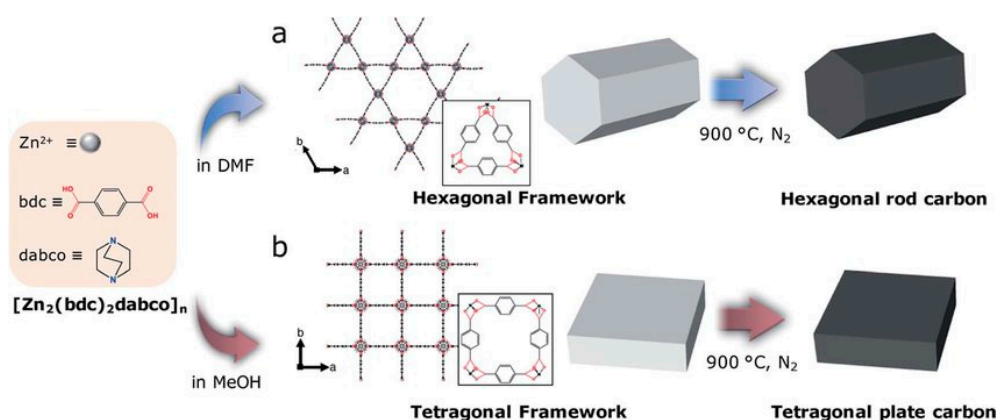


**Scheme 32.** UiO-66-NH<sub>2</sub>-Mlm/CuO nanoparticle catalyzed synthesis of biphenyl ethers.

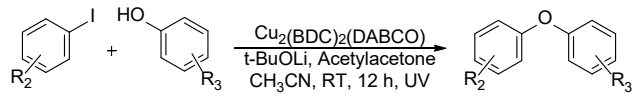
Later on, Hiep Q. Ha's team synthesized MOF-supported copper catalyst Cu<sub>2</sub>(BDC)<sub>2</sub>(DABCO) using benzene-1,4-dicarboxylate (BDC) and 1,4-diazabicyclo (2.2.2) (DABCO) in dimethylformamide (Scheme 33) [101]. The solvent-mediated method strongly affected the morphology of nano-MOF. Hwang Jong Kook observed that dimethylformamide (DMF) preferably forms a hexagonal rod MOF (ZBDh) and methanol preferably forms a tetragonal plate MOF (ZBDt) (Figure 11) [102]. This Cu-MOF utilized as a heterogeneous photocatalyst for the arylation of phenol in the presence of *t*-BuOLi as a base and acetylacetone as a ligand under 365 nm light at rt (Table 7) [101].



**Scheme 33.** Synthetic route of Cu<sub>2</sub>(BDC)<sub>2</sub>(DABCO).



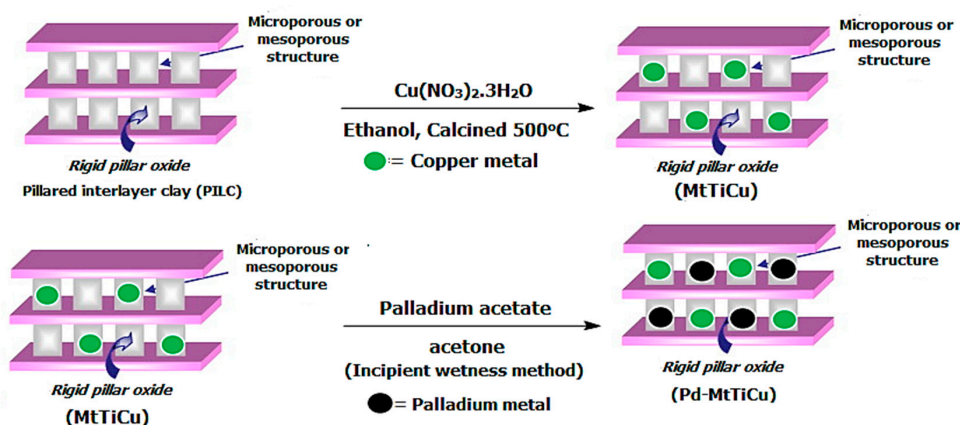
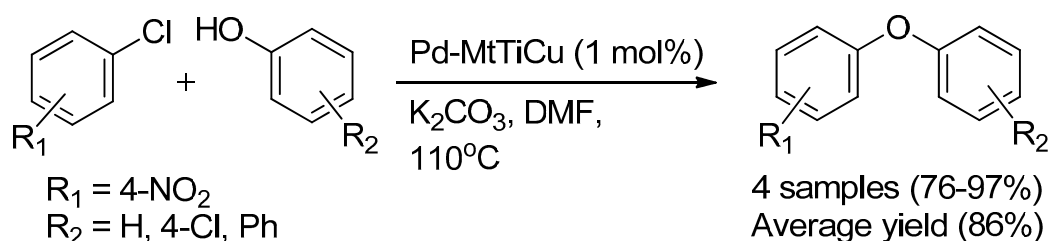
**Figure 11.** Solvent mediated synthesis of (Zn<sub>2</sub>(BDC)<sub>2</sub>(DABCO))<sub>n</sub> (ZBD) with controlled size, morphology, and polymorphism. (a) ZBD with a hexagonal framework (ZBDh), (b) ZBD with a tetragonal framework (ZBDt), and their transformation into nanoporous carbon. Reproduced by permission of Royal Society of Chemistry.

**Table 7.** MOF-based  $\text{Cu}_2(\text{BDC})_2(\text{DABCO})$  catalyzed synthesis of diphenyl ethers.


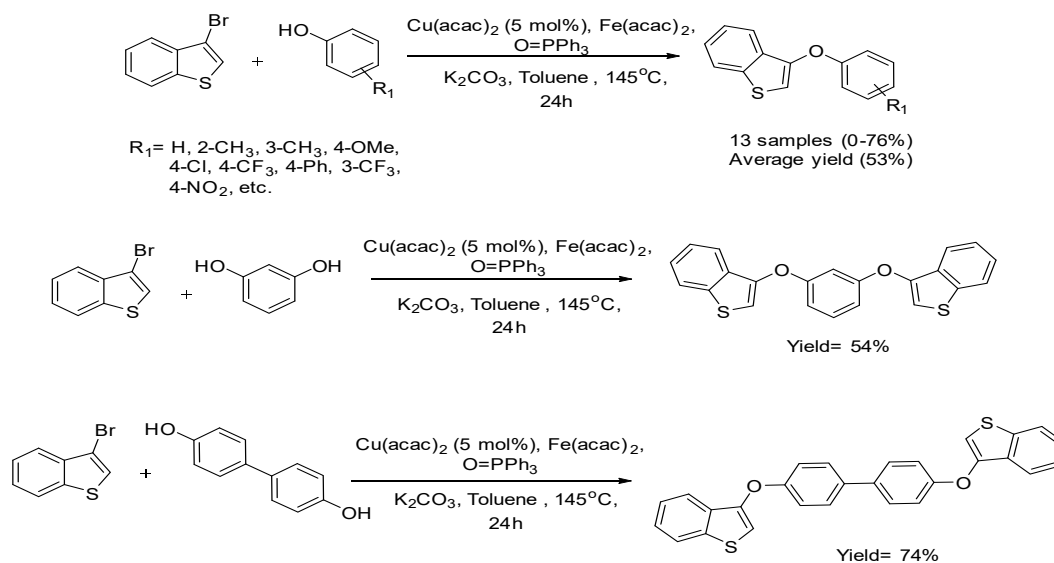
Type of Supported Catalyst	Substrates		Yield (%)	Reusability
	Ar-R <sub>2</sub>	Nucleophile		
$\text{Cu}_2(\text{BDC})_2(\text{DABCO})$	R <sub>2</sub> = H, 4-Me, 4-OCH <sub>3</sub> , 4-COCH <sub>3</sub> , 4-CN, 4-I, 2-Me, 3-F	R <sub>3</sub> = H, 4-Br, 3-NO <sub>2</sub> , 4-COOMe, 2-OMe, 3-OH	42–81	Up to 7 times

### 2.1.6. Cooperative Catalyst (Co-Catalyst)

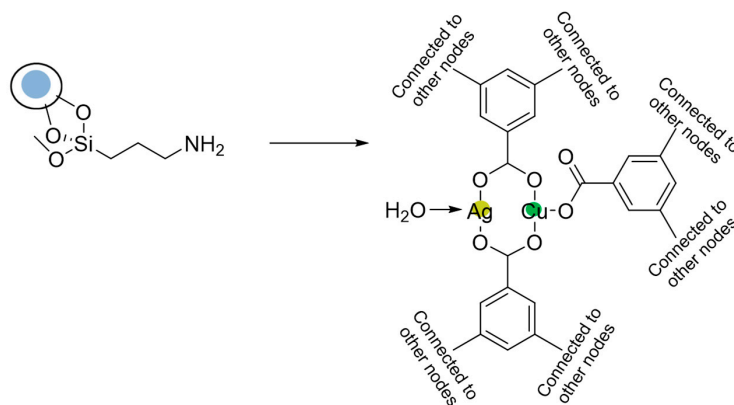
The word cooperative catalysis is applied when “two types of catalysts, as well as two catalytic cycles, are performed to construct a single new bond”. Alternatively stated, a single organic transformation is succeeded by stimulating both the nucleophile and electrophile by two different and distinct catalysts [103]. Besides the term co-catalyst, other authors also use a different word to express the same principle (1) Synergistic catalyst [103], (2) Cooperative dual catalysis [104], and (3) Contemporaneous catalyst [105]. The power and the benefit of explicitly applied cooperative catalyst can (i) create new, earlier inaccessibility chemical transformations, (ii) enhance the efficiency of previous organic transformation, and (iii) establish with improving catalytic enantioselectivity where stereocontrol was early omitted or challenging. In 2017, Kannan Vellayan et al. described the preparation of Cu-doped Ti-pillared montmorillonite as catalyst and utilized it in the O-, N- and S-arylation reactions. The co-catalysis was prepared through interpenetration of the copper doped clay supports with a Pd-precursor by the incipient wetness method (Scheme 34). The co-palladium with copper supported clay catalyst was found to be effective and gave good to extraordinary yield in the etherification reactions, and it can be reused up to three times without loss of its catalytic activity (Scheme 35) [106].

**Scheme 34.** Synthetic route for the preparation of Pd-MtTiCu.**Scheme 35.** Co-catalyst Pd-MtTiCu catalyzed of O-aryl compound.

In 2018, Koichi Mitsudo and Leila Ramezani also introduced a co-catalyst for Ullmann O-arylation cross-coupling reaction. Koichi's group utilized copper and iron nanoparticles in the presence of triphenylphosphine oxide (PPh<sub>3</sub>) for synthesis of aryl 3-benzo[b]thienyl ethers (Scheme 36) [107], whereas Leila's group proposed copper and gold nanoparticles onto BTC-MOF (Scheme 37). The co-catalyst of gold with copper exhibited is unexpected high catalytic activity for aryl-Cl in coupling of chloroarenes with phenols without presence of ligands (Scheme 38). The AgCuBTC-MOF shown high TON value (>15,000), which is better than using only Pd as a catalyst [108]. Table 8 was depicted the comparison of a single catalyst and with a combined catalyst in the Ullmann O-arylation reaction.



**Scheme 36.** Synthesis of aryl 1,3-benzo[b]thienyl ethers.



**Scheme 37.** The proposed defects formed in the structure of maghemite anchored AgCuBTC.



**Scheme 38.** The synthesis of various type biphenyl ethers in the presence of maghemite anchored AgCuBTC.

**Table 8.** The comparison of a single catalyst and with a combined catalyst in the Ullmann O-arylation reaction.

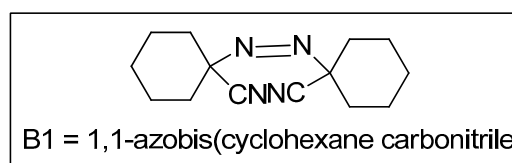
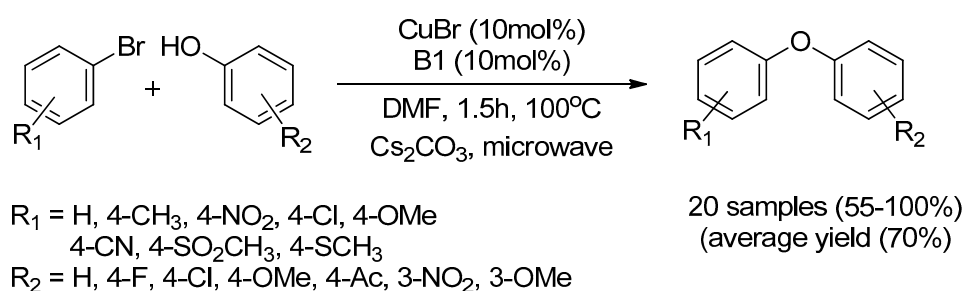
Entry	Catalytic System	Centre	Catalyst Loading	Yield (%)	Ref.
1	Fe <sub>3</sub> O <sub>4</sub> @SiO <sub>2</sub> @PPh <sub>2</sub> @Pd	Pd/Fe	1.6 × 10 <sup>-3</sup> mol%	83	[109]
2	AT-Nano CP-Pd	Pd	6 × 10 <sup>-5</sup> mol%	80	[110]
3					
4	Pd(dba) <sub>2</sub>	Pd	1 mol%	90	[111]
5	GO-Pd <sub>17</sub> Se <sub>15</sub>	Pd	1 mol%	73	[112]
6	Fe <sub>3</sub> O <sub>4</sub> @mesoporous PANI	Fe	4.69 mol%	56	[113]
7	CuI/Oxalamide	Cu	1.5 mol%	90	[114]
8	CuBr	Cu	10 mol%	81	[115]
9	CuI nanoparticles	Cu	1.25 mol%	47	[116]
10	CuI/Raney Ni-Al alloy	Cu/Ni	10 mol%	32	[117]
11	Cu <sub>2</sub> O/graphene	Cu	5 mol%	5	[76]
12	Nano CuO	Cu	5 mol%	17	[42]
13	CuO NPs into UiO-66-NH <sub>2</sub>	Cu	5 × 10 <sup>-3</sup> mol%	30	[43]
14	AgOAc	Ag	0.5–2 mol%	81	[118]
15	Maghemite anchored AgCuBTC	Ag/Cu	0.03 mol%	88	[108]
16	Cu/Fe/O = PPh <sub>3</sub>	Cu/Fe	5 mol%	84	[107]

## 2.2. Homogeneous Catalyst

A homogeneous catalyst is referred to as a catalytic reaction where the catalyst has the same phase with the reactant. In short, it is a soluble catalyst in a solution [119]. Homogeneous catalyst generally provides short reaction time and needs a few amounts of catalyst in the catalytic system owing to it can contact with reactant adequately compare to the heterogeneous catalyst [120].

### CuI Nanoparticle with the Present of Ligand Precursor (B)

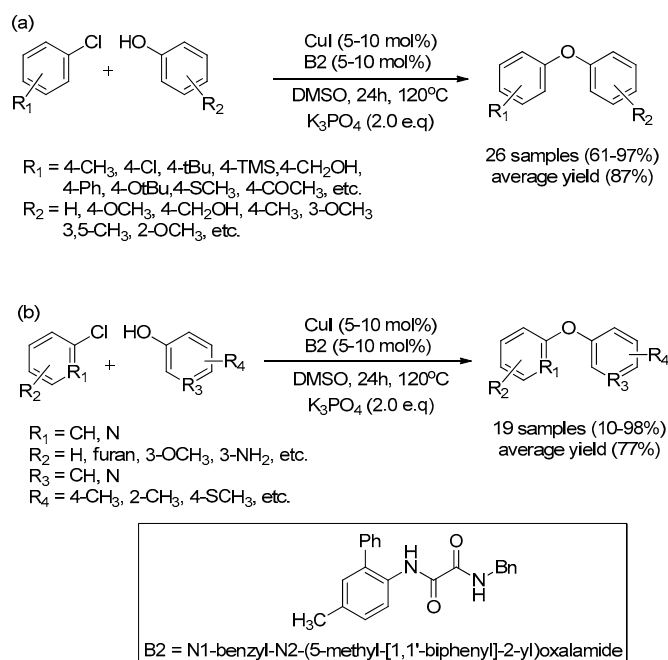
In 2015, Lorena Navarro reported a new ligand; 1,1-azobis(cyclohexane carbonitrile) (ACHN), to stabilize the Cu(I) salt. A new, useful, and eco-friendly ligand achieved an excellent protocol for the O-arylation using CuBr as a catalyst under microwave irradiation. This single process provides a clean, faster, and simple method in the Ullmann cross-coupling reaction. His method offers a competitive advantage, such as low catalyst and ligand loaded, low temperature, suitable for electron-withdrawing substituent of aryl halides, and electron-donating substituted phenols (51–100% yield) (Scheme 39) [121].



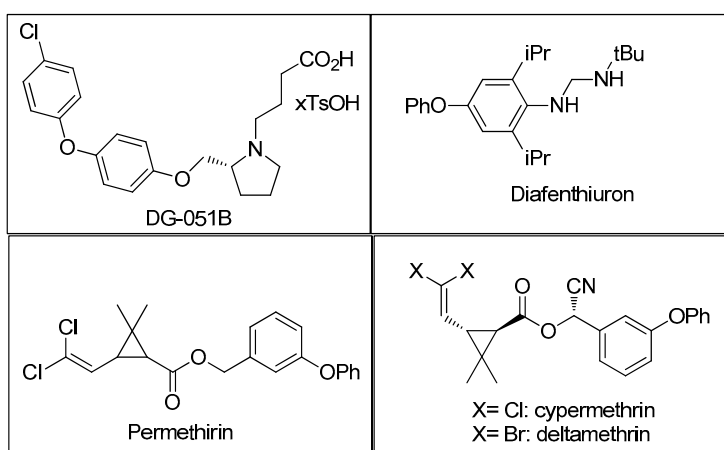
**Scheme 39.** CuBr-NPs catalyzed O-arylation in the presence of 1,1-azobis(cyclohexane carbonitrile) ligand (B1).

One year later, Fan Mei Yan's team focused on utilization of the low activity aryl chloride and (hetero)aryl chloride to the Ullmann O-arylation in the presence of CuI and *N*-aryl-*N'*-alkyl-substituted oxalamide ligand (B2). Fan Mei Yan found only 44% of aryl ether when bis(*N*-aryl)-substituted oxalamides was used. The *N*-aryl-*N'*-alkyl-substituted oxalamides showed excellent ligands for CuI catalyzed Ullmann O-arylation of low activity aryl chloride and (hetero)aryl chlorides.

Interestingly, the ligand 4-methyl-2-phenylaniline-derived oxalamide is tolerated in a broad range of functional groups, including amines, alcohols, amides, halides, esters, ketones, and nitriles, as well as several heterocycles (Scheme 40). An exciting part of this research is the combination of *N*-aryl-*N*-alkyl-substituted oxalamides ligand and CuI could be utilized in the synthesis of useful products, such as insecticide diafenthiuron, DG-051B for the treatment medicine of stroke and myocardial infarction, and so on (Scheme 41) [114].



**Scheme 40.** (a) CuI-NPs with *N*-aryl-*N*-alkyl-substituted oxalamides ligand (B2) for O-arylation reaction; (b) heterocyclic biaryl ether.

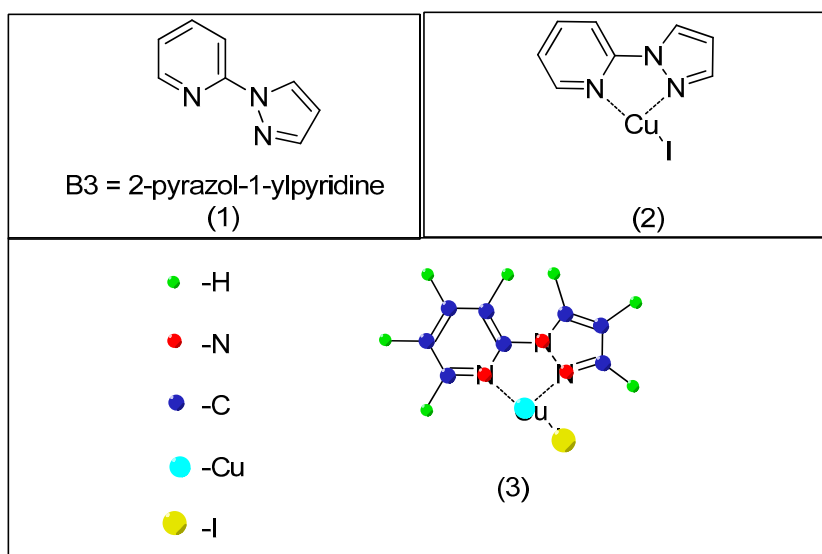


**Scheme 41.** The scaled-up product used in the industry.

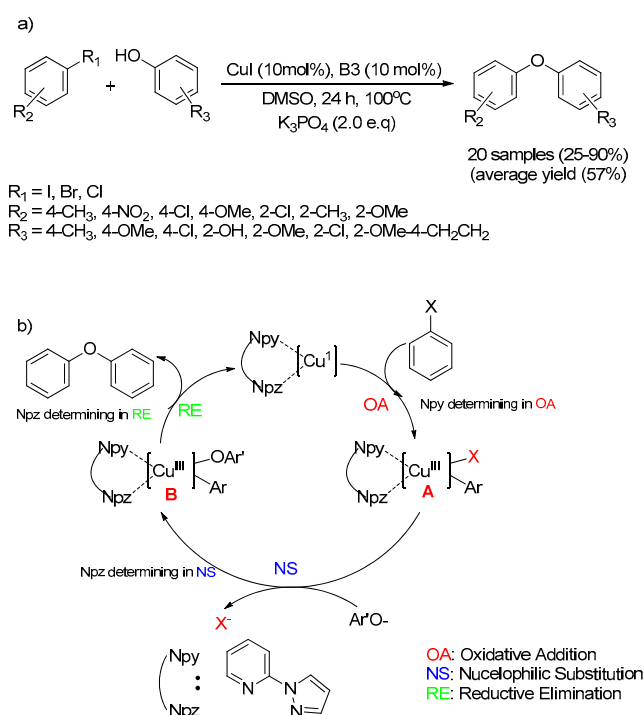
Zhao Ying Ying reported a pleasant, mild condition for Ullmann-type C-O bond formation using homogeneous Cu(I) ion solution with assisting an efficient pyrazole moiety-containing ligand: 2-pyrazol-1-ylpyridine ( $N_{py}, N_{pz}$ ) (B3), Figure 12.

In this study, a non-radical mechanism was proposed in the Ullmann-type C-O bond formation reaction. Initially, pyrazole ligand makes a coordination complex with copper ion. When the reaction is started, oxidative addition (OA) will first occur, in which the  $\text{Cu}^+$  undergoes OA with aryl halide to

form  $\text{Cu}^{3+}$  intermediate A. Then, the phenoxide undergoes nucleophilic substitution (NS) and through the reductive elimination (RE) biaryl ether is generated and the  $\text{Cu}^{3+}$  reduced to  $\text{Cu}^+$ . The proposed ligand B3, which has  $\text{N}_{\text{py}}$  and  $\text{N}_{\text{pz}}$ , play a different role in the reaction, where  $\text{N}_{\text{py}}$  is more likely the electron-rich copper center and encourages the coordination of aryl halide.  $\text{N}_{\text{pz}}$  play the role to lower and speed up the NS and RE step. This mechanism corresponds to the steric effect of the substituent at ortho-position in aryl halide rather than phenol due to an aromatic group of the former binding straight to the copper atom in the intermediate A (Scheme 42b), and Cu-O bond is formed when phenol is in the intermediate B (Scheme 42b). The O-arylation reaction was conducted in the presence of pyrazole ligands, CuI salt, and  $\text{K}_3\text{PO}_4$  in DMSO at 100 °C (Scheme 42a) [122].

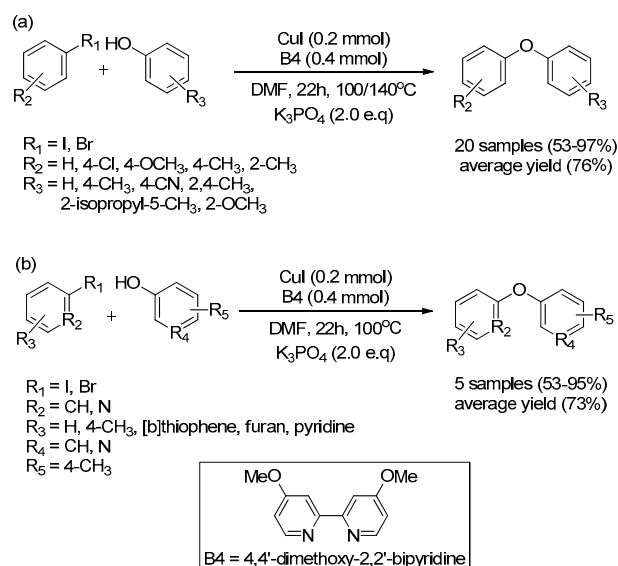


**Figure 12.** (1) 2-pyrazol-1-ylpyridine ligand (B3); (2) 2-pyrazol-1-ylpyridine ligand with CuI; (3) structures of monomeric complexes of a 2-pyrazol-1-ylpyridine ligand with CuI.

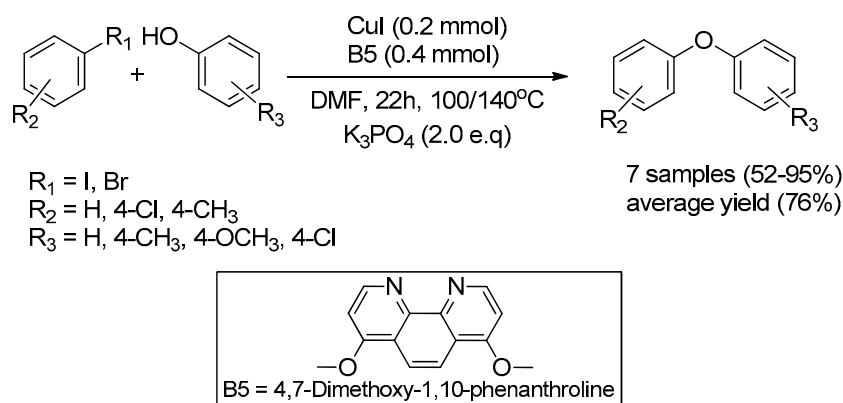


**Scheme 42.** (a) CuI-NPs with ligand (B3) in Ullmann etherification reaction; (b) the non-radical mechanism for the formation of biaryl ethers.

Besides pyrazole moiety-containing ligands, Zhao Ying Ying also reported a 2,2'-bipyridines as a ligand in the Ullmann O-arylation reaction. However, 4,4'-dimethoxy-2,2'-bipyridine ligand (B4) and 4,7-Dimethoxy-1,10-phenanthroline (B5) was found to be the best ligand which efficiently forwarded Ullmann reaction of the electron-donating methoxy substituent. The 4,4'-dimethoxy-2,2'-bipyridine ligand provided up to 95% yield of corresponding product from aryl and heteroaryl iodides and bromides with phenols (Scheme 43). The 4,7-Dimethoxy-1,10-phenanthroline ligand is a planar and rigid structure; therefore, it is less reactive and provided 52–95% yield of the aryl ether (Scheme 44) [123].



**Scheme 43.** (a) CuI-NPs with 2,2-bipyridine ligand (B4) in the formation of C-O bond; (b) heterocyclic biaryl ether.



**Scheme 44.** CuI-NPs with 4,7-Dimethoxy-1,10-phenanthroline ligand (B5) in the formation of biphenyl ether.

In 2019, Sudeep's team described a new type of imidazolium-based NHC ligand precursor in the Ullmann O-arylation. In their studies, 1,3-bis-(2,6-diisopropylphenyl)-imidazolium chloride (IPrHCl) (B6) salt showed best performance to the Ullmann reaction (Figure 13). The aryl bromide/heteroaryl bromide coupled with phenol to give corresponding biaryl ethers with excellent yield; however, highly substituted phenols gave a comparatively low yield of biaryl products. The electron-withdrawing substituted aryl bromide gave a better results (Scheme 45) [124].

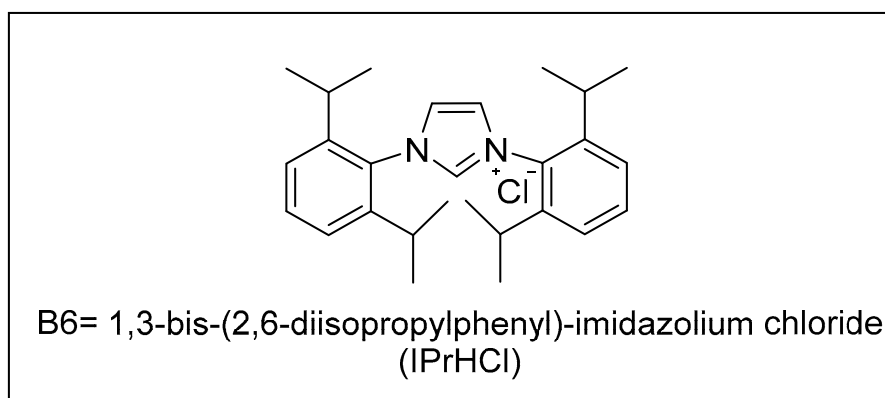
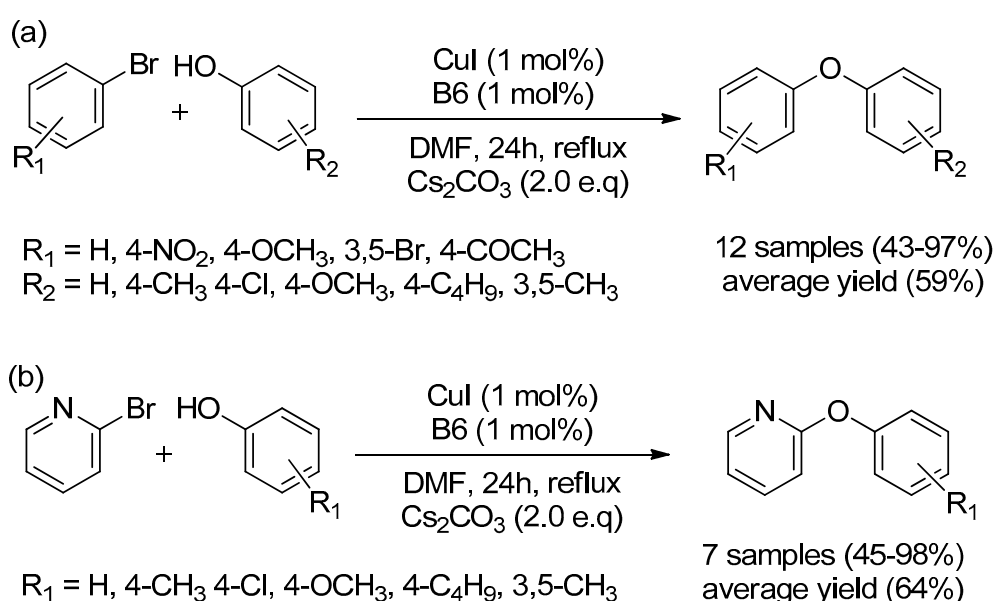


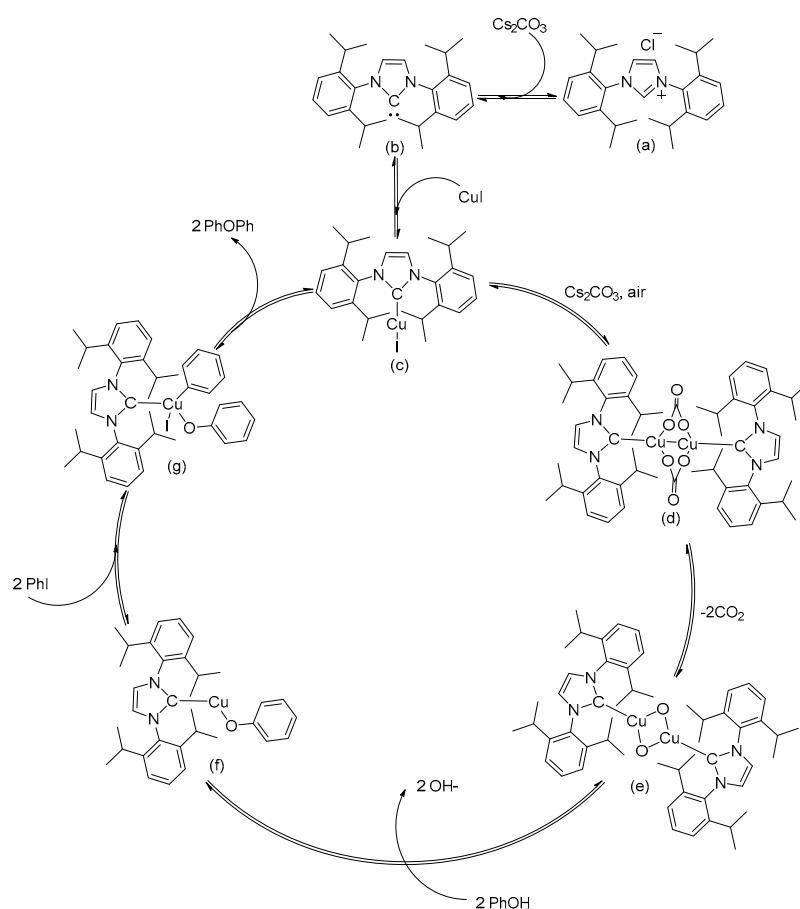
Figure 13. Imidazolium-based NHC ligands precursor.



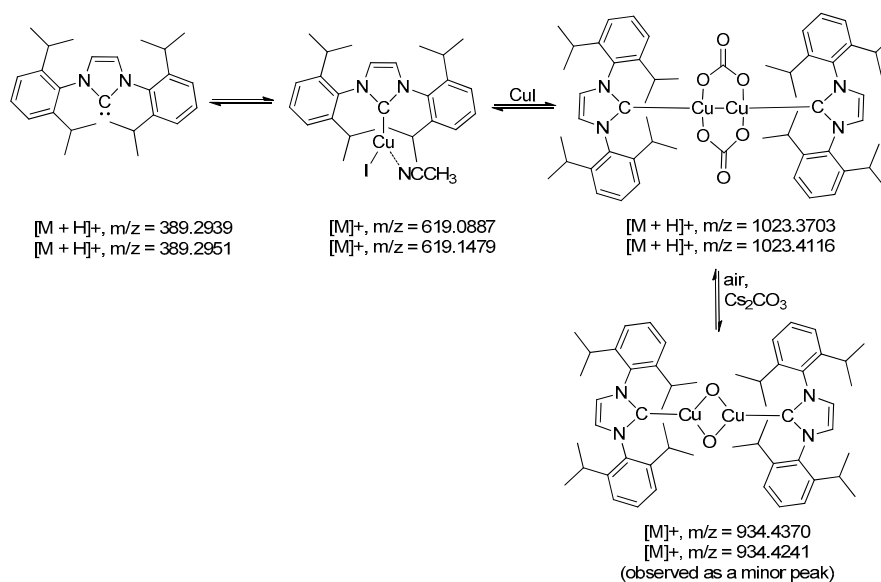
Scheme 45. (a) Formation of biaryl ethers in the presence of CuI salt and 1,3-bis-(2,6-diisopropylphenyl)-imidazolium chloride (IPrHCl) (B6) ligand; (b) heterocyclic biaryl ether.

In the Sudeep study, the mechanistic aspect of the catalyst was studied using high resolution mass spectrometry (HRMS) techniques systematically. The O-arylation of Ullmann coupling by the Sudeep study was the non-radical fashion of catalyst mechanism (Scheme 46). The catalysis reaction was proceeded through NHC-copper carbonate species (d) and followed by a bis- $\mu$ -oxo NHC-copper complex (e) formation. These intermediates play a critical part in the catalysis and produce the nucleophile incorporated complex (d), which undergoes the addition of aryl halide, followed by a final reductive elimination step yielding the desired biaryl ether and regenerate the intermediate (c) (see Figure 14) [124].



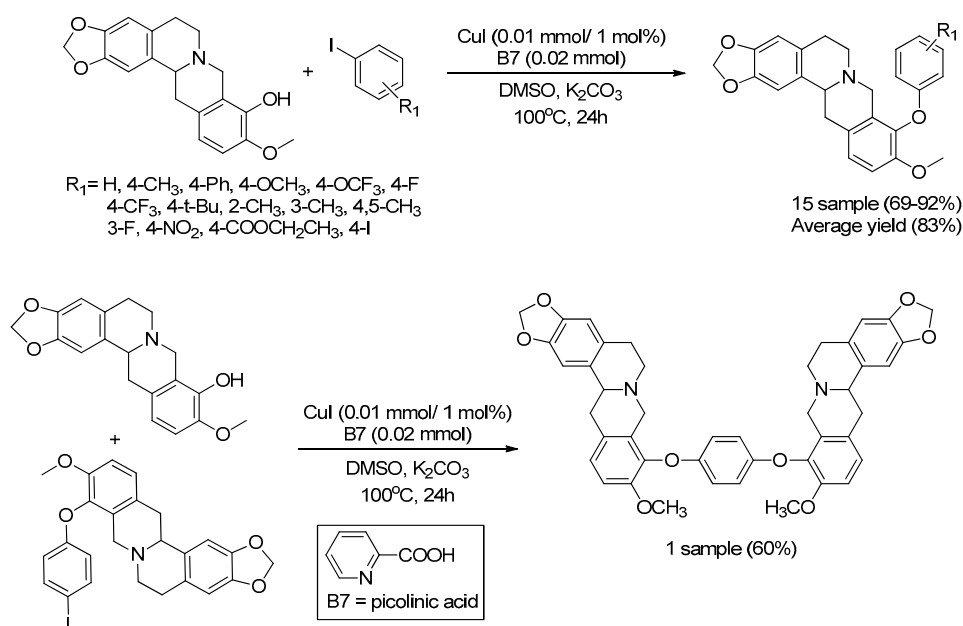


**Scheme 46.** The non-radical mechanism for the formation of biphenyl ethers using IPrHCl ligand.



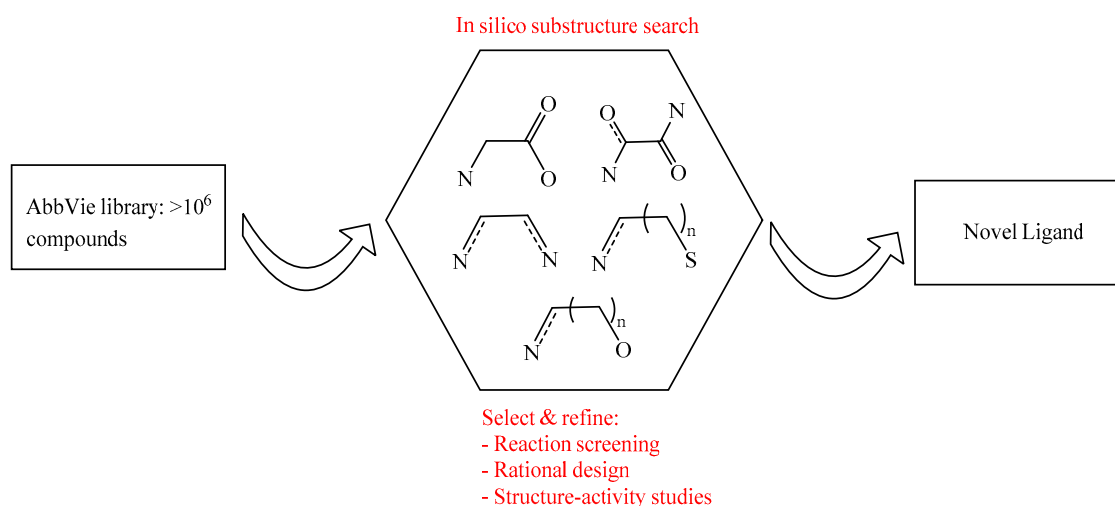
**Figure 14.** HRMS analysis of the reaction mixture (IPrHCl: CuI = 1:1).

Shortly afterwards, Teng Xiao Qing's team reported the use of pyridine base ligand in the synthesis of 9-O-arylated berberines. Berberine is a type of antimicrobial agent that widely applies in the medical field. Nevertheless, the high dosage of Berberine is required due to its low lipophilicity and bioavailability. The group of Teng applied the O-arylation Ullmann reaction in the modification of the structure of berberine with a potentially lipophilic aryl group (Scheme 47) [125].

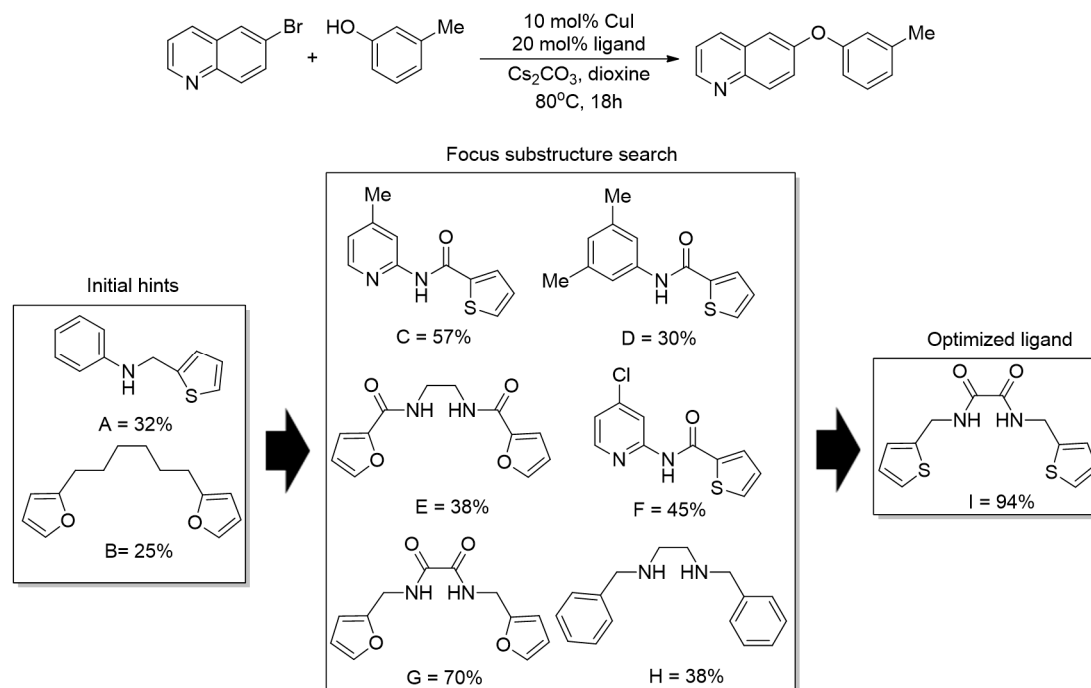


**Scheme 47.** Synthesis of 9-O-arylated berberines via CuI with picolinic acid (B7), aryl-iodide, and Levo-tetrahydro-berberrubine (l-THBr).

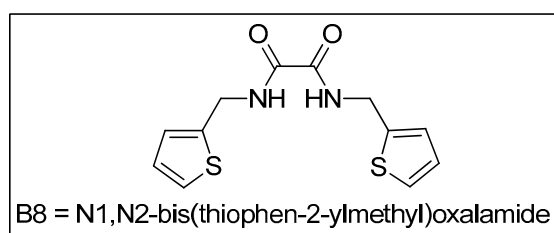
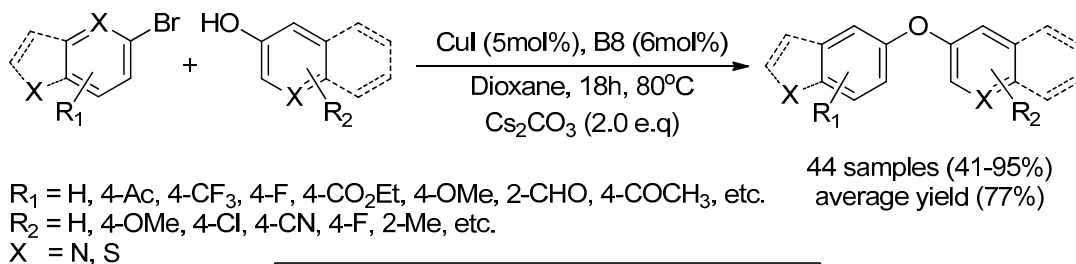
In 2019, Vincent Chan et al. described the standard pharmaceutical compound library with molecular diversity as the new pathway for discovery of new ligand structures that used in biaryl ethers formation. They used the AbbVie compound library as the source in finding, recognition, and development of new ligands (Figure 15). By using this new pathway for high throughput screening, he found that *N,N'*-bis(thiophene-2-ylmethyl)oxalamide is the potential ligand that efficiently promotes C-O bond formation reaction. The high throughput of compound screening process for new ligand and complete testing is shown in Scheme 48. Based on this screening methods, the yield of biaryl ethers is shown in (Scheme 49) [126].



**Figure 15.** Method for utilizing the AbbVie compound library as an origin for finding, recognition, and development of new ligands.



**Scheme 48.** High output compound finding for ligand identification in a Cu-mediated biaryl ether formation.



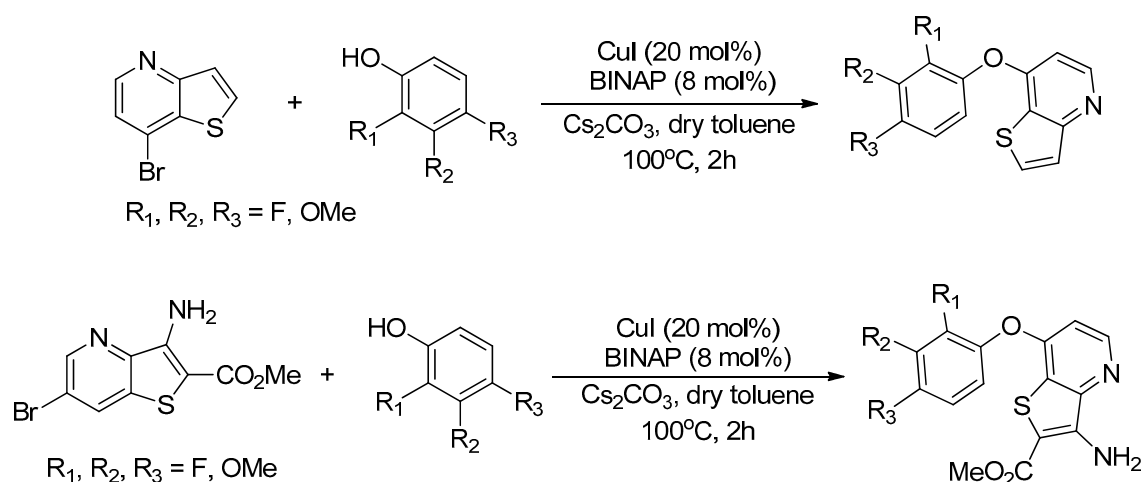
**Scheme 49.** C-O bond formation of heteroaryl bromide/aryl bromide with phenol/heteroaryl phenol.

### 3. Recent Application of Synthetic Ethers in Pharmaceutical and Natural Product

The aromatic C-O bonds are widely introduced in natural products and pharmaceutical-like molecules. Although the Pd-catalyzed cross-coupling reaction is a powerful system in the synthesis of this type of compounds, a constitutional problem, such as high cost and high toxicity, might restrict its application in pharmaceutical and medicinal industry. Back to front, the current breakthrough and growing of copper-mediated Ullmann etherification reactions offer an optional and practical selection. In this segment, we emphasize some current and representative applications of Ullmann O-arylation reaction in the medicinal chemistry and natural products.

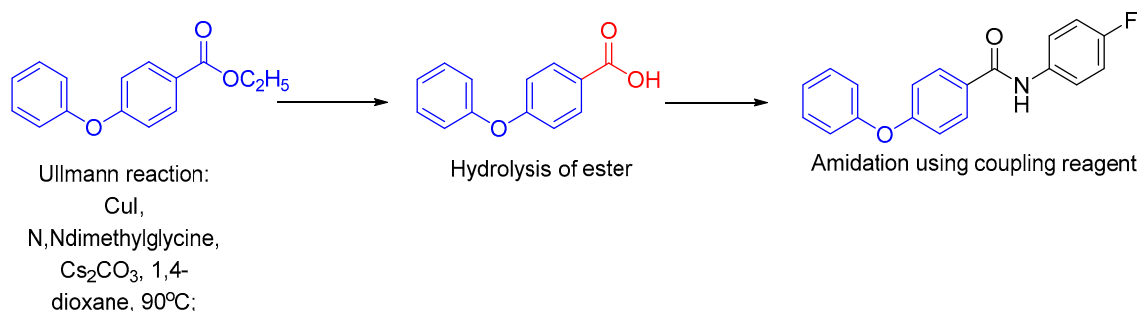
### 3.1. Medicinal Chemistry

The Ullmann etherification is comprehensively worked in the synthesis of pharmaceuticals-like derivatives. In 2013, di(hetero)aryl ether derivative compound containing a thieno (3,2-b) pyridyl ring system was prepared by Queiroz et al. through Ullmann O-arylation reaction (Scheme 50). The efficiency of anticancer inhibitory of these compounds fights a group of human tumor cell lines, including MCF-7 (breast adenocarcinoma), A375-C5 (melanoma), and NCI-H460 (non-small cell lung cancer); HCT15 (colon carcinoma), HepG2 (hepatocellular carcinoma), and HeLa (cervical carcinoma) were biologically evaluated. The biological evaluation demonstrated that the di(hetero)aryl ether compound with ortho- and meta-methoxy group (MeO-) showed encouraging antitumoral properties [127].



**Scheme 50.** New di(hetero)aryl ethers in the thieno [3,2-b]pyridine series.

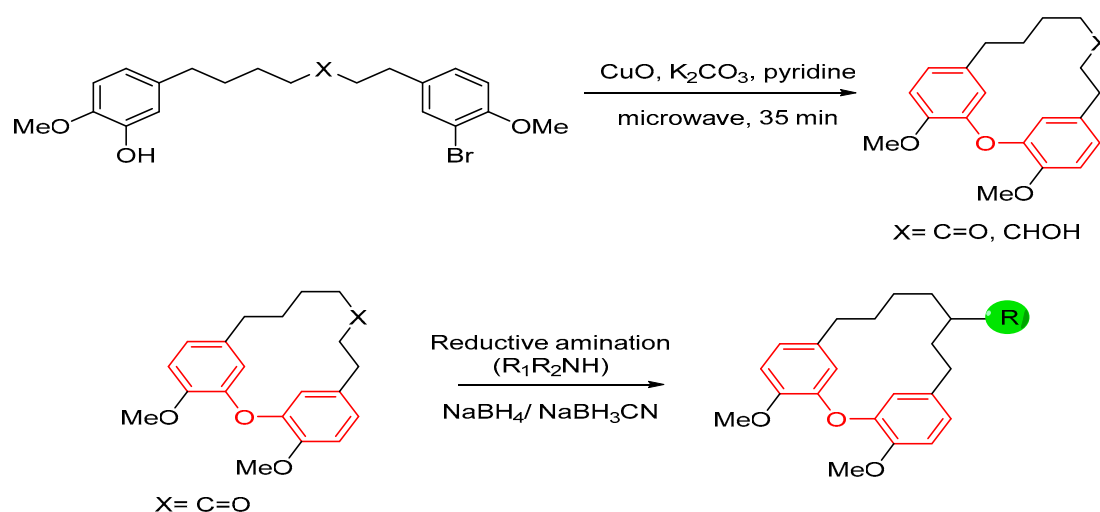
In 2015, Yang Shao Mei's team reported the structure-based pattern, structure-action connection study of a series of biaryl ether derivatives as potential antitumor agents. She found that the presence of Cl- and OH- group at para-position was significantly enhanced antitumor activity. The compound *N*-(4-fluorophenyl)-4-phenoxybenzamide can be mediated by improving the expression of P21 and Cl-caspase 3 and leading to apoptosis of tumor (Scheme 51) [128].



**Scheme 51.** The scheme reaction of antitumor agent starting from Ullman O-arylation reaction.

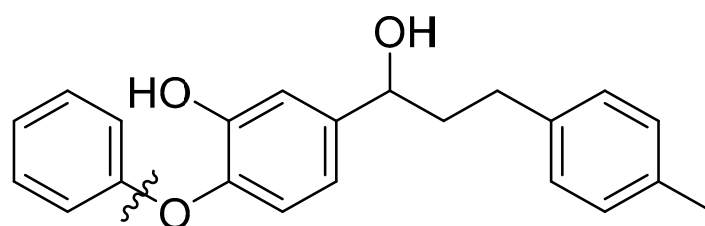
Bacterial contagion triggered by *Mycobacterium tuberculosis* (TB) and various problematic bacterial germ keep posing a vital threat to world public health. Therefore, novel chemotype antibacterial agents are doubtfully needed to fuel and boost the antibacterial drug discovery and development pipeline. Hao Lin's research group reported the structure-activity, route of synthesis, and antibacterial study of macrocyclic diarylheptanoids compound with the various amine, amide, urea, and sulfonamide functionalities in the extended pharmaceutical library. The outcome of their study produced macrocyclic

geranylamine and 4-fluorophenethylamine substituted derivatives, which can be performed reasonable activity against *M. tuberculosis* and picked Gram-positive bacterial pathogens (Scheme 52) [129].



**Scheme 52.** Synthesis pathway of macrocyclic amine derivative via Ullmann coupling reaction.

In 2018, Sidhartha S. Kar et al. developed a series of novel druggable biphenyl ethers as possibility antitubercular agents. The respective compound can be promising in vitro activity against drug-sensitive, isoniazid-resistant, and various drug-resistant strains of *Mycobacterium tuberculosis* (TB) (Scheme 53) [130].



### Ullmann coupling

## 1-(3-hydroxy-4-phenoxyphenyl)-3-p-tolylpropan-1-ol

**Scheme 53.** Anti-tuberculosis (TB) agent via Ullmann coupling reaction.

### 3.2. Natural Product

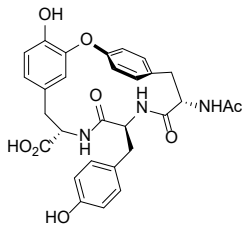
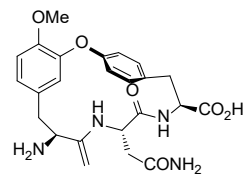
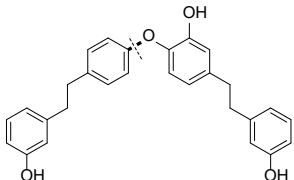
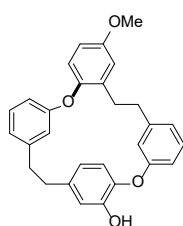
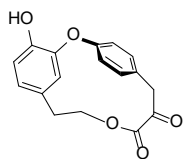
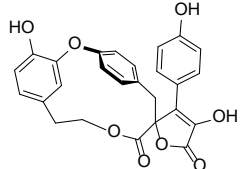
Biaryl ether compounds are the structure portion generally discovered in an extended natural product and display miscellaneous biological activities [131]. The most general compound includes amino acid derivatives, which commonly begin from oxidative phenol coupling of aromatic amino acid. The typical examples are the glycopeptide antibiotic vancomycin, neolignans, chalcones bisbenzyls, cyclic diarylheptanoids, and benzyloquinoline alkaloids [132]. Undoubtedly intentional of the carbon-oxygen bond transformation and refinement of instantaneous study are on the skyline. The significant evolution in this field was started in 1968 by Tomita, Fujitani, and Aoyagi, who discovered the proficiency of the Ullmann etherification cross-coupling reaction was powerfully enhanced by using copper oxide as a catalyst [133]. The complete synthesis of racemic bisbenzyltetrahydroisoquinoline alkaloids cycleanine [133], cephradine [134], phaeanthine [135], and isotetrandrin [135] is highlighted in Table 9. Various groups of researchers implemented the breakthrough of modified conditions by the

Tomita, Fujitani, and Aoyagi for the installation of biaryl ether derivative of a range of natural products. The representative example of a natural product using these modified methods is cyclic isodityrosine natural products, such as K-13 [136] or OF4949-III [137], perrottetin E [138], the bisbibenzyl natural product marchantin I [139], ornatipolide [140], retipolide E [140], and other related natural products (Table 10).

**Table 9.** The complete synthesis of various natural product compound.

R-X	R-OH	Condition	Diaryl Ether	Natural Product
		CuO (28 mol%), K <sub>2</sub> CO <sub>3</sub> , Pyridine, 150 °C, 4 h		
		CuO (26 mol%), K <sub>2</sub> CO <sub>3</sub> , Pyridine, 150 °C, 4 h		
		CuO (15 mol%), K <sub>2</sub> CO <sub>3</sub> , Pyridine, 150 °C, 4h		
		CuO (2 equiv.), K <sub>2</sub> CO <sub>3</sub> , Pyridine, 130 °C, 16 h		
		CuO (2 equiv.), K <sub>2</sub> CO <sub>3</sub> , Pyridine, 130 °C, 5 h		

**Table 10.** The representative example of a natural product using modified methods in cyclic isodityrosine natural products.

Compound	Condition	Structure
K-13	CuO (2.0 equiv.), K <sub>2</sub> CO <sub>3</sub> , pyridine, 145 °C, 24 h ≥91% (from bromide)	
OF4949-III	CuO (2.0 equiv.), K <sub>2</sub> CO <sub>3</sub> , pyridine, 130–145 °C, 12–24 h ≥91–93% (from bromide)	
Perrottetin E	CuO, K <sub>2</sub> CO <sub>3</sub> , pyridine, reflux, 24 h ≥60% (from bromide)	
Marchantin I	CuO (6.0 equiv.), K <sub>2</sub> CO <sub>3</sub> , pyridine, reflux, 24 h ≥60% (from bromide)	
Ornatipolide	CuO (2.5 equiv.), K <sub>2</sub> CO <sub>3</sub> , pyridine, 135 °C, 18 h ≥82% (from bromide)	
Retipolide E	CuO (2.5 equiv.), K <sub>2</sub> CO <sub>3</sub> , pyridine, 135 °C, 18 h ≥82% (from bromide)	

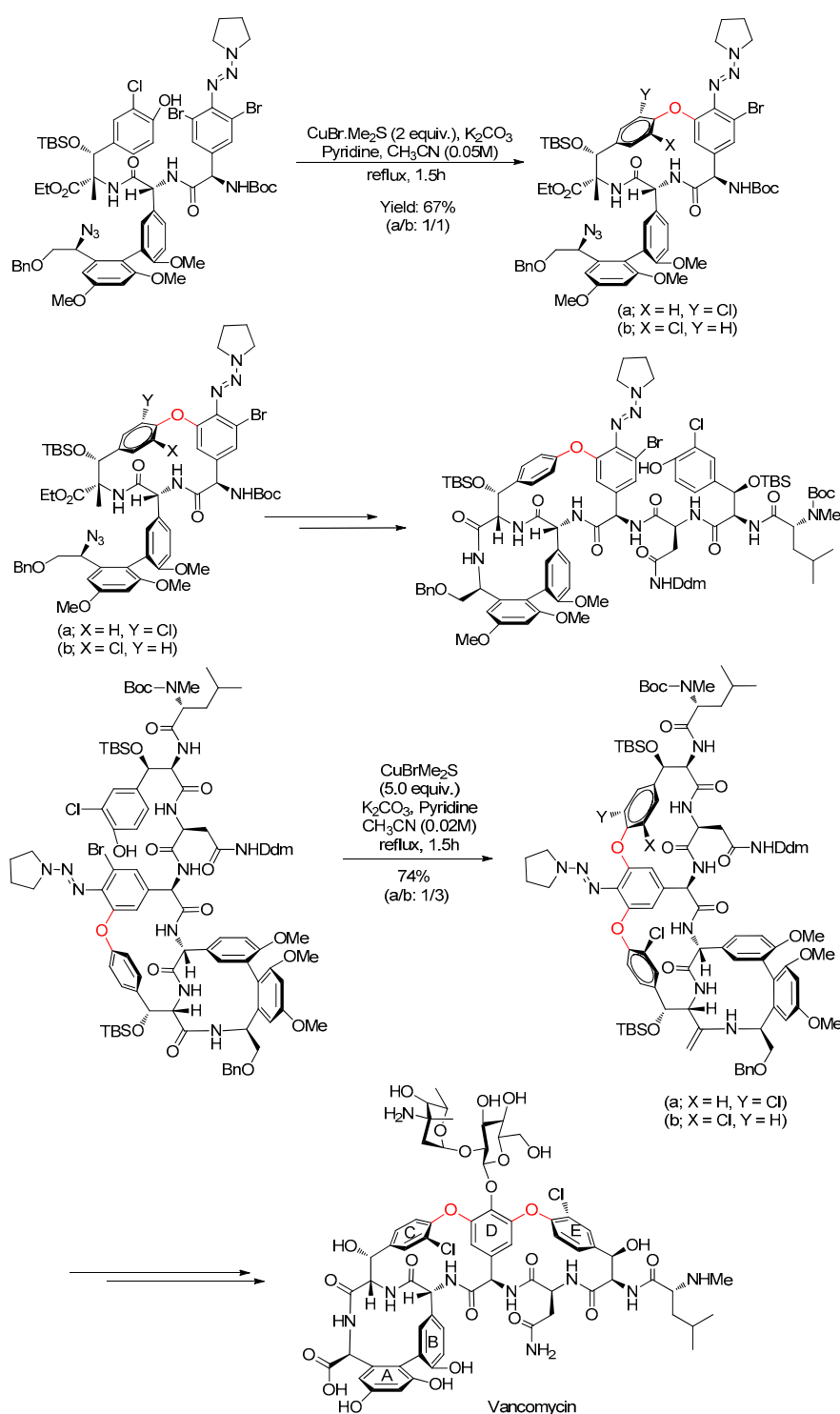
The same advancement can be seen retroactively for the transformations of the procedure used in intramolecular Ullman reactions. The ideal condition of intramolecular Ullmann coupling reaction could only be applied for the macrocyclization yielding to simple macrocyclic biphenyl ethers that are in a majority situation devoid of any functional group. As proved by the representative sample mentioned in this division, which was initially being plagued by harsh reaction conditions, it has also undergone a short transformation by Tomita, Fujitani, and Aoyagi. They reported that the most efficient procedure that progressively led the macrocyclic biaryl ether formation is using the caesium carbonate and/or chelating ligand in the reaction Table 11.

**Table 11.** The macrocyclic ether compound heptanoids that occur naturally prepared through an intramolecular Ullmann coupling reaction based on the condition that proposed by Tomita, Fujitani, and Aoyagi.

Substituents	Conditions	Yield	Precursor to	Ref.
R <sub>1</sub> = Me R <sub>2</sub> = R <sub>3</sub> = H	CuO (2.5 equiv.), K <sub>2</sub> CO <sub>3</sub> , pyridine (0.02 M), 90 °C, 48 h	49%	Acerogenin L (R <sub>1</sub> = R <sub>2</sub> = R <sub>3</sub> = H)	[141]
R <sub>1</sub> = iPr R <sub>2</sub> = R <sub>3</sub> = H	CuO (2.5 equiv.), Cs <sub>2</sub> CO <sub>3</sub> , pyridine (0.007 M), reflux, 48 h	81%	Acerogenin L (R <sub>1</sub> = R <sub>2</sub> = R <sub>3</sub> = H)	[142]
R <sub>1</sub> = Bn R <sub>2</sub> = OMe R <sub>3</sub> = H	CuO (2.5 equiv.), K <sub>2</sub> CO <sub>3</sub> , pyridine (0.02 M), 90 °C, 48 h	52%	(±)-Galeon (R <sub>1</sub> = R <sub>3</sub> = H, R <sub>2</sub> = OMe)	[141]
R <sub>1</sub> = iPr R <sub>2</sub> = OMe R <sub>3</sub> = H	CuO (2.5 equiv.), Cs <sub>2</sub> CO <sub>3</sub> , pyridine (0.007 M), reflux, 48 h	73%	(±)-Pterocarine = (±)-Engelhardione (R <sub>1</sub> = R <sub>3</sub> = H, R <sub>2</sub> = OH)	[142]
R <sub>1</sub> = H R <sub>2</sub> = OMe R <sub>3</sub> = H	CuO (10.0 equiv.), K <sub>2</sub> CO <sub>3</sub> , pyridine (0.1 M), 200 °C, 30 h	13%	(±)-Galeon (R <sub>1</sub> = R <sub>3</sub> = H, R <sub>2</sub> = OMe) Direct Obtained	[143]
R <sub>1</sub> = Me R <sub>2</sub> = OMe R <sub>3</sub> = H	CuO (2.5 equiv.), K <sub>2</sub> CO <sub>3</sub> , pyridine (0.02 M), 175 °C, 4.5 h	54%	(±)-Pterocarine = (±)-Engelhardione (R <sub>1</sub> = R <sub>3</sub> = H, R <sub>2</sub> = OH)	[144]
	CuO (2.5 equiv.), K <sub>2</sub> CO <sub>3</sub> , pyridine (0.01 M), 220 °C (Microwave), 35 min	85%		[145]
	CuO (10.0 equiv.), K <sub>2</sub> CO <sub>3</sub> , pyridine (0.1 M), 200 °C, 30 h	12%	(±)-Platycaryinol (R <sub>1</sub> = Me, R <sub>2</sub> = OMe, R <sub>3</sub> = H, alcohol instead of ketone)	[143]
R <sub>1</sub> = iPr R <sub>2</sub> = OMe R <sub>3</sub> = OiPr	CuO (2.5 equiv.), Cs <sub>2</sub> CO <sub>3</sub> , pyridine (0.007 M), reflux, 69 h	74%	(±)-Myricatomentogenin (R <sub>1</sub> = H, R <sub>2</sub> = OMe, R <sub>3</sub> = OH)	[142]
R <sub>1</sub> = Me R <sub>2</sub> = OMe R <sub>3</sub> = OiPr	CuO (2.5 equiv.), Cs <sub>2</sub> CO <sub>3</sub> , pyridine (0.007 M), reflux, 48 h	63%	(±)-Jugcathanin (R <sub>1</sub> = Me, R <sub>2</sub> = OMe, R <sub>3</sub> = OH)	[142]

There are two choices that can be imperfect when endeavoring to prepare a complex and highly sensitive compound, such as natural product by an intramolecular Ullmann etherification, with the intention of then stepping away from several reaction conditions. The first option is involved in the chelating ligand for copper that enabled the breakthrough of remarkably efficient processes operating under gentlest conditions. The second option is based on the *ortho*-effect with presence of copper that allows the desired product more accessible achieved. These *ortho*-effects touched upon by Ullman himself, who reported in 1903 the copper-mediated reaction between aniline and *ortho*-chloro-benzoic acid [132]. This is the key success of the Nicolaou group in the total synthesis of vancomycin (Scheme 54), with the gold of gentlest conditions in copper-mediated Ullmann reaction and *ortho* effect. Nicolaou designed the total synthesis of vancomycin based on the ingenious incorporation of a triazene unit in the starting materials that were place in *ortho* position to the aromatic bromine compound. The triazene serves as a potential “electron sink” and coordinate or stabilizer. The intermediate copper species turned out to be an outstanding achievement of biaryl ether compound in the synthesis of vancomycin [146–149].

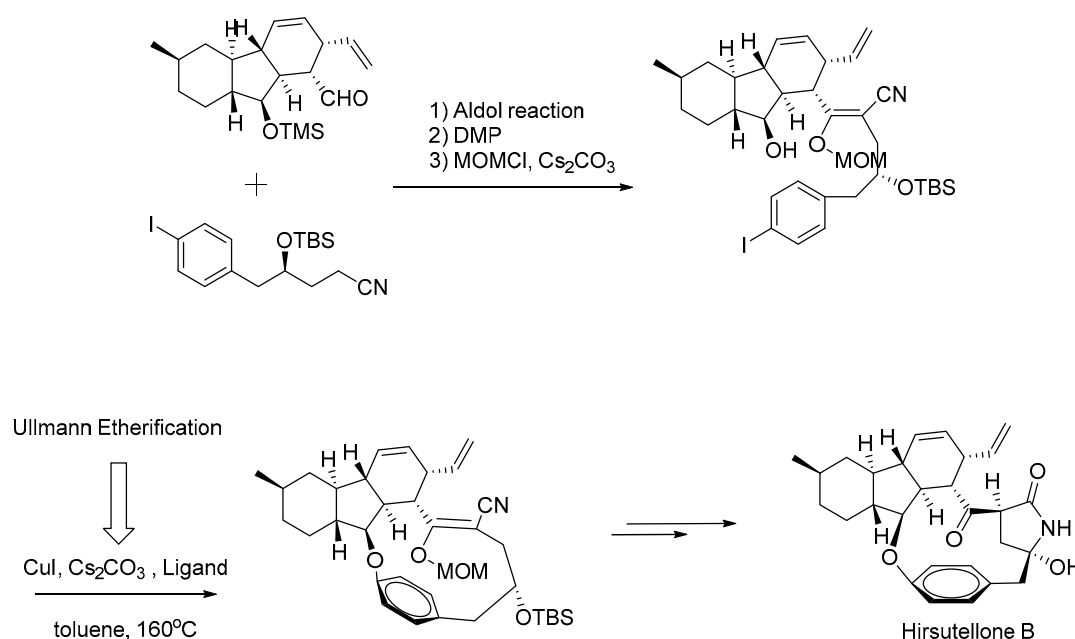




**Scheme 54.** The consecutive intramolecular condensations accelerated by ortho effects for synthesis of vancomycin.

Recently, *Hirsutellone B* is one of the members under family of decahydrofluorene class bioactive natural products [150]. The direct synthesis of strained 13-membered macrocycle is the challenge for organic chemists. Below is the first reported on the total synthesis of *Hirsutellones B* by Nicolaou's research team in 2009 [151]. In 2011, researcher Uchiro's team reported the synthesis of *Hirsutellone B* via

successful application of Ullmann etherification coupling reaction in the formation of the 13-membered ring (Scheme 55) [152].



**Scheme 55.** Total synthesis of bioactive natural products; *Hirsutellone B* via Ullmann etherification.

#### 4. Conclusions

Ullmann C–O bond arylation reaction has become dominant and plays a vital role in organic synthesis, medicinal, agrochemical chemistry, with its being present in a broad range of natural products and biologically active compounds. Copper-mediated Ullmann reactions were virtuously developed for some time by utilizing novel ligands and synthetic ancillary tools. In this review, we summarized some recent advances and applications of the copper-mediated Ullmann coupling reaction in the synthesis of heterocycles, pharmaceutical molecules, and natural products. A marvelous agreement of work has been reliable for establishing a more effortless and fast method of Ullmann type C–O bond formation, mainly capital on catalysts. Among many novels and speedy breakthrough of this reaction, we understand the eco-synthetic methodologies, such as nanosized metal-, ligand-, additive-free condition, and the reusable heterogeneous catalyst will develop in a parallel line to significantly give impact in this Ullmann O-arylation cross-coupling reaction. We notice that the involvement of low catalyst loading (<1 mol%) in the reaction is invariably limited with aryl chlorides, and tosylates are substantially expelled as the initial substrate in most of the situation. These challenges obligate the synthetic organic transformation to study further and explore with develop a novel method and catalytic system to extend the scope and generality of century-old Ullmann condition. As illustrated, the use of all kinds of various copper-mediated catalysts in Ullmann O-arylation allows for rapid transformations under relatively mild and ligand-free conditions, with the benefits of the excellent yield of products with the ease of catalyst separation and recover. As a summary, the outcome of most of the reactions highly depended on different diverse variables, and their connection has not been confirmed yet. The following are the tabulated part affecting the Ullmann O-arylation cross-coupling reaction.

- Ion form of copper: Either metallic copper, Cu(I), Cu(II), or Cu(0) salts and oxides have been applied, but Cu(I) salts commonly provide the extraordinary performance.
- Amount of copper: Commonly in the scope of 5–15 mol% based on the substrate, yet as a typical order higher loaded of copper provides a faster rate of reaction with an excellent outcome.

- Ligand form: Bi-dentate ligands are generally chosen, and the pyridine nucleus, secondary or tertiary amines, carbonyl groups, and imino-groups are generally suitable working ligand moieties; phosphine ligands are generally not very active.
- Ligand loaded: Bi-dentate ligands are used on average in a ratio of (copper: ligand); 1:1 or 1:2, while most of the conditions, a higher ratio leading a better outcome.
- Base: Organic bases, such as amines, do not work well with C-O Ullmann etherification. On the other hand, inorganic bases, such as potassium phosphate or carbonate and cesium carbonate, give better results in the reaction. The most general loading of the base is 3 equivalents relative to the substrate.
- Solvent: Depending on the reaction and reactant used, polar/non-polar solvents give a better outcome; DMF, DMSO, toluene, or acetonitrile are among the most used; N-Methyl-2-pyrrolidone (NMP) is basically utilized in microwave reactions.
- Temperature: The comment temperature in Ullmann etherification is in the range 70–120 °C, but some cases also conduct at room temperature; a better outcome of the product is generally in higher temperatures.
- Aryl halide: The reactivity of the aryl halide follows the trend: I > Br > Cl; the reactivity of aryl-chlorides can be activated via the strong electron-withdrawing group as substituents, ortho position of substituents/adding a source of I<sup>-</sup> the reaction (ion exchange reactions are catalyzed by Cu).
- Nucleophile: The better the nucleophile, the better the results, such as amines/thiols > phenol; amides are more active than imides.
- Steric hindrance: A noticeable sensitivity is usually observed, both on the aryl halide and the nucleophile. For example, the presence of the methyl group in the ortho position to the nucleophilic site can significantly reduce the corresponding product.
- Atmosphere: Usually an inert condition; nitrogen/argon atmosphere gives a better organic transformation in Cu-catalyzed ether bond couplings.

**Funding:** This work was funded by the Skim UMGreat, funding no. GUG0382-1/2019, the postgraduate student research grant, University Malaysia Sabah, Malaysia.

**Acknowledgments:** Generous support of the Skim UMGreat, funding no. GUG0382-1/2019 initiated by the University Malaysia Sabah is gratefully acknowledge.

**Conflicts of Interest:** The authors declare no conflict of interest.

## References

1. Ayogu, J.I.; Onoabedje, E.A. Recent advances in transition metal-catalysed cross-coupling of (hetero)aryl halides and analogues under ligand-free conditions. *Catal. Sci. Technol.* **2019**, *9*, 5233–5255. [[CrossRef](#)]
2. Ciulla, M.G.; Zimmermann, S.; Kumar, K. Cascade reaction based synthetic strategies targeting biologically intriguing indole polycycles. *Org. Biomol. Chem.* **2019**, *17*, 413–431. [[CrossRef](#)] [[PubMed](#)]
3. Boström, J.; Brown, D.G.; Young, R.J.; Keserü, G.M. Expanding the medicinal chemistry synthetic toolbox. *Nat. Rev. Drug Discov.* **2018**, *17*, 709–727. [[CrossRef](#)]
4. Tahmasbi, B.; Ghorbani-Choghamarani, A.; Moradi, P. Palladium fabricated on boehmite as an organic–inorganic hybrid nanocatalyst for C–C cross coupling and homoselective cycloaddition reactions. *New J. Chem.* **2020**, *44*, 3717–3727. [[CrossRef](#)]
5. Mäkelä, E.; González Escobedo, J.L.; Lindblad, M.; Käldestrom, M.; Meriö-Talvio, H.; Jiang, H.; Puurunen, R.L.; Karinen, R.J.C. Hydrodeoxygenation of levulinic acid dimers on a zirconia-supported ruthenium catalyst. *Catalysts* **2020**, *10*, 200. [[CrossRef](#)]
6. Hasija, D.C.; Gopalakrishnan, J.; Mishra, A.V.; Ghase, V.D.; Patil, V.R.J.S.A.S. Exploring copper as a catalyst for cost effective synthesis of polyfluorenes: An alternative to platinum and palladium. *SN Appl. Sci.* **2020**, *2*, 1–9. [[CrossRef](#)]

7. Padín, D.; Varela, J.A.; Saá, C. Ruthenium-Catalyzed Tandem Carbene/Alkyne Metathesis/N–H Insertion: Synthesis of Benzofused Six-Membered Azaheterocycles. *Org. Lett.* **2020**. [[CrossRef](#)]
8. Amariucaí-Mantu, D.; Mangalagiu, V.; Danac, R.; Mangalagiu, I.I. Microwave Assisted Reactions of Azaheterocycles Formedicinal Chemistry Applications. *Molecules* **2020**, *25*, 716. [[CrossRef](#)]
9. National Research Council (US) Chemical Sciences Roundtable. Replacing Critical Materials with Abundant Materials. In *The Role of the Chemical Sciences in Finding Alternatives to Critical Resources: A Workshop Summary*; National Academies Press: Washington, DC, USA, 2012.
10. Fan, Q.; Zhu, J.; Gottfried, J.M. On-Surface Ullmann Reaction for the Synthesis of Polymers and Macrocycles. In *On-Surface Synthesis II*; Springer: Cham, Switzerland, 2018; pp. 83–112.
11. Abyzaisani, M.; Jayalatharachchi, V.; MacLeod, J. 2.14—Directed On-Surface Growth of Covalently-Bonded Molecular Nanostructures. In *Comprehensive Nanoscience and Nanotechnology*, 2nd ed.; Andrews, D.L., Lipson, R.H., Nann, T., Eds.; Academic Press: Oxford, UK, 2019; pp. 299–326. [[CrossRef](#)]
12. Ullmann, F.; Bielecki, J. Ueber Synthesen in der Biphenylreihe. *Ber. Dtsch. Chem. Ges.* **1901**, *34*, 2174–2185. [[CrossRef](#)]
13. Gong, X.; Wu, J.; Meng, Y.; Zhang, Y.; Ye, L.-W.; Zhu, C.J.G.C. Ligand-free palladium catalyzed Ullmann biaryl synthesis: ‘household’ reagents and mild reaction conditions. *Green Chem.* **2019**, *21*, 995–999. [[CrossRef](#)]
14. Jiang, J.; Du, L.; Ding, Y. Aryl-Aryl Bond Formation by Ullmann Reaction: From Mechanistic Aspects to Catalyst. *Mini Rev. Org. Chem.* **2020**, *17*, 26–46. [[CrossRef](#)]
15. Gurjar, K.K.; Sharma, R.K.J.H. Synthetic and computational studies on Cu/ligand pair promoted activation of C (Aryl)-Cl bond in C–N coupling reactions. *Heliyon* **2020**, *6*, e03233. [[CrossRef](#)] [[PubMed](#)]
16. Rovira, M.; Soler, M.; Guell, I.; Wang, M.-Z.; Gomez, L.; Ribas, X. Orthogonal Discrimination among Functional Groups in Ullmann-Type C–O and C–N Couplings. *J. Org. Chem.* **2016**, *81*, 7315–7325. [[CrossRef](#)]
17. Cirigottis, K.A.; Ritchie, E.; Taylor, W.C. Studies on the Hurltley reaction. *Aust. J. Chem.* **1974**, *27*, 2209–2228. [[CrossRef](#)]
18. Evano, G.; Blanchard, N. *Copper-Mediated Cross-Coupling Reactions*; John Wiley & Sons: Hoboken, NJ, USA, 2013.
19. Ullmann, F. Ueber eine neue Bildungsweise von Diphenylaminderivaten. *Ber. Dtsch. Chem. Ges.* **1903**, *36*, 2382–2384. [[CrossRef](#)]
20. Ullmann, F.; Sponagel, P. Ueber die phenylierung von phenolen. *Ber. Dtsch. Chem. Ges.* **1905**, *38*, 2211–2212. [[CrossRef](#)]
21. Goldberg, I. Ueber phenylierungen bei gegenwart von kupfer als katalysator. *Ber. Dtsch. Chem. Ges.* **1906**, *39*, 1691–1692. [[CrossRef](#)]
22. Hurltley, W.R.H. CCXLIV—Replacement of halogen in orthobromo-benzoic acid. *J. Chem. Soc.* **1929**, 1870–1873. [[CrossRef](#)]
23. Khan, F.; Dlugosch, M.; Liu, X.; Banwell, M.G. The Palladium-Catalyzed Ullmann Cross-Coupling Reaction: A Modern Variant on a Time-Honored Process. *Acc. Chem. Res.* **2018**, *51*, 1784–1795. [[CrossRef](#)]
24. Egorova, K.S.; Ananikov, V.P. Toxicity of Metal Compounds: Knowledge and Myths. *Organometallics* **2017**, *36*, 4071–4090. [[CrossRef](#)]
25. Tepale, N.; Fernández-Escamilla, V.V.A.; Carreon-Alvarez, C.; González-Coronel, V.J.; Luna-Flores, A.; Carreon-Alvarez, A.; Aguilar, J. Nanoengineering of Gold Nanoparticles: Green Synthesis, Characterization, and Applications. *Crystals* **2019**, *9*, 612. [[CrossRef](#)]
26. Prabusankar, G.; Babu, C.N.; Raju, G.; Sampath, N. Silver (I) and copper (II)-imidazolium carboxylates: Efficient catalysts in Ullmann coupling reactions. *J. Chem. Sci.* **2017**, *129*, 553–559. [[CrossRef](#)]
27. Rosen, B.M.; Quasdorf, K.W.; Wilson, D.A.; Zhang, N.; Resmerita, A.-M.; Garg, N.K.; Percec, V. Nickel-Catalyzed Cross-Couplings Involving Carbon–Oxygen Bonds. *Chem. Rev.* **2011**, *111*, 1346–1416. [[CrossRef](#)] [[PubMed](#)]
28. Tobisu, M.; Chatani, N. Cross-Couplings Using Aryl Ethers via C–O Bond Activation Enabled by Nickel Catalysts. *Acc. Chem. Res.* **2015**, *48*, 1717–1726. [[CrossRef](#)]
29. Van der Boom, M.E.; Liou, S.-Y.; Ben-David, Y.; Shimon, L.J.W.; Milstein, D. Alkyl- and Aryl-Oxygen Bond Activation in Solution by Rhodium(I), Palladium(II), and Nickel(II). Transition-Metal-Based Selectivity. *J. Am. Chem. Soc.* **1998**, *120*, 6531–6541. [[CrossRef](#)]
30. Sun, Y.; Yang, Z.; Tian, P.; Sheng, Y.; Xu, J.; Han, Y.-F. Oxidative degradation of nitrobenzene by a Fenton-like reaction with Fe-Cu bimetallic catalysts. *Appl. Catal. B Environ.* **2019**, *244*, 1–10. [[CrossRef](#)]
31. Schlögl, R. Heterogeneous Catalysis. *Angew. Chem. Int. Ed.* **2015**, *54*, 3465–3520. [[CrossRef](#)]

32. Chatterjee, S.; Bhattacharya, S.K. Size-Dependent Catalytic Activity and Fate of Palladium Nanoparticles in Suzuki-Miyaura Coupling Reactions. *ACS Omega* **2018**, *3*, 12905–12913. [[CrossRef](#)]
33. Kidwai, M.; Mishra, N.K.; Bansal, V.; Kumar, A.; Mozumdar, S. Cu-nanoparticle catalyzed O-arylation of phenols with aryl halides via Ullmann coupling. *Tetrahedron Lett.* **2007**, *48*, 8883–8887. [[CrossRef](#)]
34. Benaskar, F.; Ben-Abdelmoumen, A.; Patil, N.G.; Rebrov, E.V.; Meuldijk, J.; Hulshof, L.A.; Hessel, V.; Krtschil, U.; Schouten, J.C. Cost Analysis for a Continuously Operated Fine Chemicals Production Plant at 10 Kg/Day Using a Combination of Microprocessing and Microwave Heating. *J. Flow Chem.* **2011**, *1*, 74–89. [[CrossRef](#)]
35. Benaskar, F.; Engels, V.; Patil, N.; Rebrov, E.V.; Meuldijk, J.; Hessel, V.; Hulshof, L.A.; Jefferson, D.A.; Schouten, J.C.; Wheatley, A.E.J.T.L. Copper (0) in the Ullmann heterocycle-aryl ether synthesis of 4-phenoxy pyridine using multimode microwave heating. *Tetrahedron Lett.* **2010**, *51*, 248–251. [[CrossRef](#)]
36. Isomura, Y.; Narushima, T.; Kawasaki, H.; Yonezawa, T.; Obora, Y. Surfactant-free single-nano-sized colloidal Cu nanoparticles for use as an active catalyst in Ullmann-coupling reaction. *Chem. Commun.* **2012**, *48*, 3784–3786. [[CrossRef](#)] [[PubMed](#)]
37. Nasrollahzadeh, M.; Sajadi, S.M.; Khalaj, M. Green synthesis of copper nanoparticles using aqueous extract of the leaves of *Euphorbia esula* L and their catalytic activity for ligand-free Ullmann-coupling reaction and reduction of 4-nitrophenol. *RSC Adv.* **2014**, *4*, 47313–47318. [[CrossRef](#)]
38. Garel, C.; Renard, B.-L.; Escande, V.; Galtayries, A.; Hesemann, P.; Grison, C. CC bond formation strategy through ecocatalysis: Insights from structural studies and synthetic potential. *Appl. Catal. A Gen.* **2015**, *504*. [[CrossRef](#)]
39. Deyris, P.-A.; Grison, C. Nature, ecology and chemistry: An unusual combination for a new green catalysis, ecocatalysis. *Curr. Opin. Green Sustain. Chem.* **2018**, *10*, 6–10. [[CrossRef](#)]
40. Clavé, G.; Garel, C.; Poullain, C.; Renard, B.-L.; Olszewski, T.K.; Lange, B.; Shutcha, M.; Faucon, M.-P.; Grison, C. Ullmann reaction through ecocatalysis: Insights from bioresource and synthetic potential. *RSC Adv.* **2016**, *6*, 59550–59564. [[CrossRef](#)]
41. Olszewski, T.K.; Adler, P.; Grison, C. Bio-based Catalysts from Biomass Issued after Decontamination of Effluents Rich in Copper—An Innovative Approach towards Greener Copper-based Catalysis. *Catalysts* **2019**, *9*, 214. [[CrossRef](#)]
42. Damkaci, F.; Sigindere, C.; Sobiech, T.; Vik, E.; Malone, J. N-Picolinamides as ligands in Ullman type C–O coupling reactions. *Tetrahedron Lett.* **2017**, *58*, 3559–3564. [[CrossRef](#)]
43. Zhang, J.; Zhang, Z.; Wang, Y.; Zheng, X.; Wang, Z. Nano-CuO-Catalyzed Ullmann Coupling of Phenols with Aryl Halides under Ligand-Free Conditions. *Eur. J. Org. Chem.* **2008**, *2008*, 5112–5116. [[CrossRef](#)]
44. Kim, J.Y.; Park, J.C.; Kim, A.; Kim, A.Y.; Lee, H.J.; Song, H.; Park, K. Cu<sub>2</sub>O Nanocube-Catalyzed Cross-Coupling of Aryl Halides with Phenols via Ullmann Coupling. *Eur. J. Org. Chem.* **2009**, *2009*, 4219–4223. [[CrossRef](#)]
45. Babu, S.G.; Karvembu, R. Room temperature Ullmann type C–O and C–S cross coupling of aryl halides with phenol/thiophenol catalyzed by CuO nanoparticles. *Tetrahedron Lett.* **2013**, *54*, 1677–1680. [[CrossRef](#)]
46. Khalilzadeh, M.A.; Keipour, H.; Hosseini, A.; Zareyee, D. KF/Clinoptilolite, an effective solid base in Ullmann ether synthesis catalyzed by CuO nanoparticles. *New J. Chem.* **2014**, *38*, 42–45. [[CrossRef](#)]
47. Derakhshankhah, H.; Jafari, S.; Sarvari, S.; Barzegari, E.; Moakedi, F.; Ghorbani, M.; Varnamkhasti, B.S.; Jaymand, M.; Izadi, Z.; Tayebi, L. Biomedical Applications of Zeolitic Nanoparticles, with an Emphasis on Medical Interventions. *Int. J. Nanomed.* **2020**, *15*, 363. [[CrossRef](#)] [[PubMed](#)]
48. Pabalan, R.; Bertetti, F.P. Cation-Exchange Properties of Natural Zeolites. *Rev. Mineral. Geochem.* **2001**, *45*, 453–518. [[CrossRef](#)]
49. Zhang, Y.-P.; Shi, A.-H.; Yang, Y.-S.; Li, C.-L. Impregnated copper on magnetite as catalyst for the O-arylation of phenols with aryl halides. *Chin. Chem. Lett.* **2014**, *25*, 141–145. [[CrossRef](#)]
50. Gawande, M.B.; Bonifácio, V.D.B.; Varma, R.S.; Nogueira, I.D.; Bundaleski, N.; Ghumman, C.A.A.; Teodoro, O.M.N.D.; Branco, P.S. Magnetically recyclable magnetite–ceria (Nanocat-Fe-Ce) nanocatalyst—Applications in multicomponent reactions under benign conditions. *Green Chem.* **2013**, *15*, 1226–1231. [[CrossRef](#)]
51. Sharma, R.K.; Gaur, R.; Yadav, M.; Rathi, A.K.; Pechousek, J.; Petr, M.; Zboril, R.; Gawande, M.B. Maghemite-Copper Nanocomposites: Applications for Ligand-Free Cross-Coupling (C–O, C–S, and C–N) Reactions. *ChemCatChem* **2015**, *7*, 3495–3502. [[CrossRef](#)]
52. Kazemi, N.; Mahdavi Shahri, M. Magnetically Separable and Reusable CuFe<sub>2</sub>O<sub>4</sub> Spinel Nanocatalyst for the O-Arylation of Phenol with Aryl Halide Under Ligand-Free Condition. *J. Inorg. Organomet. Polym. Mater.* **2017**, *27*, 1264–1273. [[CrossRef](#)]

53. Jeevanandam, J.; Barhoum, A.; Chan, Y.S.; Dufresne, A.; Danquah, M.K. Review on nanoparticles and nanostructured materials: History, sources, toxicity and regulations. *Beilstein J. Nanotechnol.* **2018**, *9*, 1050–1074. [[CrossRef](#)]
54. Kovtyukhova, N.I.; Ollivier, P.J.; Martin, B.R.; Mallouk, T.E.; Chizhik, S.A.; Buzaneva, E.V.; Gorchinskiy, A. Layer-by-layer assembly of ultrathin composite films from micron-sized graphite oxide sheets and polycations. *Chem. Mater.* **1999**, *11*, 771–778. [[CrossRef](#)]
55. Bagherzadeh, M.; Heydari, M. Electrochemical detection of dopamine based on pre-concentration by graphene nanosheets. *Analyst* **2013**, *138*, 6044–6051. [[CrossRef](#)] [[PubMed](#)]
56. Nasrollahzadeh, M.; Maham, M.; Rostami-Vartooni, A.; Bagherzadeh, M.; Sajadi, S.M. Barberry fruit extract assisted in situ green synthesis of Cu nanoparticles supported on a reduced graphene oxide–Fe<sub>3</sub>O<sub>4</sub> nanocomposite as a magnetically separable and reusable catalyst for the O-arylation of phenols with aryl halides under ligand-free conditions. *RSC Adv.* **2015**, *5*, 64769–64780.
57. Nakhate, A.; Yadav, G. Solvothermal Synthesis of CuFe<sub>2</sub>O<sub>4</sub>@rGO: Efficient Catalyst for C-O Cross Coupling and N-arylation Reaction under Ligand-Free Condition. *ChemistrySelect* **2017**, *2*, 7150–7159. [[CrossRef](#)]
58. Radfar, I.; Kazemi Miraki, M.; Esfandiary, N.; Ghandi, L.; Heydari, A. Fe<sub>3</sub>O<sub>4</sub>@SiO<sub>2</sub>-copper sucrose xanthate as a green nanocatalyst for N-, O- and S-arylation. *Appl. Organomet. Chem.* **2019**, *33*, e4619. [[CrossRef](#)]
59. Bagheri, S.; Pazoki, F.; Radfar, I.; Heydari, A. Copper(I)-creatine complex on magnetic nanoparticles as a green catalyst for N- and O-arylation in deep eutectic solvent. *Appl. Organomet. Chem.* **2020**, *34*, e5447. [[CrossRef](#)]
60. Ashraf, M.; Liu, Z.; Peng, W.-X.; Zhou, L. Glycerol Cu(II) Complex Supported on Fe<sub>3</sub>O<sub>4</sub> Magnetic Nanoparticles: A New and Highly Efficient Reusable Catalyst for the Formation of Aryl-Sulfur and Aryl-Oxygen Bonds. *Catal. Lett.* **2019**, *150*. [[CrossRef](#)]
61. Khalili, D.; Rezaei, M.; Koohgard, M. Ligand-free copper-catalyzed O-arylation of aryl halides using impregnated copper ferrite on mesoporous graphitic carbon nitride as a robust and magnetic heterogeneous catalyst. *Microporous Mesoporous Mater.* **2019**, *287*, 254–263. [[CrossRef](#)]
62. Khodaei, M.M.; Alizadeh, A.; Haghipour, M. Preparation and characterization of isatin complexed with Cu supported on 4-(aminomethyl) benzoic acid-functionalized Fe<sub>3</sub>O<sub>4</sub> nanoparticles as a novel magnetic catalyst for the Ullmann coupling reaction. *Res. Chem. Intermed.* **2019**, *45*. [[CrossRef](#)]
63. Mousavi Mashhadi, S.A.; Kassaee, M.Z.; Eidi, E. Magnetically recyclable nano copper/chitosan in O-arylation of phenols with aryl halides. *Appl. Organomet. Chem.* **2019**, *33*, e5042. [[CrossRef](#)]
64. Zahedi, R.; Asadi, Z.; Firuzabadi, F.D. Anchored N,O-Cu complex over Fe<sub>3</sub>O<sub>4</sub>@SiO<sub>2</sub> as a highly efficient and reusable catalyst for CO coupling reaction. *Colloids Surf. A Physicochem. Eng. Asp.* **2019**, *580*, 123728. [[CrossRef](#)]
65. Yang, H.; Ye, S.; Zhou, J.; Liang, T. Biomass-Derived Porous Carbon Materials for Supercapacitor. *Front. Chem.* **2019**, *7*, 274. [[CrossRef](#)] [[PubMed](#)]
66. Huang, J.; Liu, Y.; You, T. Carbon nanofiber based electrochemical biosensors: A review. *Anal. Methods* **2010**, *2*, 202–211. [[CrossRef](#)]
67. Dante, R.C. 7—Carbon materials. In *Handbook of Friction Materials and Their Applications*; Dante, R.C., Ed.; Woodhead Publishing: Boston, MA, USA, 2016; pp. 93–103. [[CrossRef](#)]
68. Luciano, M.A.; Ribeiro, H.; Bruch, G.E.; Silva, G.G. Efficiency of capacitive deionization using carbon materials based electrodes for water desalination. *J. Electroanal. Chem.* **2020**, *859*, 113840. [[CrossRef](#)]
69. Wang, Q.; Yan, S.; Han, G.; Li, X.; You, R.; Zhang, Q.; Li, M.; Kaplan, D.L. Facile production of natural silk nanofibers for electronic device applications. *Compos. Sci. Technol.* **2020**, *187*, 107950. [[CrossRef](#)]
70. Mergen, Ö.B.; Arda, E.; Evingür, G.A. Electrical, optical, and mechanical percolations of multi-walled carbon nanotube and carbon mesoporous-doped polystyrene composites. *J. Compos. Mater.* **2020**, *54*, 31–44. [[CrossRef](#)]
71. Goto, T.; Ito, T.; Mayumi, K.; Maeda, R.; Shimizu, Y.; Hatakeyama, K.; Ito, K.; Hakuta, Y.; Terashima, K. Movable cross-linked elastomer with aligned carbon nanotube/nanofiber as high thermally conductive tough flexible composite. *Compos. Sci. Technol.* **2020**, *190*, 108009. [[CrossRef](#)]
72. Wang, C.-C.; Hung, K.-Y.; Ko, T.-E.; Hosseini, S.; Li, Y.-Y. Carbon-nanotube-grafted and nano-Co<sub>3</sub>O<sub>4</sub>-doped porous carbon derived from metal-organic framework as an excellent bifunctional catalyst for zinc-air battery. *J. Power Sources* **2020**, *452*, 227841. [[CrossRef](#)]
73. Jenie, S.N.A.; Kristiani, A.; Khaerudini, D.S.; Takeishi, K. Magnetic Nanobiochar as Heterogeneous Acid Catalyst for Esterification Reaction. *J. Environ. Chem. Eng.* **2020**, *8*, 103912. [[CrossRef](#)]
74. Widiyastuti, W.; Setyawan, H. Sulfonated carbon aerogel derived from coir fiber as high performance solid acid catalyst for esterification. *Adv. Powder Technol.* **2020**, *31*, 1412–1419.

75. Guo, X.; Hao, C.; Jin, G.; Zhu, H.-Y.; Guo, X.-Y. Copper Nanoparticles on Graphene Support: An Efficient Photocatalyst for Coupling of Nitroaromatics in Visible Light. *Angew. Chem. Int. Ed.* **2014**, *53*, 1973–1977. [[CrossRef](#)]
76. Zhai, Z.; Guo, X.; Jiao, Z.; Jin, G.; Guo, X.-Y. Graphene-supported Cu<sub>2</sub>O nanoparticles: An efficient heterogeneous catalyst for C–O cross-coupling of aryl iodides with phenols. *Catal. Sci. Technol.* **2014**, *4*, 4196–4199. [[CrossRef](#)]
77. Singh, V.V.; Singh, A.K. Nanoflowers of Cu<sub>1.85</sub>: Free and Decorated on Graphene Oxide (GO–Cu<sub>1.85</sub>) as Efficient and Recyclable Catalysts for C–O Coupling. *ACS Appl. Nano Mater.* **2018**, *1*, 2164–2174. [[CrossRef](#)]
78. Lou, Y.; Chen, X.; Samia, A.C.; Burda, C. Femtosecond Spectroscopic Investigation of the Carrier Lifetimes in Digenite Quantum Dots and Discrimination of the Electron and Hole Dynamics via Ultrafast Interfacial Electron Transfer. *J. Phys. Chem. B* **2003**, *107*, 12431–12437. [[CrossRef](#)]
79. Du, X.-S.; Yu, Z.-Z.; Dasari, A.; Ma, J.; Meng, Y.-Z.; Mai, Y.-W. Facile synthesis and assembly of Cu<sub>2</sub>S nanodisks to corncoblike nanostructures. *Chem. Mater.* **2006**, *18*, 5156–5158. [[CrossRef](#)]
80. Yang, W.; Vogler, B.; Lei, Y.; Wu, T. Metallic ion leaching from heterogeneous catalysts: An overlooked effect in the study of catalytic ozonation processes. *Environ. Sci. Water Res. Technol.* **2017**, *3*, 1143–1151. [[CrossRef](#)]
81. Vasquez-Céspedes, S.; Chepiga, K.M.; Möller, N.; Schäfer, A.H.; Glorius, F. Direct C–H arylation of heteroarenes with copper impregnated on magnetite as a reusable catalyst: Evidence for CuO nanoparticle catalysis in solution. *ACS Catal.* **2016**, *6*, 5954–5961. [[CrossRef](#)]
82. Alshehri, R.; Ilyas, A.M.; Hasan, A.; Arnaout, A.; Ahmed, F.; Memic, A. Carbon Nanotubes in Biomedical Applications: Factors, Mechanisms, and Remedies of Toxicity. *J. Med. Chem.* **2016**, *59*, 8149–8167. [[CrossRef](#)]
83. Abdalla, S.; Al-Marzouki, F.; Al-Ghamdi, A.A.; Abdel-Daiem, A. Different Technical Applications of Carbon Nanotubes. *Nanoscale Res. Lett.* **2015**, *10*, 358. [[CrossRef](#)]
84. Kharisov, B.I.; Kharissova, O.V.; Dimas, A.V. The dispersion, solubilization and stabilization in “solution” of single-walled carbon nanotubes. *RSC Adv.* **2016**, *6*, 68760–68787. [[CrossRef](#)]
85. Akhavan, E.; Hemmati, S.; Hekmati, M.; Veisi, H. CuCl heterogenized on metformine-modified multi walled carbon nanotubes as a recyclable nanocatalyst for Ullmann-type C–O and C–N coupling reactions. *New J. Chem.* **2018**, *42*, 2782–2789. [[CrossRef](#)]
86. Kolanowska, A.; Kuziel, A.W.; Jedrysiak, R.G.; Krzywiecki, M.; Korczeniewski, E.; Wisniewski, M.; Terzyk, A.P.; Boncel, S. Ullmann Reactions of Carbon Nanotubes-Advantageous and Unexplored Functionalization toward Tunable Surface Chemistry. *Nanomaterials* **2019**, *9*, 1619. [[CrossRef](#)] [[PubMed](#)]
87. Mu, H.; Li, C.; Bai, J.; Sun, W. In situ synthesis of Cu/CNFs composite catalyst by electrospun nanofibers wrapped copper chloride and applied for Ullmann coupling reaction. *J. Mol. Struct.* **2018**, *1165*, 90–100. [[CrossRef](#)]
88. Chawla, S.; Cai, J.; Naraghi, M. Mechanical tests on individual carbon nanofibers reveals the strong effect of graphitic alignment achieved via precursor hot-drawing. *Carbon* **2017**, *117*, 208–219. [[CrossRef](#)]
89. Bin Ali, A.; Renz, F.; Koch, J.; Tegenkamp, C.; Sindelar, R. Graphene Nanoplatelet (GNPs) Doped Carbon Nanofiber (CNF) System: Effect of GNPs on the Graphitic Structure of Creep Stress and Non-Creep Stress Stabilized Polyacrylonitrile (PAN). *Nanomaterials* **2020**, *10*, 351. [[CrossRef](#)] [[PubMed](#)]
90. Li, Y.; Li, L.; Yu, J. Applications of Zeolites in Sustainable Chemistry. *Chem* **2017**, *3*, 928–949. [[CrossRef](#)]
91. Tahraoui, Z.; Nouali, H.; Marichal, C.; Forler, P.; Klein, J.; Daou, T.J. Influence of the Compensating Cation Nature on the Water Adsorption Properties of Zeolites. *Molecules* **2020**, *25*, 944. [[CrossRef](#)]
92. Tuel, A.; Farrusseng, D. Perspectives on Zeolite-Encapsulated Metal Nanoparticles and Their Applications in Catalysis. *New J. Chem.* **2015**, *40*. [[CrossRef](#)]
93. Magné, V.; Garnier, T.; Danel, M.; Pale, P.; Chassaing, S. CuI–USY as a Ligand-Free and Recyclable Catalytic System for the Ullmann-Type Diaryl Ether Synthesis. *Org. Lett.* **2015**, *17*, 4494–4497. [[CrossRef](#)]
94. Garnier, T.; Danel, M.; Magné, V.; Pujol, A.; Bénétteau, V.; Pale, P.; Chassaing, S. Copper(I)–USY as a Ligand-Free and Recyclable Catalyst for Ullmann-Type O-, N-, S-, and C-Arylation Reactions: Scope and Application to Total Synthesis. *J. Org. Chem.* **2018**, *83*, 6408–6422. [[CrossRef](#)]
95. Choi, D.-Y.; Lee, J.W.; Peng, J.; Lee, Y.J.; Han, J.-Y.; Lee, Y.H.; Choi, I.S.; Han, S.B.; Jung, J.K.; Lee, W.S.; et al. Obovatol improves cognitive functions in animal models for Alzheimer’s disease. *J. Neurochem.* **2012**, *120*, 1048–1059. [[CrossRef](#)]
96. Elsaïdi, S.K.; Mohamed, M.H.; Banerjee, D.; Thallapally, P.K. Flexibility in Metal–Organic Frameworks: A fundamental understanding. *Coord. Chem. Rev.* **2018**, *358*, 125–152. [[CrossRef](#)]
97. Lin, Z.-J.; Lü, J.; Hong, M.; Cao, R. Metal–organic frameworks based on flexible ligands (FL-MOFs): Structures and applications. *Chem. Soc. Rev.* **2014**, *43*, 5867–5895. [[CrossRef](#)]

98. Zhao, S.-N.; Song, X.-Z.; Song, S.-Y.; Zhang, H.-j. Highly efficient heterogeneous catalytic materials derived from metal-organic framework supports/precursors. *Coord. Chem. Rev.* **2017**, *337*, 80–96. [[CrossRef](#)]
99. Doonan, C.J.; Sumby, C.J. Metal-organic framework catalysis. *CrystEngComm* **2017**, *19*, 4044–4048. [[CrossRef](#)]
100. Sadeghi, S.; Jafarzadeh, M.; Reza Abbasi, A.; Daasbjerg, K. Incorporation of CuO NPs into modified UiO-66-NH<sub>2</sub> metal-organic frameworks (MOFs) with melamine for catalytic C–O coupling in the Ullmann condensation. *New J. Chem.* **2017**, *41*, 12014–12027. [[CrossRef](#)]
101. Ha, H.Q.; Nguyen, H.T.D.; Pham, T.H.M.; Pham, V.T.; Truong, T. Towards optical application of metal-organic frameworks: Cu-MOFs as sole heterogeneous photocatalyst for arylation of phenols at room temperature. *Catal. Commun.* **2018**, *117*, 79–84. [[CrossRef](#)]
102. Hwang, J.; Yan, R.; Oschatz, M.; Schmidt, B. Solvent Mediated Morphology Control of Zn MOFs as Carbon Templates for Application in Supercapacitors. *J. Mater. Chem. A* **2018**, *6*. [[CrossRef](#)]
103. Allen, A.E.; MacMillan, D.W.C. Synergistic catalysis: A powerful synthetic strategy for new reaction development. *Chem. Sci.* **2012**, *3*, 633–658. [[CrossRef](#)] [[PubMed](#)]
104. Sammis, G.M.; Danjo, H.; Jacobsen, E.N. Cooperative Dual Catalysis: Application to the Highly Enantioselective Conjugate Cyanation of Unsaturated Imides. *J. Am. Chem. Soc.* **2004**, *126*, 9928–9929. [[CrossRef](#)]
105. Trost, B.M.; Luan, X. Contemporaneous Dual Catalysis by Coupling Highly Transient Nucleophilic and Electrophilic Intermediates Generated in Situ. *J. Am. Chem. Soc.* **2011**, *133*, 1706–1709. [[CrossRef](#)]
106. Vellayan, K.; González, B.; Trujillano, R.; Vicente, M.A.; Gil, A. Pd supported on Cu-doped Ti-pillared montmorillonite as catalyst for the Ullmann coupling reaction. *Appl. Clay Sci.* **2018**, *160*, 126–131. [[CrossRef](#)]
107. Mitsudo, K.; Asada, T.; Inada, T.; Kurimoto, Y.; Mandai, H.; Suga, S. Cu/Fe/O= PPh<sub>3</sub>-Catalyzed Etherification for the Synthesis of Aryl 3-Benzo [b] thienyl Ethers. *Chem. Lett.* **2018**, *47*, 1044–1047. [[CrossRef](#)]
108. Ramezani, L.; Yahyazadeh, A.; Sheykhani, M. The First C–Cl Activation in Ullmann C–O Coupling by MOFs. *ChemCatChem* **2018**, *10*, 4636–4651. [[CrossRef](#)]
109. Zolfigol, M.A.; Khakyzadeh, V.; Moosavi-Zare, A.R.; Rostami, A.; Zare, A.; Iranpoor, N.; Beyzavi, M.H.; Luque, R. A highly stable and active magnetically separable Pd nanocatalyst in aqueous phase heterogeneously catalyzed couplings. *Green Chem.* **2013**, *15*, 2132–2140. [[CrossRef](#)]
110. Baghbanian, S.M.; Yadollahy, H.; Tajbakhsh, M.; Farhang, M.; Biparva, P. Palladium nanoparticles supported on natural nanozeolite clinoptilolite as a catalyst for ligand and copper-free C–C and C–O cross coupling reactions in aqueous medium. *RSC Adv.* **2014**, *4*, 62532–62543. [[CrossRef](#)]
111. Zhang, Y.; Ni, G.; Li, C.; Xu, S.; Zhang, Z.; Xie, X. The coupling reactions of aryl halides and phenols catalyzed by palladium and MOP-type ligands. *Tetrahedron* **2015**, *71*, 4927–4932. [[CrossRef](#)]
112. Joshi, H.; Sharma, K.N.; Sharma, A.K.; Prakash, O.; Singh, A.K. Graphene oxide grafted with Pd 17 Se 15 nano-particles generated from a single source precursor as a recyclable and efficient catalyst for C–O coupling in O-arylation at room temperature. *Chem. Commun.* **2013**, *49*, 7483–7485. [[CrossRef](#)]
113. Arundhathi, R.; Damodara, D.; Likhar, P.R.; Kantam, M.L.; Saravanan, P.; Magdaleno, T.; Kwon, S.H. Fe<sub>3</sub>O<sub>4</sub>@ mesoporous polyaniline: A Highly Efficient and Magnetically Separable Catalyst for Cross-Coupling of Aryl Chlorides and Phenols. *Adv. Synth. Catal.* **2011**, *353*, 1591–1600. [[CrossRef](#)]
114. Fan, M.; Zhou, W.; Jiang, Y.; Ma, D. CuI/Oxalamide catalyzed couplings of (Hetero) aryl chlorides and phenols for diaryl ether formation. *Angew. Chem. Int. Ed.* **2016**, *55*, 6211–6215. [[CrossRef](#)]
115. Xia, N.; Taillefer, M. Copper- or Iron-Catalyzed Arylation of Phenols from respectively Aryl Chlorides and Aryl Iodides. *Chem. A Eur. J.* **2008**, *14*, 6037–6039. [[CrossRef](#)]
116. Sreedhar, B.; Arundhathi, R.; Reddy, P.L.; Kantam, M.L. CuI Nanoparticles for C–N and C–O Cross Coupling of Heterocyclic Amines and Phenols with Chlorobenzenes. *J. Org. Chem.* **2009**, *74*, 7951–7954. [[CrossRef](#)] [[PubMed](#)]
117. Xu, L.-W.; Xia, C.-G.; Li, J.-W.; Hu, X.-X. Highly efficient CO cross-coupling reactions with unactivated halides by ligandless, heterogeneous raney Ni-Al alloy/copper (I) salts. *Synlett* **2003**, *2003*, 2071–2073.
118. Truong, T.; Daugulis, O. Divergent reaction pathways for phenol arylation by arynes: Synthesis of helicenes and 2-arylphenols. *Chem. Sci.* **2013**, *4*, 531–535. [[CrossRef](#)] [[PubMed](#)]
119. Ke, J. Semiconductor Nanocrystals for Environmental Catalysis. In *Advanced Nanomaterials for Pollutant Sensing and Environmental Catalysis*; Elsevier: Amsterdam, The Netherlands, 2020; pp. 119–163.
120. Shende, V.S.; Saptal, V.B.; Bhanage, B.M. Recent Advances Utilized in the Recycling of Homogeneous Catalysis. *Chem. Rec.* **2019**, *19*, 2022–2043. [[CrossRef](#)]
121. Navarro, L.; Pujol, M.D. Microwave assisted synthesis of selected diaryl ethers under Cu(I)-catalysis. *Tetrahedron Lett.* **2015**, *56*, 1812–1815. [[CrossRef](#)]



122. Zhao, Y.; Wang, X.; Kaneyama, R.; Kodama, K.; Hirose, T. Efficient Pyrazole Moiety-Containing Ligands for Cu-Catalyzed O-Arylation of Phenols. *Beilstein Arch.* **2019**, *1*, 94.
123. Zhao, Y.; Wang, X.; Kodama, K.; Hirose, T. Copper-Catalyzed Coupling Reactions of Aryl Halides and Phenols by 4,4'-Dimethoxy-2,2'-bipyridine and 4,7-Dimethoxy-1,10-phenanthroline. *ChemistrySelect* **2018**, *3*, 12620–12624. [[CrossRef](#)]
124. Paul, S.; Joy, B.P.; Rajendran, R.; Gudimetla, V.B. Cost Efficient Synthesis of Diaryl Ethers Catalysed by CuI, Imidazolium Chloride and Cs<sub>2</sub>CO<sub>3</sub>. *ChemistrySelect* **2019**, *4*, 7181–7186. [[CrossRef](#)]
125. Teng, Q.; Zhu, X.; Guo, Q.; Jiang, W.; Liu, J.; Meng, Q. Synthesis of 9-O-arylated berberines via copper-catalyzed C(Ar)-O coupling reactions. *Beilstein J. Org. Chem.* **2019**, *15*, 1575–1580. [[CrossRef](#)]
126. Chan, V.S.; Krabbe, S.W.; Li, C.; Sun, L.; Liu, Y.; Nett, A.J. Identification of an Oxalamide Ligand for Copper-Catalyzed C–O Couplings from a Pharmaceutical Compound Library. *ChemCatChem* **2019**, *11*, 5748–5753. [[CrossRef](#)]
127. Queiroz, M.-J.R.P.; Peixoto, D.; Calhelha, R.C.; Soares, P.; dos Santos, T.; Lima, R.T.; Campos, J.F.; Abreu, R.M.V.; Ferreira, I.C.F.R.; Vasconcelos, M.H. New di(hetero)arylethers and di(hetero)arylamines in the thieno[3,2-b]pyridine series: Synthesis, growth inhibitory activity on human tumor cell lines and non-tumor cells, effects on cell cycle and on programmed cell death. *Eur. J. Med. Chem.* **2013**, *69*, 855–862. [[CrossRef](#)] [[PubMed](#)]
128. Yang, S.-M.; Huang, Z.-N.; Zhou, Z.-S.; Hou, J.; Zheng, M.-Y.; Wang, L.-J.; Jiang, Y.; Zhou, X.-Y.; Chen, Q.-Y.; Li, S.-H.; et al. Structure-based design, structure–activity relationship analysis, and antitumor activity of diaryl ether derivatives. *Arch. Pharmacol. Res.* **2015**, *38*, 1761–1773. [[CrossRef](#)]
129. Lin, H.; Bruhn, D.F.; Maddox, M.M.; Singh, A.P.; Lee, R.E.; Sun, D. Synthesis and antibacterial evaluation of macrocyclic diarylheptanoid derivatives. *Bioorg. Med. Chem. Lett.* **2016**, *26*, 4070–4076. [[CrossRef](#)]
130. Kar, S.S.; Bhat, V.G.; Shenoy, V.P.; Bairy, I.; Shenoy, G.G. Design, synthesis, and evaluation of novel diphenyl ether derivatives against drug-susceptible and drug-resistant strains of *Mycobacterium tuberculosis*. *Chem. Biol. Drug Des.* **2019**, *93*, 60–66. [[CrossRef](#)] [[PubMed](#)]
131. Choudhary, A.; Naughton, L.M.; Montánchez, I.; Dobson, A.D.W.; Rai, D.K. Current status and future prospects of marine natural products (MNPs) as antimicrobials. *Mar. Drugs* **2017**, *15*, 272. [[CrossRef](#)] [[PubMed](#)]
132. Evano, G.; Wang, J.; Nitelet, A. Metal-mediated C–O bond forming reactions in natural product synthesis. *Org. Chem. Front.* **2017**, *4*, 2480–2499. [[CrossRef](#)]
133. Tomita, M.; Aoyagi, Y.; Sakatani, Y.; Fujitani, K. Studies on the Alkaloids of Menispermaceous Plants. CCXLI. Synthesis of Cycleanine.(2). Bischler-Napieralski Reaction of N-Acyl-3, 4-dimethoxy-5-(4-substituted-phenoxy)- $\beta$ -phenethylamines. *Chem. Pharm. Bull.* **1968**, *16*, 56–61. [[CrossRef](#)]
134. Tomita, M.; Fujitani, K.; Aoyagi, Y.; Kajita, Y. Studies on the alkaloids of menispermaceous plants. CCXLIV. Synthesis of dl-cepharanthine. *Chem. Pharm. Bull.* **1968**, *16*, 217–226. [[CrossRef](#)]
135. Inubushi, Y.; Masaki, Y.; Matsumoto, S.; Takami, F. Studies on the alkaloids of menispermaceous plants. Part CCXLIX. Total synthesis of optically active natural isotetrandrine, phaeanthine, and tetrandrine. *J. Chem. Soc. C Org.* **1969**, *11*, 1547–1556. [[CrossRef](#)]
136. Evans, D.A.; Ellman, J.A. The total syntheses of the isodityrosine-derived cyclic tripeptides OF4949-III and K-13. Determination of the absolute configuration of K-13. *J. Am. Chem. Soc.* **1989**, *111*, 1063–1072. [[CrossRef](#)]
137. Lygo, B.; Humphreys, L.D. Enantioselective synthesis of renieramide. *Synlett* **2004**, *2004*, 2809–2811. [[CrossRef](#)]
138. Toyota, M.; Tori, M.; Takikawa, K.; Shiobara, Y.; Kodama, M.; Asakawa, Y. Perrottetins E, F, and G from *Radula perrottetii* (liverwort)—isolation, structure determination, and synthesis of perrottetin e. *Tetrahedron Lett.* **1985**, *26*, 6097–6100. [[CrossRef](#)]
139. Miao, T.; Wang, L. Immobilization of copper in organic–inorganic hybrid materials: A highly efficient and reusable catalyst for the Ullmann diaryl etherification. *Tetrahedron Lett.* **2007**, *48*, 95–99. [[CrossRef](#)]
140. Ingerl, A.; Justus, K.; Hellwig, V.; Steglich, W. Syntheses of retipolide E and ornatipolide, 14-membered biaryl-ether macrolactones from mushrooms. *Tetrahedron* **2007**, *63*, 6548–6557. [[CrossRef](#)]
141. Jeong, B.-S.; Wang, Q.; Son, J.-K.; Jahng, Y. A Versatile Synthesis of Cyclic Diphenyl Ether-Type Diarylheptanoids: Acerogenins, ( $\pm$ )-Galeon, and ( $\pm$ )-Pterocaraine. *Eur. J. Org. Chem.* **2007**, *2007*, 1338–1344. [[CrossRef](#)]
142. Salih, M.Q.; Beaudry, C.M. Chirality in diarylether heptanoids: Synthesis of myricatomentogenin, jugcathanin, and congeners. *Org. Lett.* **2012**, *14*, 4026–4029. [[CrossRef](#)]
143. Bryant, V.C.; Kumar, G.D.K.; Nyong, A.M.; Natarajan, A. Synthesis and evaluation of macrocyclic diarylether heptanoid natural products and their analogs. *Bioorg. Med. Chem. Lett.* **2012**, *22*, 245–248. [[CrossRef](#)]

144. Shen, L.; Sun, D. Total synthesis and structural revision of engelhardione. *Tetrahedron Lett.* **2011**, *52*, 4570–4574. [[CrossRef](#)]
145. Shen, L.; Simmons, C.J.; Sun, D. Microwave-assisted synthesis of macrocycles via intramolecular and/or bimolecular Ullmann coupling. *Tetrahedron Lett.* **2012**, *53*, 4173–4178. [[CrossRef](#)]
146. Nicolaou, K.C.; Li, H.; Boddy, C.N.C.; Ramanjulu, J.M.; Yue, T.Y.; Natarajan, S.; Chu, X.J.; Bräse, S.; Rübsam, F. Total synthesis of vancomycin—Part 1: Design and development of methodology. *Chem. A Eur. J.* **1999**, *5*, 2584–2601. [[CrossRef](#)]
147. Nicolaou, K.C.; Boddy, C.N.C.; Li, H.; Koumbis, A.E.; Hughes, R.; Natarajan, S.; Jain, N.F.; Ramanjulu, J.M.; Bräse, S.; Solomon, M.E. Total synthesis of vancomycin—Part 2: Retrosynthetic analysis, synthesis of amino acid building blocks and strategy evaluations. *Chem. A Eur. J.* **1999**, *5*, 2602–2621. [[CrossRef](#)]
148. Nicolaou, K.C.; Koumbis, A.E.; Takayanagi, M.; Natarajan, S.; Jain, N.F.; Bando, T.; Li, H.; Hughes, R. Total synthesis of vancomycin—Part 3: Synthesis of the aglycon. *Chem. A Eur. J.* **1999**, *5*, 2622–2647. [[CrossRef](#)]
149. Nicolaou, K.C.; Mitchell, H.J.; Jain, N.F.; Bando, T.; Hughes, R.; Winssinger, N.; Natarajan, S.; Koumbis, A.E. Total synthesis of vancomycin—Part 4: Attachment of the sugar moieties and completion of the synthesis. *Chem. A Eur. J.* **1999**, *5*, 2648–2667. [[CrossRef](#)]
150. Lang, G.; Blunt, J.W.; Cummings, N.J.; Cole, A.L.J.; Munro, M.H.G. Hirsutide, a Cyclic Tetrapeptide from a Spider-Derived Entomopathogenic Fungus, *Hirsutella* sp. *J. Nat. Prod.* **2005**, *68*, 1303–1305. [[CrossRef](#)] [[PubMed](#)]
151. Nicolaou, K.C.; Sarlah, D.; Wu, T.R.; Zhan, W. Total synthesis of hirsutellone B. *Angew. Chem. (Int. Ed. Engl.)* **2009**, *48*, 6870–6874. [[CrossRef](#)]
152. Uchiro, H.; Kato, R.; Arai, Y.; Hasegawa, M.; Kobayakawa, Y. Total Synthesis of Hirsutellone B via Ullmann-Type Direct 13-Membered Macrocyclization. *Org. Lett.* **2011**, *13*, 6268–6271. [[CrossRef](#)]



© 2020 by the authors. Licensee MDPI, Basel, Switzerland. This article is an open access article distributed under the terms and conditions of the Creative Commons Attribution (CC BY) license (<http://creativecommons.org/licenses/by/4.0/>).